AD-A080 539 ARMY ARMAMENT RESEARCH AND DEVELOPMENT COMMAND ABERD--ETC F/G 20/4
MEASUREMENTS OF WEAK SHOCK WAVE REFLECTED PRESSURE HISTORIES ON--ETC(U)
OCT 79 B P BERTRAND

UNCLASSIFIED ARBRL-MR-02966 SBIE -AD-E430 357 NL

1 OF 2
AD A080539

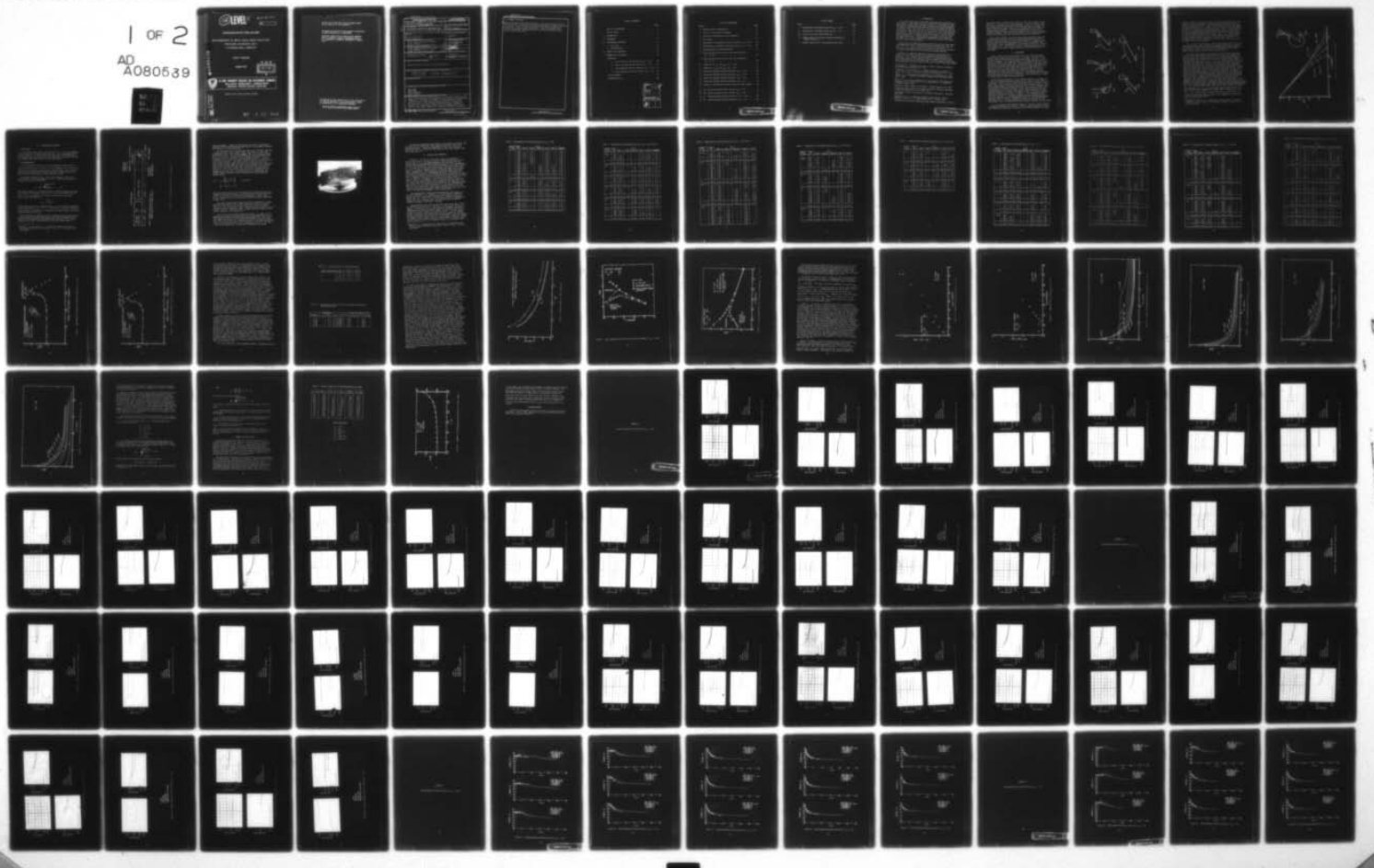

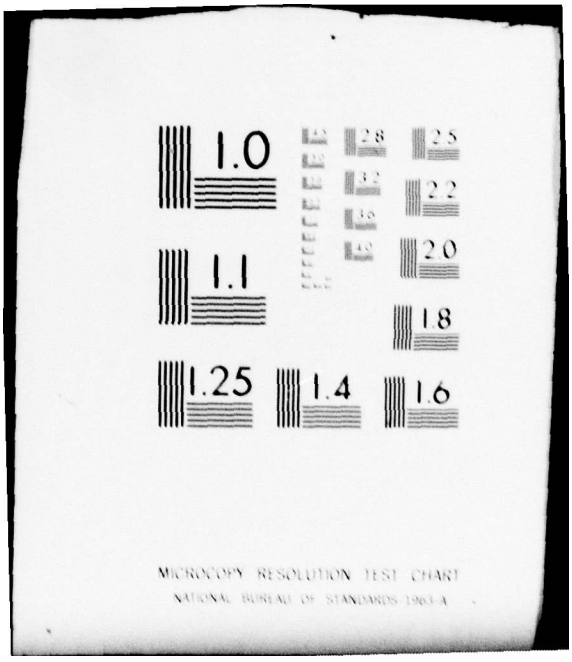
1.0
1.1
1.25
1.4
1.6
2.8
3.2
3.6
4.0
2.5
2.2
2.0
1.8
MICROCOPY RESOLUTION TEST CHART
NATIONAL BUREAU OF STANDARDS 1963-A

(12) LEVEL III

AD-E 430 357

AD

MEMORANDUM REPORT ARBRL-MR-02966

MEASUREMENTS OF WEAK SHOCK WAVE REFLECTED PRESSURE HISTORIES ON A 2-DIMENSIONAL SURFACE

Brian P. Bertrand

October 1979

US ARMY ARMAMENT RESEARCH AND DEVELOPMENT COMMAND
BALLISTIC RESEARCH LABORATORY
ABERDEEN PROVING GROUND, MARYLAND

80 1 21 036

Destroy this report when it is no longer needed.
Do not return it to the originator.

Secondary distribution of this report by originating or sponsoring activity is prohibited.

Additional copies of this report may be obtained from the National Technical Information Service, U.S. Department of Commerce, Springfield, Virginia 22151.

The findings in this report are not to be construed as an official Department of the Army position, unless so designated by other authorized documents.

The use of trade names or manufacturers' names in this report does not constitute indorsement of any commercial product.

UNCLASSIFIED

SECURITY CLASSIFICATION OF THIS PAGE (When Data Entered)

REPORT DOCUMENTATION PAGE

READ INSTRUCTIONS BEFORE COMPLETING FORM

1. REPORT NUMBER (14) MEMORANDUM REPORT ARBRL-MR-02966
2. GOVT ACCESSION NO.
3. RECIPIENT'S CATALOG NUMBER

4. TITLE (and Subtitle) (6)
MEASUREMENTS OF WEAK SHOCK WAVE REFLECTED PRESSURE HISTORIES ON A 2-DIMENSIONAL SURFACE.

5. TYPE OF REPORT & PERIOD COVERED (9)
Final rept.

6. PERFORMING ORG. REPORT NUMBER

7. AUTHOR(s) (10)
Brian P. Bertrand

8. CONTRACT OR GRANT NUMBER(s)
DNA 77-611 ?

9. PERFORMING ORGANIZATION NAME AND ADDRESS
US Army Ballistic Research Laboratory
(ATTN: DRDAR-BLT)
Aberdeen Proving Ground, MD 21005

10. PROGRAM ELEMENT, PROJECT, TASK AREA & WORK UNIT NUMBERS (16)
N990AXA E501 001AJ

11. CONTROLLING OFFICE NAME AND ADDRESS (11)
US Army Armament Research & Development Command
US Army Ballistic Research Laboratory
(ATTN: DRDAR-BL)
Aberdeen Proving Ground, MD 21005

12. REPORT DATE (12)
OCT [redacted] 79

13. NUMBER OF PAGES
115

14. MONITORING AGENCY NAME & ADDRESS (if different from Controlling Office)
Defense Nuclear Agency
Washington, D.C. 20305 (12) 108

15. SECURITY CLASS. (of this report)
UNCLASSIFIED

15a. DECLASSIFICATION/DOWNGRADING SCHEDULE

16. DISTRIBUTION STATEMENT (of this Report)

Approved for public release; distribution unlimited.

62704H

17. DISTRIBUTION STATEMENT (of the abstract entered in Block 20, if different from Report)
(18) SBIE (19) AD-E430 357

18. SUPPLEMENTARY NOTES

19. KEY WORDS (Continue on reverse side if necessary and identify by block number)

Shock Waves
Shock Tubes
Shock Reflection
Mach Reflection

20. ABSTRACT (Continue on reverse side if necessary and identify by block number)

Reflected pressures have been measured on a 2-dimensional wedge over the range of 0 to 90 degrees of incidence for shock waves of 13.8 and 34.5 kPa overpressure. The higher than normal pressures predicted by regular reflection theory in the range of angles just prior to the onset of Mach reflection are found to agree closely with theory. Reflected pressures for a small range of angles of shock incidence greater than those for which regular reflection is predicted are found to exceed the

(over)

DD FORM 1 JAN 73 1473 EDITION OF 1 NOV 65 IS OBSOLETE

UNCLASSIFIED

SECURITY CLASSIFICATION OF THIS PAGE (When Data Entered)

393471

20. ABSTRACT (Continued):

highest predicted regular reflection values. The pressure history scales as expected in time as a function of distance from the starting edge of the reflecting surface. Curves of reflected pressure versus angle of incidence are presented for the two incident shock levels. Curves of pressure versus distance-scaled times are presented which can be used to determine instantaneous whole surface loads.

TABLE OF CONTENTS

LIST OF ILLUSTRATIONS

LIST OF TABLES

I. INTRODUCTION

It is well known that the predicted reflected shock pressure on a flat surface in the angular region of transition from regular to Mach reflection is higher than for normal incidence for weak shock waves[1-3]. For angles of incidence beyond those for which the regular reflection (two shock) theory[2] has solutions, the three shock theory also has no solutions for weak shocks in much of the range in which Mach reflection is observed[3]. However, based on the speed of the foot of the observed Mach stem one would also surmise that the pressure is higher than for normal incidence for a range of angles of incidence above the limit for regular reflection. Experimental measurements of the enhanced pressures and of their durations are needed to determine their significance in blast loading problems.

Curves have been published showing reflected pressure versus angle of incidence for various strength shock waves incident on a flat surface[4,5,6,7,8,9]. These curves often differ from each other. In some cases, engineering judgment apparently has been used to disregard or to modify the magnitude of the predicted enhanced pressure.

There are no complete experimental pressure versus angle of incidence data available showing these enhanced pressures and their durations. This is because pressure measuring instrumentation until recent years did not have adequate frequency response to follow this short-lived enhanced pressure phenomenon. Another probable reason that this problem has not been pursued in the past is that it has been assumed

---

[1] *von Neumann, J. "Oblique Reflection of Shocks." Bureau of Ordnance Explosives Research Report 12. 1943*

[2] *Polacheck, H. and Seeger, R. J., "Regular Reflection of Shocks in Ideal Gases" Bureau of Ordnance Explosives Research Report 13. 1944*

[3] *Smith, L. G. "Photographic Investigation of the Reflection of Plane Shocks in Air." Office of Scientific Research and Development Report 6271. 1945*

[4] *Emmons, H. W. (Editor) Fundamentals of Gas Dynamics, High Speed Aerodynamics and Jet Propulsion, Vol. III, Princeton, N. J., Princeton University Press, 1958.*

[5] *Glasstone, Samuel (Editor) The Effects of Atomic Weapons, June 1950.*

[6] *Glasstone, Samuel (Editor) The Effects of Nuclear Weapons, Department of the Army Pamphlet No. 39-3, April 1962.*

[7] *Structures to Resist the Effects of Accidental Explosions. TM5-1300, June 1969.*

[8] *Swisdak, M. M., Jr., "Explosion Effects and Properties: Part I, Explosion Effects in Air, "NSWC/WOL/TR-75-116. October 1975.*

[9] *"Capabilities of Nuclear Weapons" Defense Nuclear Agency EM-1, Nov 1974.*

that normal shock incidence, which loads an entire flat surface instantaneously, is the most severe load possible. It may be, however, that for certain situations the higher than normal pressure associated with shock reflection at angles close to the limiting angle for regular reflection may be important. One needs pressure history data in this enhanced pressure region to assess its significance as it pertains to a specific problem. One could then proceed to a more simplified approximation for load calculations if this were found to be warranted.

This report documents a series of shock tube experiments that were performed to measure the reflected shock overpressure histories for angles of shock incidence on a flat surface from 0 to 90 degrees using incident shock waves of approximately 13.8 and 34.5 kilopascal (kPa) overpressure. These corresponded to shock pressure ratios of 1.136 and 1.34, respectively. These pressure ratios were chosen because of the susceptibility to damage of most structures, vehicles and aircraft in this range.

II. BACKGROUND

Figure 1 depicts several possibilities for the reflection phenomenon of weak, constant pressure shocks on a wedge. In Figure 1A the incident shock strikes the flat surface of the wedge face-on, or at 0° angle of incidence. The reflected shock, S_R, brings the flow to rest on the entire surface at a higher pressure and temperature than that existing behind the incident shock wave. Conditions in this reflected shock gas may be calculated using shock equations for normal reflection. If there is a corner, C, that allows part of the incident shock wave to travel past the reflecting surface, a rarefaction wave, R, will be generated that travels from the corner into the quiescent reflected shock gas at the speed of sound in that gas. The rarefaction wave lowers the pressure of the gas that it overtakes at A and accelerates it toward the lower pressure region beyond the corner.

If the reflecting surface is then slightly tilted, as in Figure 1B, so that the incident shock wave arrives at the surface at some angle of incidence, α, the gas in the region behind the point of contact T of the shock front on the surface will have a velocity along the surface. Here the two shock theory of regular reflection may be used to determine the flow conditions behind the reflected shock. The rarefaction wave front A generated at C now travels after T at the speed of sound in the reflected shock gas, its motion superimposed on the flow velocity induced along the surface by the shock. At small α, this rarefaction speed is less than the speed of T along the surface, so the distance TA continually increases. It has been predicted and observed experimentally[3] that the entire reflection configuration grows in a self-similar manner from the corner C. The gas conditions are constant between T and A, and between A and C the pressure and flow velocity decrease for weak shocks.

As α is increased still further, Figure 1C, the flow velocity behind T becomes greater and the speed of T along the surface decreases so that the distance TA diminishes. An angle α_c, the catch-up angle, is finally

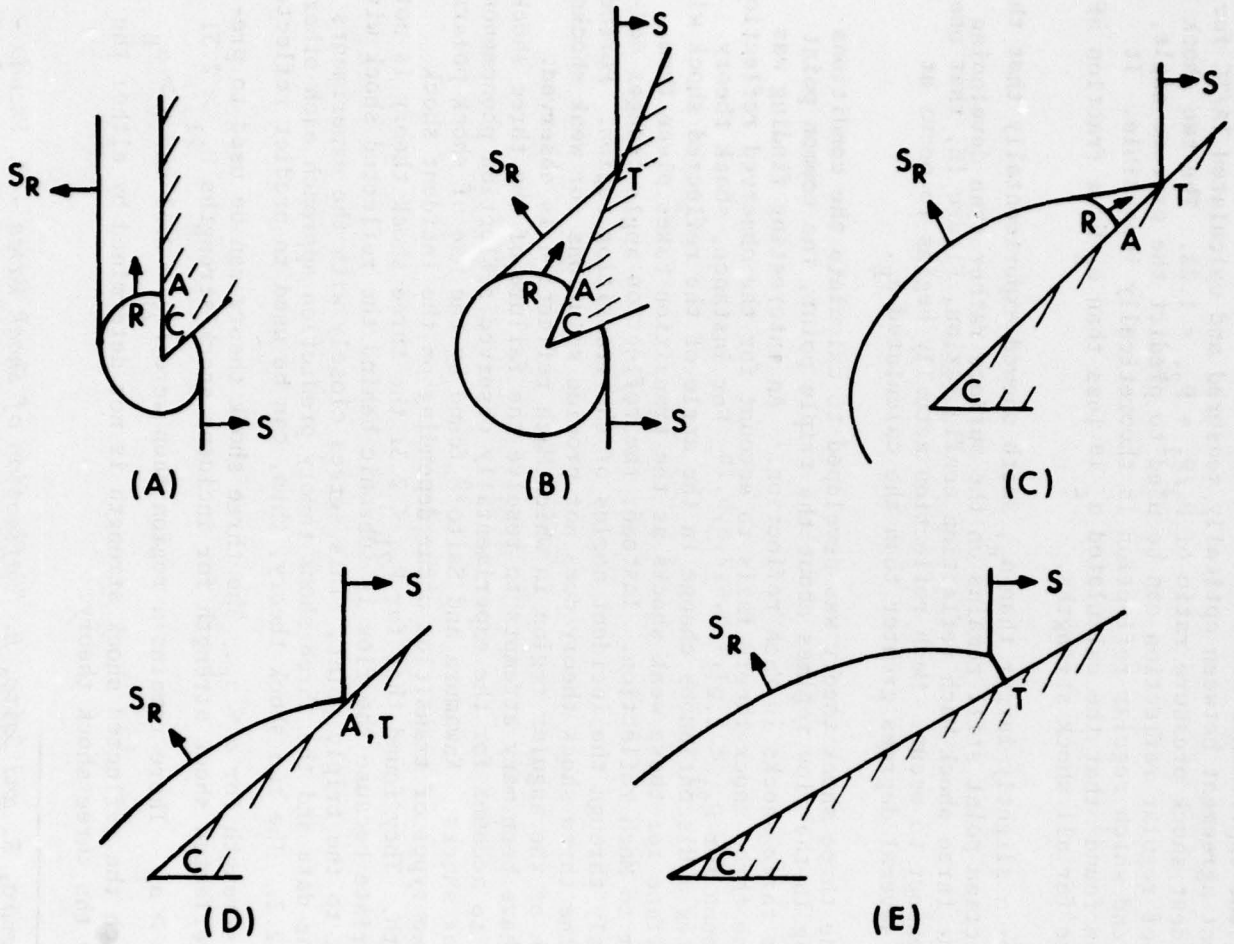

Figure 1. Reflected shock configurations.

reached at which A just keeps up with T so that TA diminishes to a point, Figure 1D. Once this occurs for weak shocks, the pressure starts decreasing immediately behind T. The ratio TA/TC can be calculated using an equation derived by L. G. Smith[3]. Plots of TA/TC versus α are shown in Figure 2 for several cases including the two levels of shock strength used in the experiments described later in this report. Smith found excellent agreement between optically measured and calculated TA/TC for an incident shock pressure ratio of $P_2/P_1 = P_{21} = 1.25$. The two shock theory of regular reflection can be used to predict the extreme angle, α_E, beyond which regular reflection is theoretically impossible. It has been found[3] that the calculated α_c is less than α_E by a fraction of a degree for all shock strengths.

For α slightly larger than α_E, Smith showed experimentally that the intersection point still remains on the surface rather than developing into the three shock Mach reflection configuration, Figure 1E, that one would expect to occur. Mach reflection actually begins to occur at angles several degrees greater than the calculated α_E.

The three shock theory was developed to calculate the conditions existing in the flow regimes about the triple point, the common point for the three shocks in Mach reflection.[1] An interesting finding was that the three shock theory fails to account for the observed reflection phenomenon for $P_{21} < 2.2$[3,4,5,6,7,8,9,10]. For instance, shock theory indicates a discontinuous change in the angle of the reflected shock with the surface for these weak shocks as the transition takes place from regular to Mach reflection. Instead, the reflection angle changes continuously through the incident angles of the transition region. Furthermore, the three shock theory does not provide solutions for weak shocks in much of the angular region in which Mach reflection is observed. There have been many attempts to resolve the failure of the three shock theory to account for the experimentally observed reflection phenomenon for weak shocks. Kawamura and Saito[10] found by the use of shock polars that two types of transition occur depending on the incident shock strength. They found that for $P_{21} < 2.31$ the three shock theory is not appropriate because the flow is subsonic behind the reflected shock with respect to the triple point. This agrees closely with the experiments which show the data and the three shock theory prediction approach each other for $P_{21} > 2.2$. The two shock theory, then, can be used to predict reflected shock strength for $\alpha \leq \alpha_E$. The three shock theory can be used to predict reflected shock strength for incident shock strengths $P_{21} > 2.31$ when $\alpha > \alpha_E$. There remains a region then were $P_{21} < 2.31$ and $\alpha > \alpha_E$ in which the reflected shock strength is not determined by either the two or the three shock theory.

---

[10] *Kawamura, R. and Saito, H. "Reflection of Shock Waves - I. Pseudo - Stationary Case." Journal of the Physical Society of Japan, Vol 11, No. 5, May 1956.*

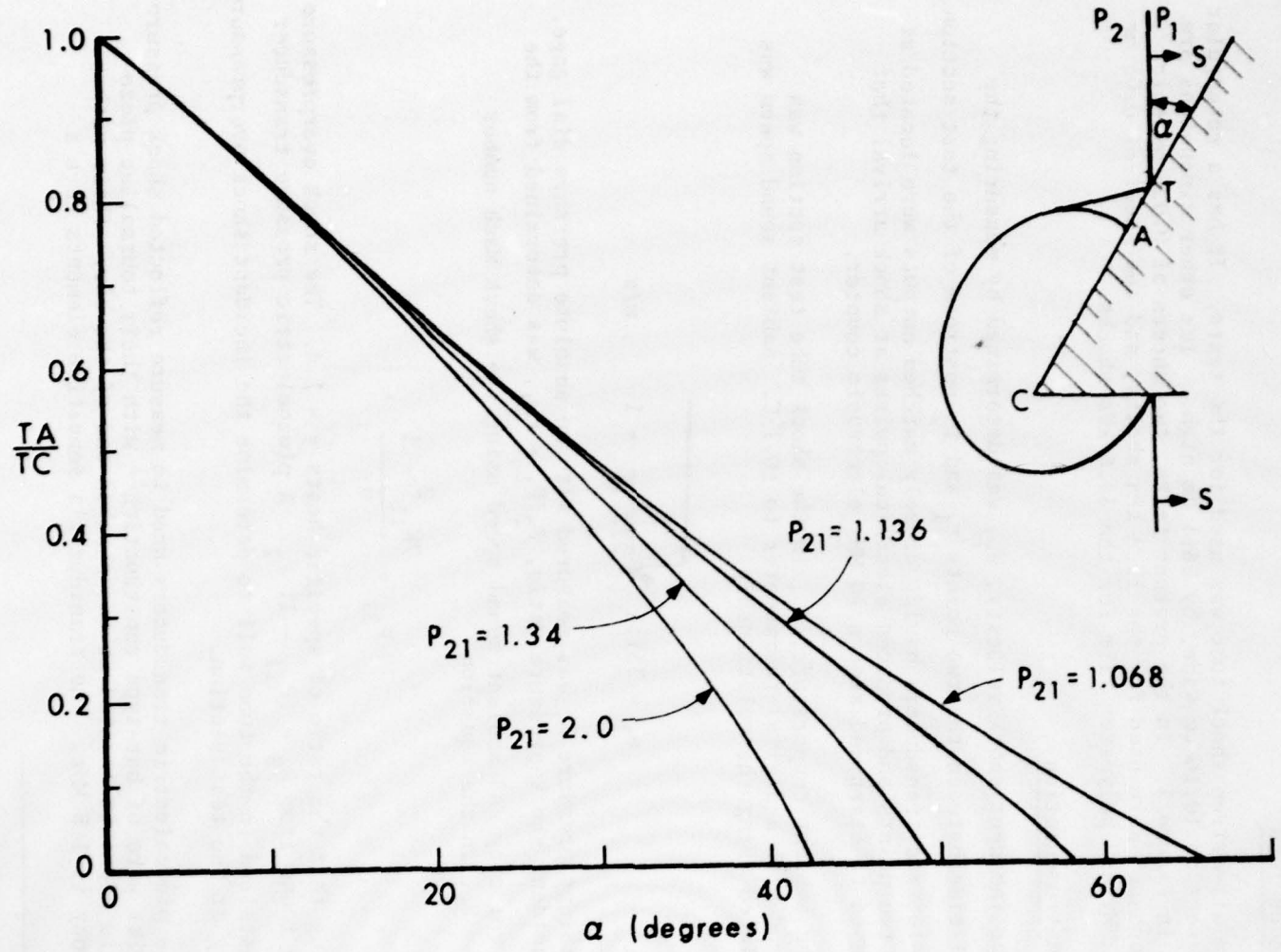

Figure 2. TA/TL for several shock strengths.

III. EXPERIMENTAL PROCEDURE

A. Shock Tube

An air-driven shock tube was used for the tests. It has a retangular cross section 10.16 cm wide, by 38.1 cm high. Its other dimensions are shown in Figure 3. In the present tests, two sheets of 0.025 mm thick "cellophane" were used for the 13.8 kPa shocks, and one sheet of 0.05 mm thick "Mylar" polyester film for the 34.5 kPa shocks.

B. Instrumentation

The incident shock velocity, W_1, was determined by measuring the travel time between the two points t_1 and t_2 upstream of the test section. Piezoelectric transducers having closely matched outputs were located at these two points and produced electrical pulses at shock arrival that were used to start and stop a 10 MHz electronic counter.

The ambient temperature, T_1, in the shock tube test section was measured with a digital thermometer to $\pm 0.1^\circ C$. Ambient sound speed was calculated using the relationship

$$a_1 = 331.4 \sqrt{\frac{T_1}{273.15} + 1} \quad , \text{m/s}$$

The ambient pressure P_1 was measured with an absolute pressure dial gage. The incident shock pressure ratio, $P_2/P_1 = P_{21}$, was determined from the shock velocity and ambient sound speed using the shock Mach number $W_1/a_1 = W_{11}$ in the equation

$$P_{21} = \frac{7W_{11}^2 - 1}{6} \quad ,$$

assuming that the ratio of specific heats $\gamma = 1.4$. The shock overpressure can be found from $P_S = (P_{21} - 1)\, P_1$. A piezoelectric pressure transducer was installed in the tube wall to determine the incident shock overpressure history at the test section.

The piezoelectric transducers used to measure reflected shock pressure histories were of bar-type construction[11] with their tourmaline piezoelectric elements located at the shocked end of the bar. Their natural frequency is 1.5 MHz. The transducer's sensitive elements have a

---

[11] *Granath, B. A. and Coulter, G. A. "Ballistic Research Laboratories Shock Tube Piezo-Electric Blast Gages." BRL T. N. 1478, August 1962.* (AD #289365)

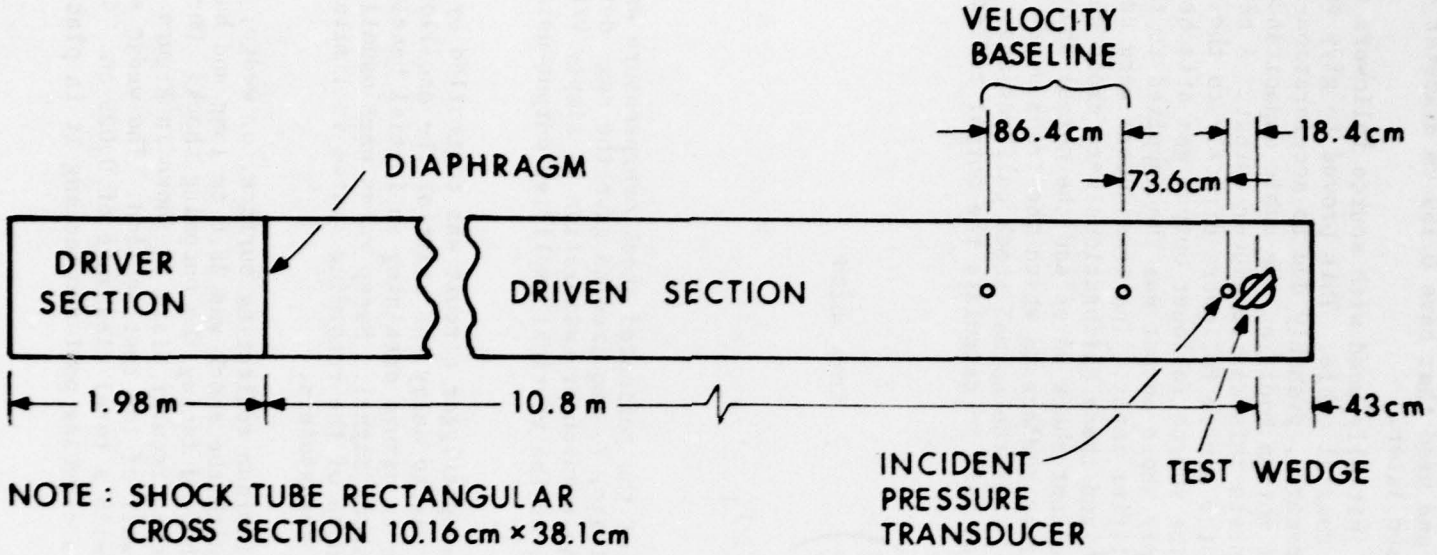

Figure 3. Shock tube experimental set up, dimensions.

0.318 cm diameter. Towards the end of the test series, two similar transducers were obtained and used that have 0.159 cm diameter elements, with results to be discussed later.

The transducers were initially used with source followers attached to them with a very short coaxial cable. This proved to give some troublesome noise on the records, probably due to acceleration-induced motion of the cable. That motion modifies the cable capacitance, and the source follower interprets this as transducer output. A better arrangement was to attach the source followers directly to the transducer output connector. The source follower output was attached to the source follower power supply whose output was then applied to the oscilloscope vertical amplifier input. The transducers were calibrated with a pulse calibrator,[11] and these calibrations were cross checked dynamically using both incident shock waves and the normal shock reflection ($\alpha = 0^{o}$) on the flat surface in which the transducers were mounted in the shock tube. For the normal shock calibrations, the incident shock strength was used to calculate the normal reflected shock strength

$$P_5/P_2 = P_{52} = \left(\frac{8 \ - P_{12}}{6 \ P_{12} \ + \ 1} \right) \quad , \quad \text{from which}$$

$$P_R = (P_{52} \ P_{21} - 1) \ P_1 \quad .$$

Each oscilloscope record of the reflected shock overpressure was then compared to the known voltage, V, required to give the same deflection on the oscilloscope so the transducer calibration is simply V/P_R. Periodic checks were made of the vertical amplifier output using known voltage inputs.

Each oscilloscope sweep trigger circuit was controlled by a delay generator whose function was to delay the start of the oscilloscope trace for a time suitable to assure obtaining an initial baseline followed by the desired shock signal. Sweep rates were usually 20 microseconds/ division. Response of the recording system is limited by the natural frequency of the transducers.

The five cm thick aluminum reflecting surface, or wedge, used to produce the interaction with the shock was 35.6 cm long and had a 30^{o} sharp edge machined on the end facing the oncoming shock. One side of this wedge was mounted on a circular plate as shown in Figure 4 that fits into a port in the wall of the test section. The wedge spanned the width of the shock tube with a total clearance of 0.025 cm. The angle α was set by rotating the circular port and locking it in place.

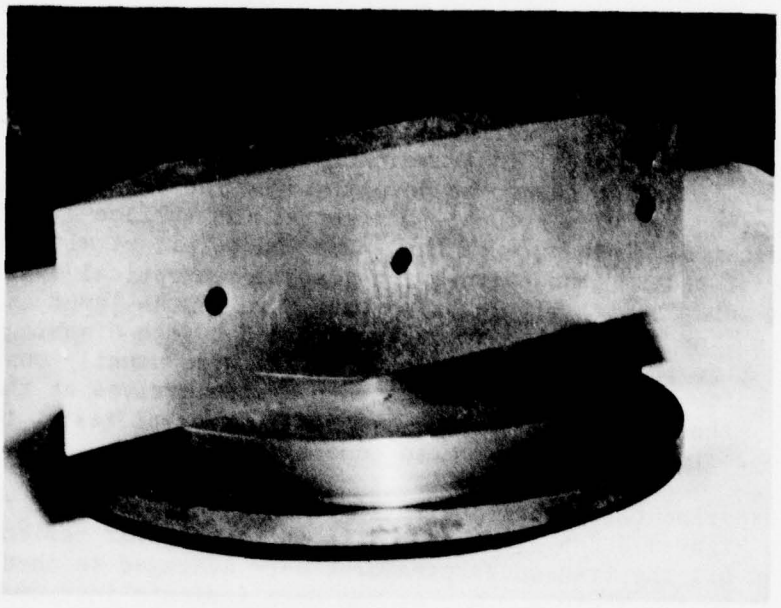

Figure 4. Test wedge.

The pressure transducers were mounted in the wedge at locations 7.62, 17.8, and 33 cm from the front edge, midway between the sides of its reflecting surface. Another instrumentation location at 33 cm was positioned 2.54 cm to one side of the center on the later stages of the tests; see Figure 4.

IV. RESULTS AND DISCUSSION

Figures A1 - A18 and B1 - B20 depict typical photographs of oscilloscope traces of pressure histories obtained during these tests. Tables I and II list the average measured shock pressures and the corresponding average measured reflected pressures at the instrumented positions for each angle. Data scatter may result from several sources: (1) variation in the incident shock strength from test to test which causes α_c to shift to higher and lower values for weaker and stronger shocks, respectively; (2) variation in α from that which is pre-set. Since there was no optical instrumentation used in the present tests, the angle of incidence has to be determined by the setting of the wedge angle. Whether the wave actually arrives at the surface with the correct α may be debated. The angle of the wedge can be preset within 1/4 degree. Past tests[12], however, using a schlieren optical system with this shock tube, showed little or no curvature of the input shock for weak shocks; and (3) transverse waves produced by the diaphragm opening characteristics in the tests mentioned in (2) were usually observed. These are quite weak by the time the wave system arrives at the test section for the weak input shocks used in the present tests, but could affect the reflection phenomena to some slight extent.

The experimentally obtained reflected pressure ratios P_R/P_S are plotted in Figures 5 & 6. Whenever α is in the regular reflection region then all the transducer pressures were averaged so that $P_R = \bar{P}_R$ for that test. Where $\alpha \geq \alpha_c$, or the data indicate instrumentation limitations to be discussed next, then the data from the smallest diameter transducer, Position 5, are used.

The transducers give fairly consistent results from shot to shot and agreement between them was good for α in the regular reflection region. At angles close to α_c the reflection phenomenon approaches a configuration in which the corner signal A is traveling very close to the point of shock interaction T with the surface. In this angular region, the physical distance between A and T, a region of constant pressure, approaches the diameter of the transducer's sensitive element. At slightly greater angles, but still in the regular reflection region, the length of this constant pressure region becomes a fraction of the element diameter so that the transducer output is an average of the

---

[12] *Bertrand, B. P. "Measurements of the Speed of a Rarefaction Wave Behind a Normally Reflected Shock Wave." BRL M.R. 1634. Jan 1965.* (AD #465397)

Table I. Experimentally Determined P_R/P_S for P_{21} = 1.136

ANGLE α, DEG	SHOT NO.	P_R/P_S POS 2	POS 3	POS 3S	POS 4	POS 5	AVERAGE
0	240	--	2.07	--	2.10	--	2.08
	241	2.14	2.11	--	2.13	--	2.13
	242	2.14	2.11	--	2.12	--	2.12
	243	2.07	2.11	--	2.12	--	2.10
	273	2.11	2.09	--	2.06	--	2.09
	274	--	2.06	--	2.12	--	2.09
	275	--	2.06	--	2.10	--	2.08
	282	2.10	2.10	--	2.10	--	2.10
	433	2.12	--	2.13	2.08	2.10	2.11
	434	2.06	--	2.08	2.13	2.13	2.10
	435	2.11	--	2.10	2.10	2.15	2.12
	493	2.10	--	2.08	2.09	2.08	2.09
	494	2.12	--	2.11	2.09	2.07	2.10
	495	2.13	--	2.14	2.10	2.09	2.12
	AVG	2.11	2.09	2.11	2.10	2.10	2.10
10	436	2.07	--	2.10	--	2.11	2.09
	437	2.04	--	2.09	2.16	2.10	2.10
	438	2.02	--	2.09	2.16	2.12	2.10
	439	2.01	--	2.07	2.13	2.11	2.08
	AVG	2.04	--	2.09	2.15	2.11	2.09
20	440	2.10	--	2.09	2.10	--	2.10
	441	2.10	--	2.10	2.13	2.12	2.11
	442	2.11	--	2.11	2.13	2.10	2.11
	AVG	2.10	--	2.10	2.12	2.11	2.11
30	443	2.12	--	2.12	2.15	2.13	2.13
	444	2.10	--	2.10	2.11	2.10	2.10
	445	2.12	--	--	2.11	2.10	2.11
	AVG	2.12	--	2.11	2.12	2.11	2.11

Table I. Experimentally Determined P_R/P_S for P_{21} = 1.136 (cont.)

ANGLE α, DEG	SHOT NO.	P_R/P_S POS 2	POS 3	POS 3S	POS 4	POS 5	AVERAGE
39½	401	--	--	--	2.10	2.14	2.12
	402	2.10	--	--	2.10	2.14	2.11
	403	2.08	--	--	2.12	2.17	2.12
	404	2.08	--	--	2.13	2.14	2.12
	AVG	2.08	--	--	2.11	2.15	2.12
40	252	2.09	2.15	--	2.11	--	2.12
	446	--	--	2.15	2.12	2.10	2.12
	447	2.13	--	2.11	2.10	2.08	2.11
	448	2.12	--	2.10	2.10	2.11	2.11
	AVG	2.11	2.15	2.12	2.11	2.10	2.12
45	449	2.09	--	2.12	2.17	2.13	2.13
	450	2.11	--	2.10	2.15	2.12	2.12
	451	2.12	--	2.13	2.18	2.15	2.15
	AVG	2.11	--	2.12	2.17	2.13	2.13
50	251	2.17	2.23	--	2.17	--	2.19
	452	2.14	--	2.19	2.19	2.16	2.17
	453	2.17	--	2.22	2.20	2.19	2.20
	454	2.15	--	2.18	2.20	2.18	2.18
	AVG	2.16	2.23	2.20	2.19	2.18	2.19
55	455	2.28	--	2.34	2.30	2.33	2.31
	456	2.27	--	2.32	2.31	2.31	2.30
	457	2.26	--	2.29	2.31	2.30	2.29
	AVG	2.27	--	2.32	2.31	2.31	2.30
57½	458	2.32	--	2.46	2.42	2.45	--
	459	2.36	--	2.48	--	--	--
	460	2.36	--	2.48	2.49	2.53	--
	461	2.34	--	2.45	2.44	2.49	--
	AVG	2.35	--	2.47	2.45	2.49	--

Table I. Experimentally Determined P_R/P_S for P_{21} = 1.136 (Cont.)

ANGLE α, DEG	SHOT NO.	P_R/P_S POS 2	POS 3	POS 3S	POS 4	POS 5
58 3/4	245	2.32	2.58	--	2.63	--
	412	2.33	--	--	2.58	2.62
	509	2.33	--	2.56	2.55	2.56
	AVG	2.33	2.58	2.56	2.59	2.59
60	246	2.33	2.66	--	2.81	--
	250	2.37	2.68	--	2.75	--
	405	2.35	--	--	2.66	2.73
	406	2.27	--	--	2.68	2.79
	462	2.40	--	2.78	2.82	2.93
	463	2.40	--	2.76	2.83	2.92
	464	2.39	--	--	2.77	2.87
	465	2.40	--	2.72	2.79	--
	466	2.39	--	2.74	2.81	2.88
	508	2.37	--	2.70	2.73	2.76
	AVG	2.37	2.67	2.74	2.77	2.84
61¼	413	2.30	--	--	2.81	3.02
	414	2.30	--	--	2.82	3.02
	415	2.29	--	--	2.85	3.03
	467	2.33	--	2.90	--	--
	468	2.39	--	2.91	--	--
	471	2.36	--	2.85	2.92	3.07
	472	2.40	--	2.86	2.91	3.01
	473	2.38	--	2.89	2.94	3.05
	475	2.36	--	2.92	2.92	3.06
	510	2.33	--	2.81	2.81	2.88
	AVG	2.34	--	2.88	2.87	3.02
62½	244	2.29	2.69	--	2.93	--
	253	2.31	--	--	3.05	--
	254	2.32	2.62	--	2.97	--
	260	--	2.71	--	2.94	--
	261	--	2.73	--	2.99	--
	262	--	2.69	--	2.91	--
	263	2.40	2.76	--	2.98	--
	264	2.40	2.70	--	2.96	--
	283	2.29	2.68	--	2.93	--
	286	2.35	2.67	--	2.92	--
	287	2.27	2.65	--	2.86	--

Table I. Experimentally Determined P_R/P_S for P_{21} = 1.136 (Cont.)

ANGLE α, DEG	SHOT NO.	P_R/P_S POS 2	POS 3	POS 3S	POS 4	POS 5
62½ (cont)	407	2.30	--	--	2.90	3.11
	408	2.37	--	--	2.90	3.12
	476	2.37	--	2.74	2.95	3.12
	477	2.34	--	2.91	2.94	3.12
	478	2.38	--	2.97	2.97	3.15
	479	--	--	2.89	2.92	3.13
	502	2.23	--	2.81	2.83	3.02
	AVG	2.33	2.69	2.86	2.94	3.11
63 3/4	416	2.25	--	--	2.87	3.06
	417	2.33	--	--	2.88	3.05
	480	2.28	2.93	--	2.83	2.98
	481	2.28	2.90	--	2.87	3.05
	482	2.30	2.90	--	2.90	--
	483	2.28	2.94	--	2.89	3.04
	AVG	2.29	2.92	--	2.87	3.04
65	247	2.16	2.54	--	2.75	--
	248	2.20	2.60	--	2.77	--
	255	2.28	2.60	--	2.82	--
	418	2.27	--	--	2.77	2.98
	419	2.18	--	--	2.74	2.93
	484	2.20	--	2.79	2.79	2.92
	485	2.20	--	2.76	2.77	2.95
	486	2.23	--	2.81	2.87	3.01
	503	2.14	--	2.71	2.70	2.87
	AVG	2.21	2.58	2.77	2.78	2.94
67½	257	2.07	--	--	2.62	--
	487	2.05	--	2.66	2.58	2.70
	488	2.17	--	2.78	2.69	2.81
	489	2.12	--	--	2.60	2.73
	504	2.03	--	2.48	2.52	2.65
	AVG	2.09	--	2.64	2.60	2.72

Table I. Experimentally Determined P_R/P_S for P_{21} = 1.136 (Cont.)

ANGLE α, DEG	SHOT NO.	P_R/P_S POS 2	POS 3	POS 3S	POS 4	POS 5
70	249	1.91	2.21	--	2.30	--
	256	1.95	--	--	2.42	--
	420	1.90	--	--	2.28	2.39
	421	1.87	--	--	2.29	2.38
	AVG	1.91	2.21	--	2.32	2.39
72½	506	1.78	--	2.11	2.12	2.20
	507	1.76	--	2.06	2.08	2.18
	AVG	1.77	--	2.09	2.10	2.19
75	490	1.56	--	--	1.91	1.90
	491	1.64	--	2.01	1.95	1.97
	492	1.61	--	2.02	1.92	1.93
	AVG	1.60	--	2.02	1.93	1.93
90	277	1.03	1.04	--	1.02	--
	278	1.03	1.03	--	1.03	--
	279	1.00	1.04	--	1.04	--
	AVG	1.02	1.04	--	1.03	--

Table II. Experimentally Determined P_R/P_S for P_{21} = 1.34

ANGLE α, DEG	SHOT NO.	P_R/P_S POS 2	POS 3	POS 3S	POS 4	POS 5	AVERAGE
0	288	2.28	2.24	--	2.29	--	2.27
	289	--	2.27	--	2.24	--	2.26
	290	2.29	2.27	--	2.30	--	2.29
	291	2.26	2.26	--	2.31	--	2.28
	292	2.28	2.22	--	2.35	--	2.28
	301	2.37	2.26	--	2.26	--	2.30
	302	--	2.25	--	2.27	--	2.26
	303	2.38	2.26	--	2.26	--	2.30
	363	2.36	--	--	2.29	2.23	2.29
	372	2.34	--	--	2.24	2.22	2.27
	AVG	2.32	2.25	--	2.28	2.23	2.27
5	373	2.31	--	--	2.24	2.24	2.25
10	304	2.30	2.25	--	--	--	2.27
	305	2.25	2.27	--	--	--	2.26
	306	2.25	2.23	--	2.33	--	2.24
	374	2.25	--	--	--	2.23	2.24
	AVG	2.26	2.25	--	2.33	2.23	2.25
20	307	2.35	2.23	--	2.22	--	2.23
	308	2.31	2.24	--	2.26	--	2.27
	309	2.40	2.25	--	2.19	--	2.28
	AVG	2.35	2.24	--	2.22	--	2.28
30	310	2.37	2.22	--	2.24	--	2.28
	311	2.24	2.24	--	2.26	--	2.24
	312	2.21	2.21	--	2.23	--	2.21
	AVG	2.21	2.21	--	2.24	--	2.24
39¼	390	--	--	--	2.28	2.30	2.29
	391	2.26	--	--	2.28	2.26	2.26
	392	2.26	--	--	2.28	2.32	2.29
	393	2.26	--	--	2.28	2.28	2.28
	AVG	2.26	--	--	2.28	2.29	2.28

Table II. Experimentally Determined P_R/P_S for P_{21} = 1.34 (Cont.)

ANGLE α, DEG	SHOT NO.	P_R/P_S POS 2	POS 3	POS 3S	POS 4	POS 5	AVERAGE
40	313	2.32	--	--	--	--	2.32
	314	2.30	2.30	--	2.26	--	2.29
	315	2.25	2.29	--	2.23	--	2.26
	AVG	2.29	2.29	--	2.25	--	2.28
45	316	2.36	2.39	--	2.36	--	2.37
	317	2.33	2.38	--	2.33	--	2.35
	318	2.37	2.39	--	2.33	--	2.36
	AVG	2.35	2.39	--	2.34	--	2.36
47½	319	2.49	2.47	--	2.47	--	2.47
	320	2.43	2.43	--	2.41	--	2.42
	321	2.50	2.56	--	2.48	--	2.51
	377	2.42	--	--	2.46	2.44	2.44
	378	2.42	--	--	2.44	2.46	2.44
	511	--	--	2.46	2.46	2.44	2.45
	512	2.44	--	2.44	2.42	2.40	2.42
50	322	2.60	2.67	--	--	--	--
	323	2.53	2.63	--	2.59	--	--
	324	2.63	2.67	--	2.69	--	--
	379	2.55	--	--	2.72	2.71	--
	380	2.56	--	--	2.74	2.72	--
	381	2.57	--	--	2.73	2.71	--
	513	2.69	--	2.73	2.81	2.79	--
	AVG	2.59	2.66	2.73	2.71	2.73	--
51⅓	333	2.68	2.79	--	2.87	--	--
	334	2.57	2.82	--	2.89	--	--
	335	2.56	2.81	--	2.85	--	--
	382	2.65	--	--	2.98	3.06	--
	383	2.61	--	--	2.92	2.98	--
	384	--	--	--	2.91	2.95	--
	514	2.63	--	2.93	3.03	3.10	--
	AVG	2.62	2.81	2.93	2.92	3.02	--

Table II. Experimentally Determined P_R/P_S for P_{21} = 1.34 (Cont.)

ANGLE α, DEG	SHOT NO.	P_R/P_S POS 2	POS 3	POS 3S	POS 4	POS 5	AVERAGE
52½	325	2.64	2.87	--	3.05	--	--
	326	2.64	2.89	--	3.05	--	--
	327	2.67	2.88	--	3.03	--	--
	328	2.75	--	--	--	--	--
	329	--	2.95	--	3.10	--	--
	330	2.69	2.88	--	3.06	--	--
	331	2.74	2.93	--	3.09	--	--
	332	2.73	2.92	--	3.09	--	--
	366	--	--	--	3.11	3.15	--
	367	2.57	--	--	3.07	3.11	--
	368	2.65	--	--	3.11	3.21	--
	375	2.58	--	--	3.06	3.13	--
	376	2.62	--	--	3.05	3.13	--
	515	2.63	--	3.00	3.02	3.02	--
	AVG	2.66	2.90	3.00	3.07	3.15	--
53 3/4	336	2.57	2.87	--	3.01	--	--
	337	2.51	2.85	--	2.98	--	--
	338	2.55	2.85	--	3.03	--	--
	398	2.58	--	--	2.99	3.15	--
	399	2.58	--	--	3.10	3.24	--
	516	2.64	--	3.01	3.07	3.18	--
	AVG	2.57	2.85	3.01	3.03	3.19	--
55	339	2.55	2.84	--	2.99	--	--
	340	2.57	2.84	--	2.99	--	--
	341	2.53	2.85	--	2.98	--	--
	385	2.55	--	--	2.98	3.10	--
	386	2.55	--	--	2.96	3.08	--
	387	2.52	--	--	2.98	3.10	--
	517	2.58	--	2.93	2.99	3.09	--
	AVG	2.55	2.84	2.93	2.98	3.09	--
56¼	342	2.52	2.76	--	2.93	--	--
	343	2.49	2.76	--	2.93	--	--
	344	2.48	2.75	--	2.90	--	--
	AVG	2.50	2.76	--	2.90	--	--

Table II. Experimentally Determined P_R/P_S for P_{21} = 1.34 (Cont.)

ANGLE α, DEG	SHOT NO.	P_R/P_S POS 2	POS 3	POS 3S	POS 4	POS 5
57½	345	2.42	2.64	--	2.77	--
	346	--	2.71	--	2.83	--
	347	2.41	2.66	--	2.81	--
	394	2.40	--	--	2.81	2.90
	395	2.41	--	--	2.80	2.90
	396	2.35	--	--	2.76	2.87
	518	2.42	--	2.77	2.81	2.88
	AVG	2.40	2.67	2.77	2.80	2.89
60	348	2.29	2.50	--	2.64	--
	349	2.29	2.50	--	2.60	--
	350	2.30	2.51	--	2.65	--
	370	--	--	--	2.63	--
	388	2.30	--	--	2.58	2.64
	389	2.28	--	--	2.58	2.68
	519	2.29	--	2.55	2.61	2.68
	AVG	2.29	2.50	2.55	2.61	2.67
65	351	1.97	--	--	2.18	--
	352	1.97	2.13	--	2.20	--
	353	1.98	2.11	--	2.23	--
	AVG	1.97	2.12	--	2.20	--
70	354	1.72	1.80	--	1.88	--
	355	1.69	1.81	--	1.87	--
	356	1.72	1.80	--	1.89	--
	520	1.73	--	1.87	1.87	1.87
	AVG	1.72	1.80	1.87	1.88	1.87
80	357	1.32	1.34	--	1.38	--
	358	1.30	1.34	--	--	--
	359	1.31	1.34	--	1.36	--
	AVG	1.31	1.34	--	1.37	--
90	366	1.02	1.02	--	1.04	--
	361	1.01	1.01	--	1.02	--
	AVG	1.01	1.02	--	1.03	--

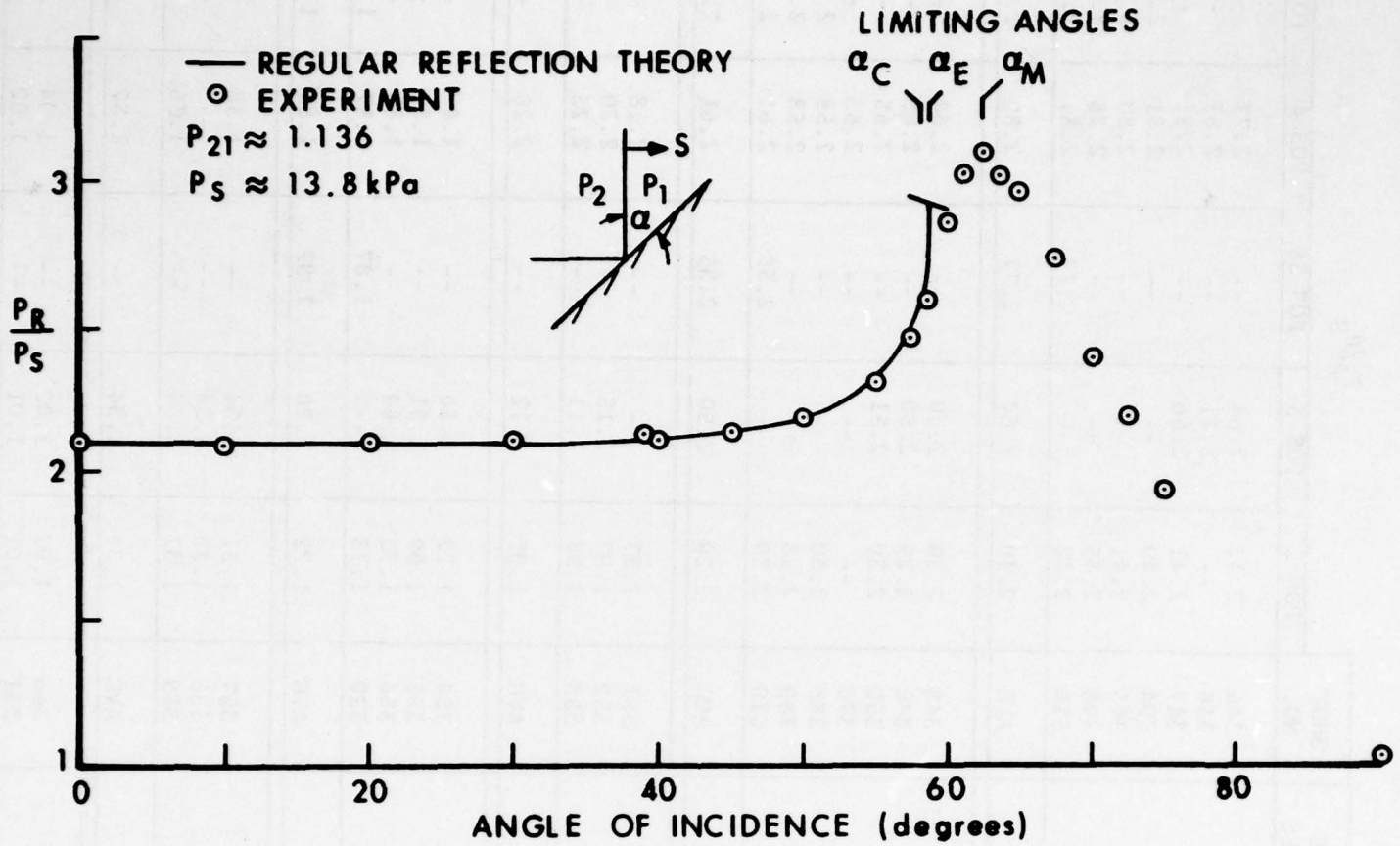

Figure 5. Experimentally determined reflection factors, $P_{21} = 1.136$.

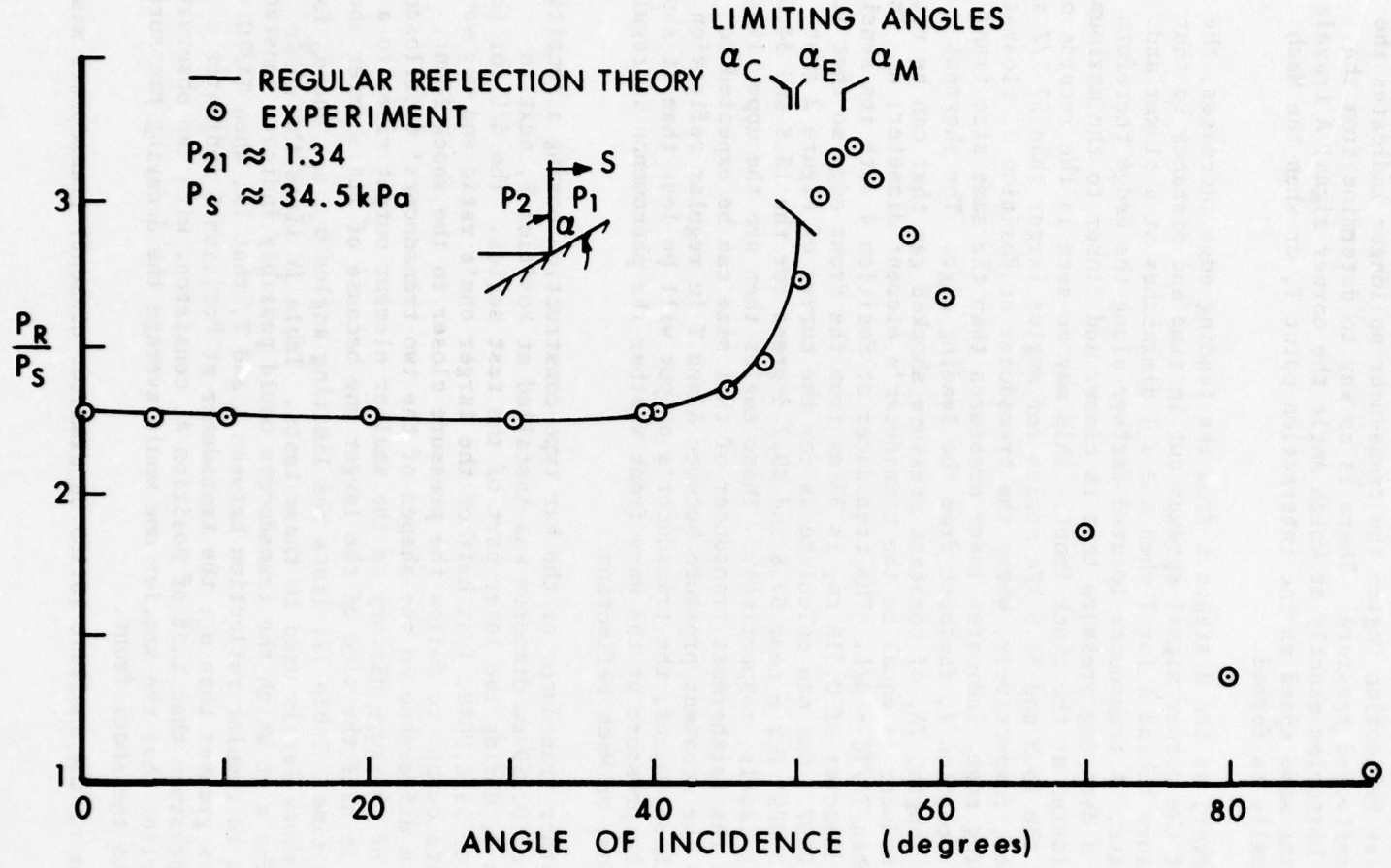

Figure 6. Experimentally determined reflection factors, $P_{21} = 1.34$.

correct regular reflection value existing between A and T, and the decaying pressure following A. At these angles and at angles beyond the regular reflection region the transducer no longer indicates the maximum reflected pressure. There is no way to determine from the pressure histories exactly at which angle the corner signal A travels just at the same speed as the interaction point T, or when the Mach stem actually is formed.

However, as the distance L from the leading edge increases, the effect of the corner signal spreads out in time and distance so that the pressure behind A (or T when $\alpha > \alpha_c$) diminishes at a slower and slower rate. A transducer located farther along the wedge therefore averages a decaying pressure that is closer and closer to the maximum value existing at the shock front. This may be seen in the records of data for the 13.8 and 34.5 kPa series for angles larger than 57 1/2 and 50 degrees, respectively, where the transducer at Position 2, closest to the leading edge, indicates lower pressures than the same size transducer at Position 4, farthest from the leading edge. The shortest possible length, TA, of constant pressure shocked gas that can be resolved by a transducer is equal to the transducer's element diameter, d. This occurs when TA/TC = d/L. The transducer at Position 4 with its sensitive element diameter of 0.318 cm, is 33 cm from the front edge so that its d/L = 0.0097. One can calculate as for the curves of Figure 2 that TA/TC = 0.0097 for α near 57.8 and 49.2 degrees for the 13.8 and 34.5 kPa shock levels, respectively. These angles then are the upper limits at which the farthermost transducer of that size can be expected to indicate the constant pressure between A and T in regular reflection. Beyond these angles, the transducer's output will be less than it should be for the pressure at the wave front whether the phenomenon is regular, transition, or Mach reflection.

Another transducer of the bar type construction having a sensitive element of 0.159 cm diameter was installed at Position 5, next to Position 4, during the later part of the test series. The d/L for this transducer is 0.0048, just half of the larger one's ratio and one would expect its output to follow the pressure closer to the shock front. We can see a difference in the shapes of the two transducers' oscilloscope records of pressure history as the smaller element output rises to a maximum in half the time of the larger one because of its shorter shock crossing time. Table III lists the limiting angles α_c, α_E, and α_M for the two shock levels used in these tests. Table IV lists the upper limits for α at which the transducers could possibly indicate constant pressure in regular reflection between A and T, that is, when TA/TC = d/L. At angles greater than α_c, the transducer at Position 5 indicates a higher pressure than that of Position 4, consistent with the observation made earlier that the smaller one would average the decaying pressure closer to the shock front.

One of the smallest (0.159 cm diameter element) transducers was also

Table III. Limiting Angles for Shock Reflection

Shock Overpressure, kPa	13.8	34.5
α_c, deg	58.2	49.4
α_E, deg	58.77	49.9
α_M, deg	62.5	53.0

Table IV. Upper Angular Limits for Accurate Transducer Response in Regular Reflection

TRANSDUCER				α, DEG, FOR TA/TC = d/L	
DIAMETER, d, cm	POS	L,cm	d/L	P_S = 13.8 Kpa	P_s = 34.5 kPa
0.159	5	33	0.0048	58.0	49.3
0.159	3S	17.7	0.009	57.9	49.2
0.318	4	33	0.0096	57.8	49.17
0.318	3	17.7	0.018	57.5	48.9
0.318	2	7.62	0.042	56.1	48.2

installed at Position 3 in place of the larger one during the final part of the series. At that position its d/L is 0.009, close to the d/L of the larger tranducer at Position 4, and both indicate pressures very close to the same values at angles beyond where TA/TC = d/L as one might expect. The lowest angles α_M at which Smith[3] observed Mach reflection in his tests are plotted on Figure 7 along with curves of α_c and α_E. By fairing a smooth curve through his data, we see that for the present tests there is a transition of several degrees between α_c and α_M. The reason for this angular delay in the onset of Mach reflection beyond α_c for weak shocks was discussed in Section II.

In view of the problem of measuring the peak pressure of a decaying wave with a finite diameter transducer, the question arises, "How do we know what the maximum pressure is at the shock front?" If all we had to work with were the pressure transducers, the answer would be at best uncertain. However, Smith's work[3] was principally with spark shadowgraphs of the entire shock reflection phenomenon. From those photographs he was able to observe when Mach reflection started and to calculate the speed of the foot of the Mach stem from which its shock strength was determined. Parts of the curves of P_R/P_S versus α presented in the original "Effects of Atomic Weapons"[5] were generated using this data. His data indicate maximum P_R/P_S near 3.4, 3.6 and 3.5 for shock pressure levels of 11.3, 25.3, and 43.4 kPa, respectively, at α_M. These are higher than those measured in the present tests in the same pressure range using pressure transducers where the average is closer to 3.1 and 3.2 for the 13.8 and 34.5 kPa series, respectively. Using the same idea, several tests were run in the present effort at different α's at both shock levels in which the velocity W_T of T along the slope between transducer Positions 2 and 4 was measured using the transducer outputs to trigger the start and stop circuits of a 10 mHz counter. The pressures at Positions 2, 3, 4 & 5 were also measured. The velocity of T was used, assuming Mach reflection, to calculate the pressure behind the foot of the Mach stem. This velocity-determined shock pressure could then be compared with the values measured with the transducers. The actual pressure of course cannot be calculated using the velocity of T along the wedge except where it is known for certain that Mach reflection is occuring. Smith's data, Figure 7, indicates that this would occur for $\alpha \geq 62.5$ and 53.0 degrees for the 13.8 and 34.5 kPa series respectively. The pressure ratios determined from the velocity measurements are shown on Figures 8 & 9 along with the values measured with pressure transducers. The measured values are those obtained at Position 5 which has the smallest transducer. It is farthest from the leading edge and should give the best approximation to the peak pressure behind the shock front. If the transducers were capable of following the pressure of the foot of the Mach stem (point T) the two curves in Figures 8 & 9 would agree for $\alpha \geq \alpha_M$. In fact, the measured pressures are lower in that angular region because of the finite size of the transducer but the curves do approach each other with increasing α.

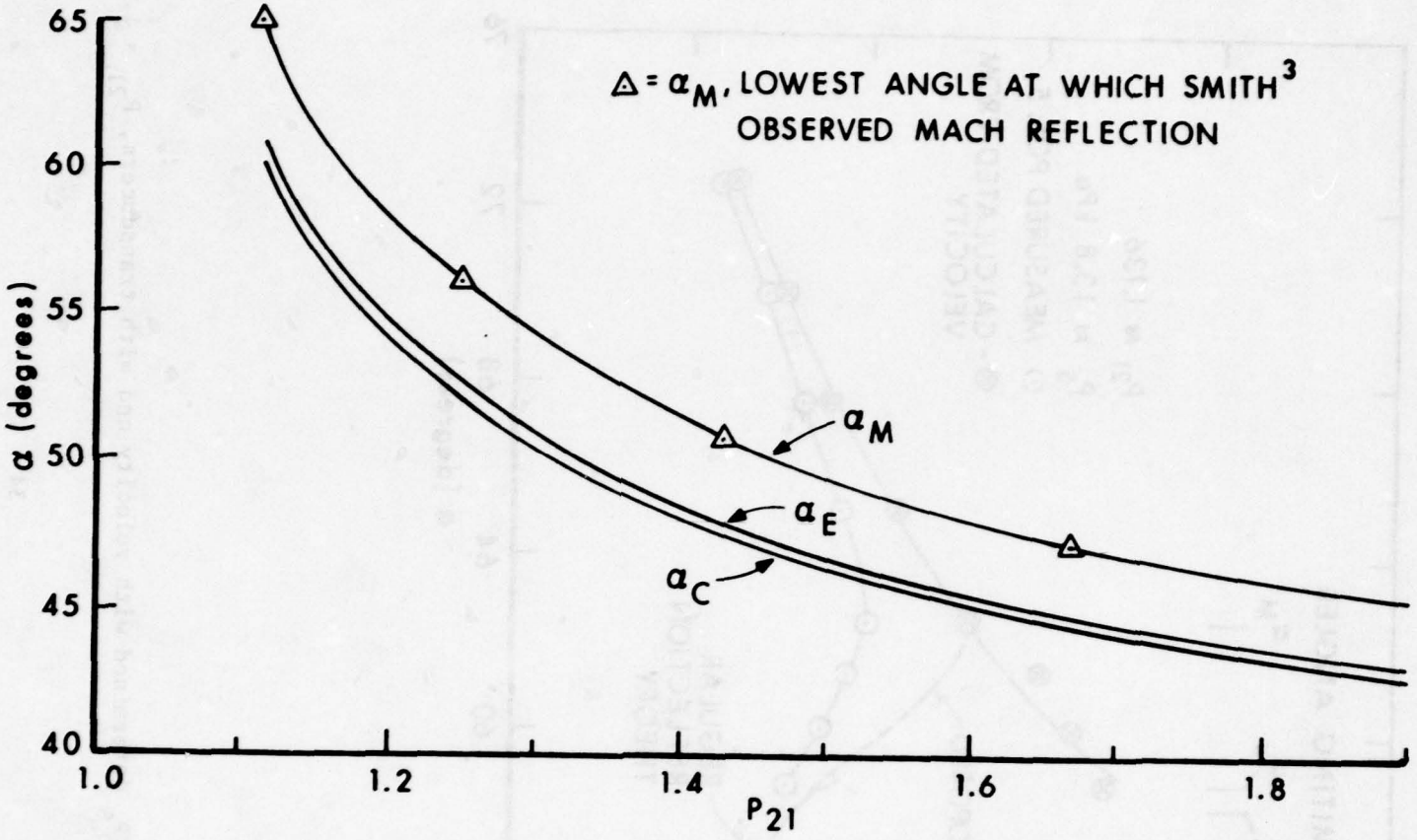

Figure 7. Limiting angles in shock reflection.

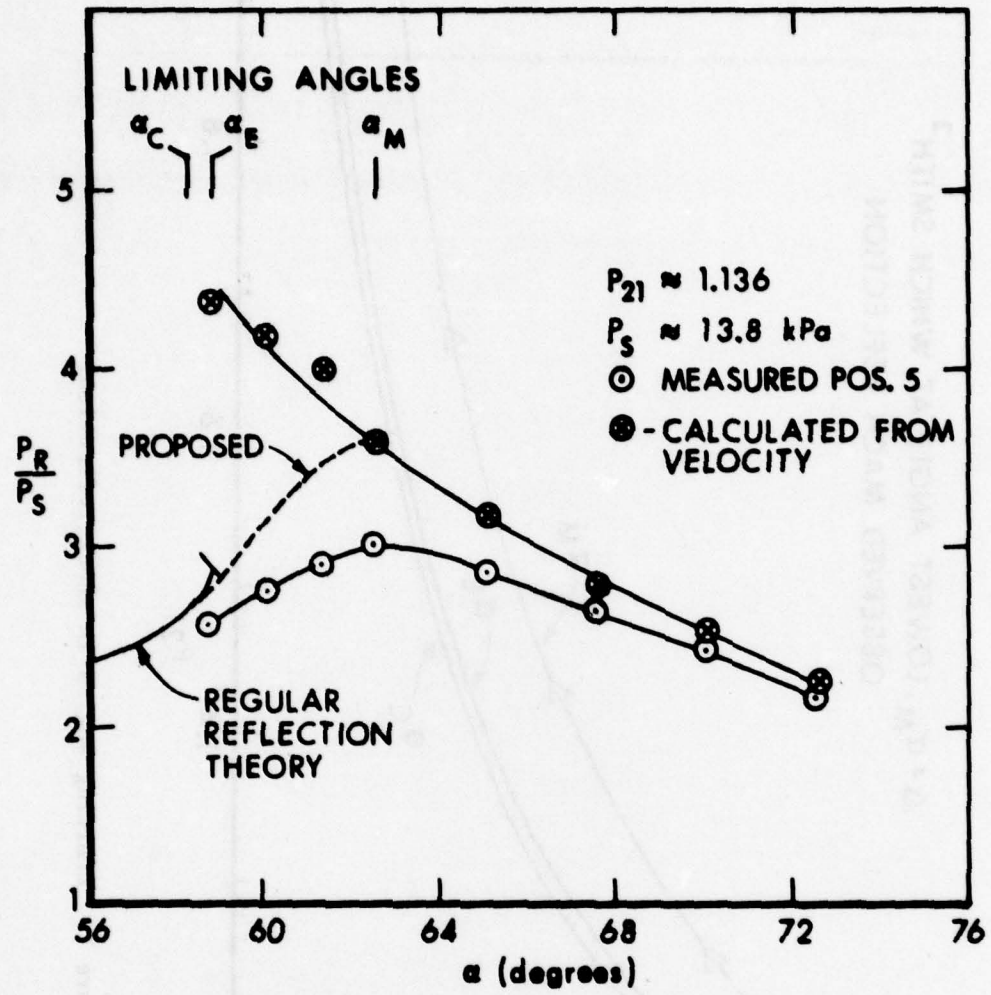

Figure 8. P_R/P_S determined with velocity and with transducers, P_{21} = 1.136.

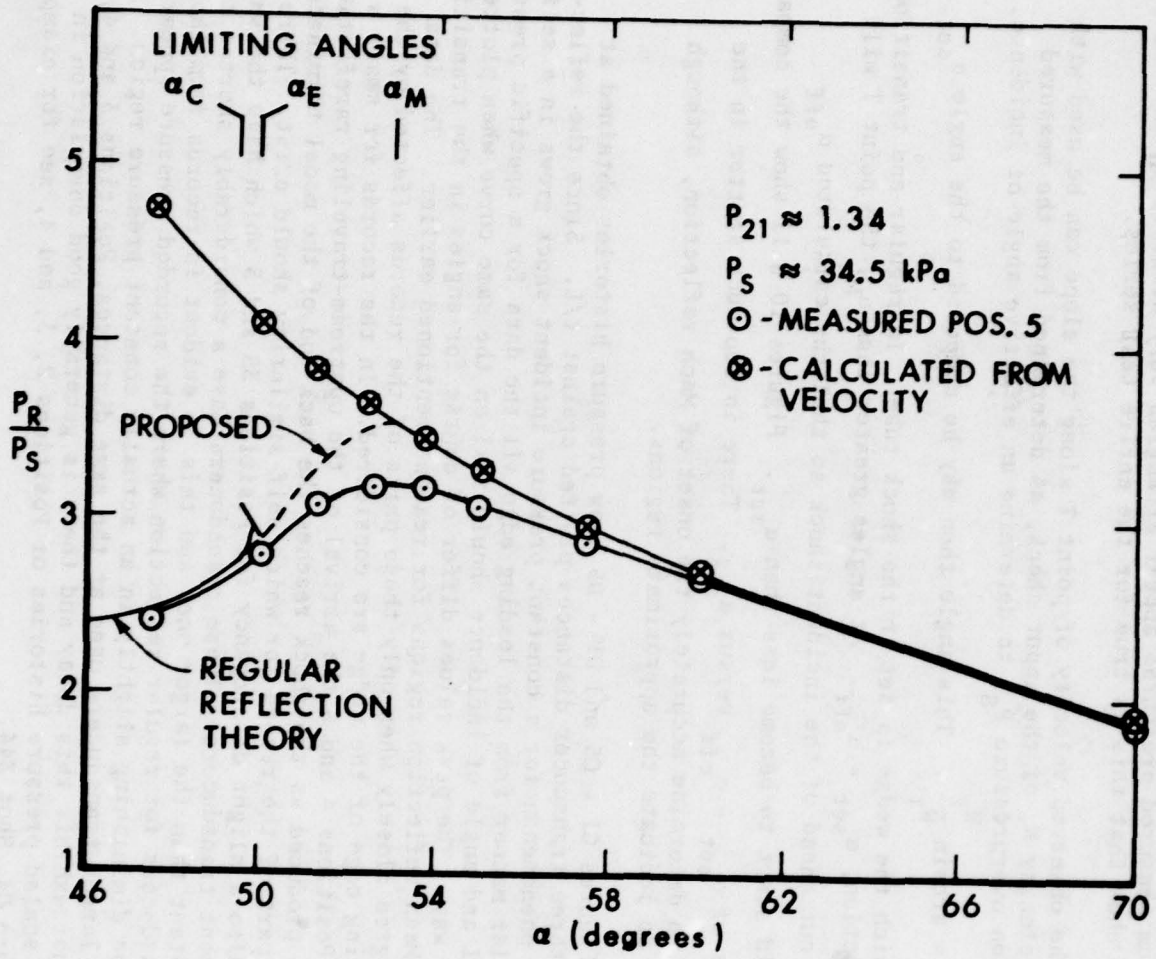

Figure 9. P_R/P_S determined with velocity and with transducers, $P_{21} = 1.34$.

The proposed curves on Figures 8 & 9 of the pressure ratio in the transition region between regular and Mach reflection start at the regular reflection-predicted value of α_c, terminate with the velocity-determined value at α_M and increase smoothly in the interval. The maximum measured pressures appear at angles very close to α_M and Figures 5 & 6 show that this is true for the entire test series.

The observed velocity of point T along the slope can be used with the velocity W_1 of the input shock, as determined from the measured side-on overpressure P_S, to determine an effective angle of incidence, $\alpha_{eff} = \arcsin \frac{W_1}{W_T}$. This angle then may be compared to the angle α_{set} at which the wedge is set in the shock tube. In regular and transition reflection, $\alpha_{set} = \alpha_{eff}$. At angles greater than α_M, the point T will pull out ahead of the incident shock so that the calculated α_{eff} should start to become less than α_{set}. Figures 10 & 11 show the comparisons of $\alpha_{set} - \alpha_{eff}$ versus α_{set}. There is too much scatter in the data to determine accurately the onset of Mach reflection, although they do indicate the approximate regions.

Figures C1 - C5 and D1 - D5 show pressure histories obtained at the three transducer distances plotted against t/L. Since the reflection phenomenon for a constant pressure incident shock grows in a self-similar manner from the leading edge all the data for a specific pressure level and angle of incidence should fall on the same curve when plotted this way. The peak values differ of course for angles in the transition and Mach reflection regions for reasons mentioned earlier. The data do agree closely when only those parts of the records affected by the leading edge of the wedge are considered. In the records for small α for Positions 4 and 5 the arrival of the upstream-traveling rarefaction wave produced as the shock reaches the back end of the model terminates the part of the record for which self-similarity should exist. There is also a slight discrepancy for Positions 3S and 5 which have the smaller element transducers. These transducers have a considerably shorter time constant than the larger ones and this is evident in records from those transducers for regular reflection where the recorded pressure appears to be diminishing slightly in an actually constant pressure region. The larger transducers used at the same distances, Positions 3 and 4, do not exhibit this decay and there is generally good correlation in the scaled pressure histories of Positions 2, 3, and 4, see for example Figure D4, Shot 344.

Figures 12 through 15 depict corrected curves of pressure history at Position 2 plotted against t/L for several angles of incidence. The experimental data have been normalized to their respective input shock pressures. Here the values of P_R/P_S at t/L = 0 are the average measured values for regular reflection and the velocity-determined values for Mach reflection. The values in the transition region are

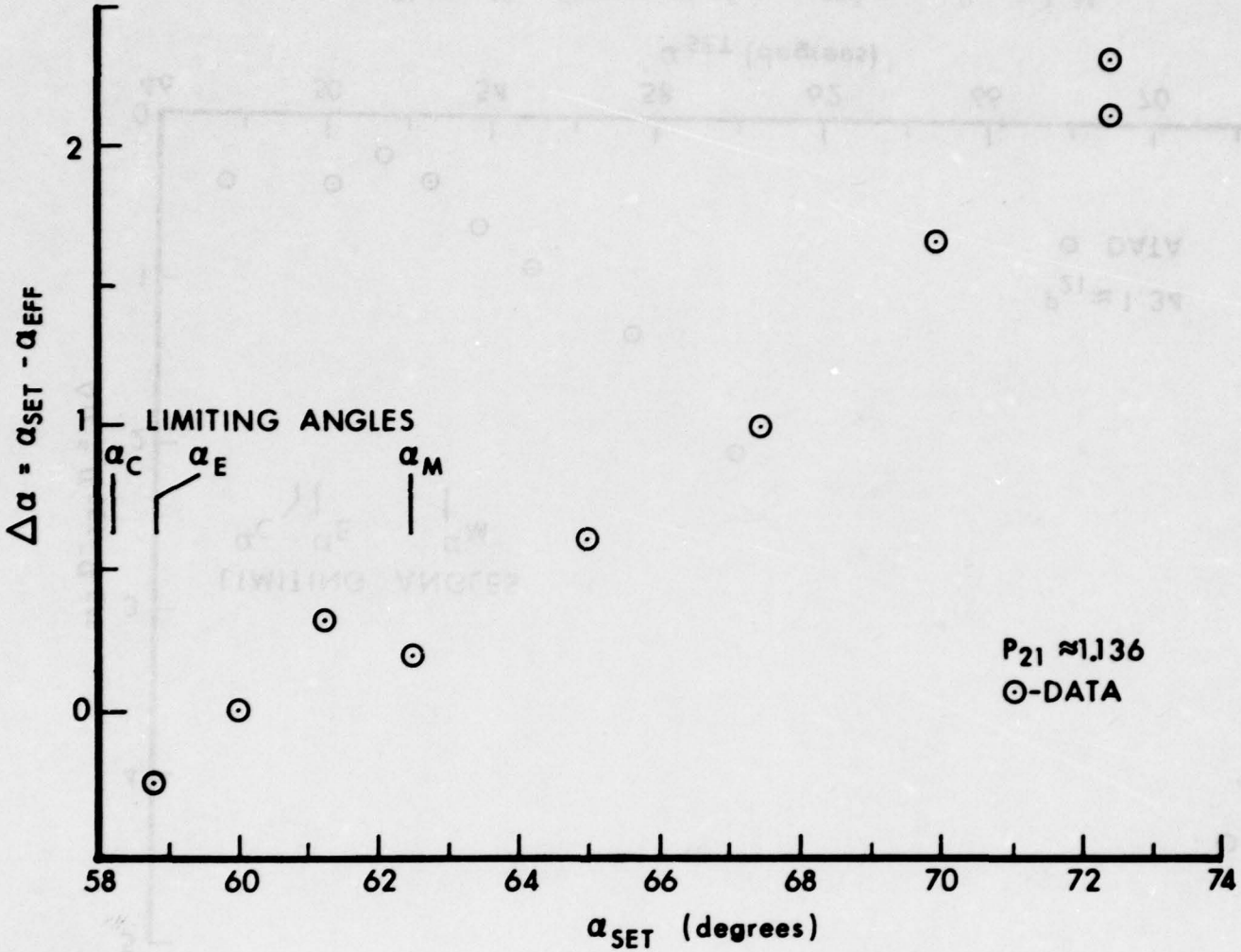

Figure 10. Comparison of α_{set} and α_{eff}, $P_{21} = 1.136$.

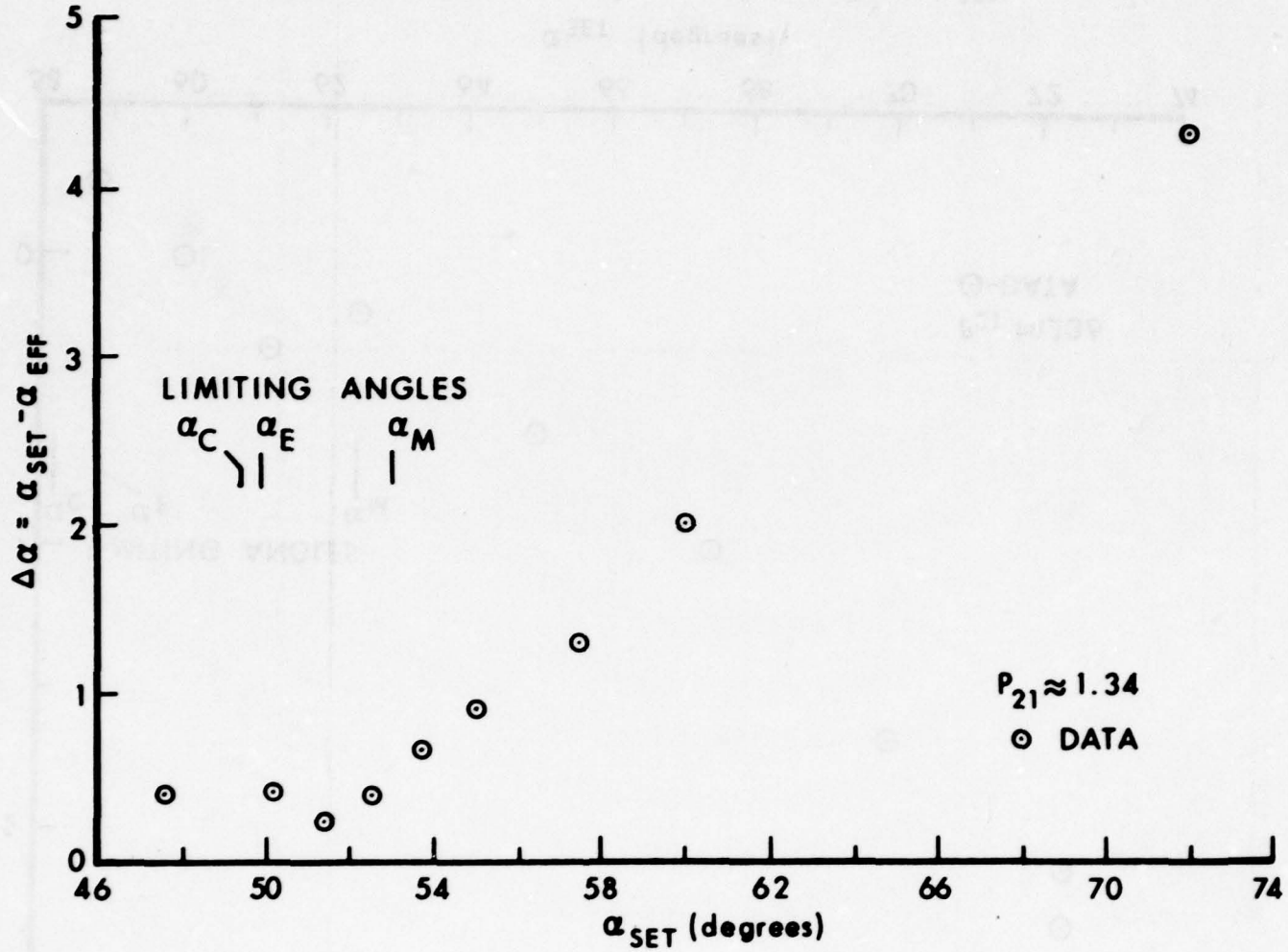

Figure 11. Comparison of α_{set} and α_{eff}, P_{21} = 1.34.

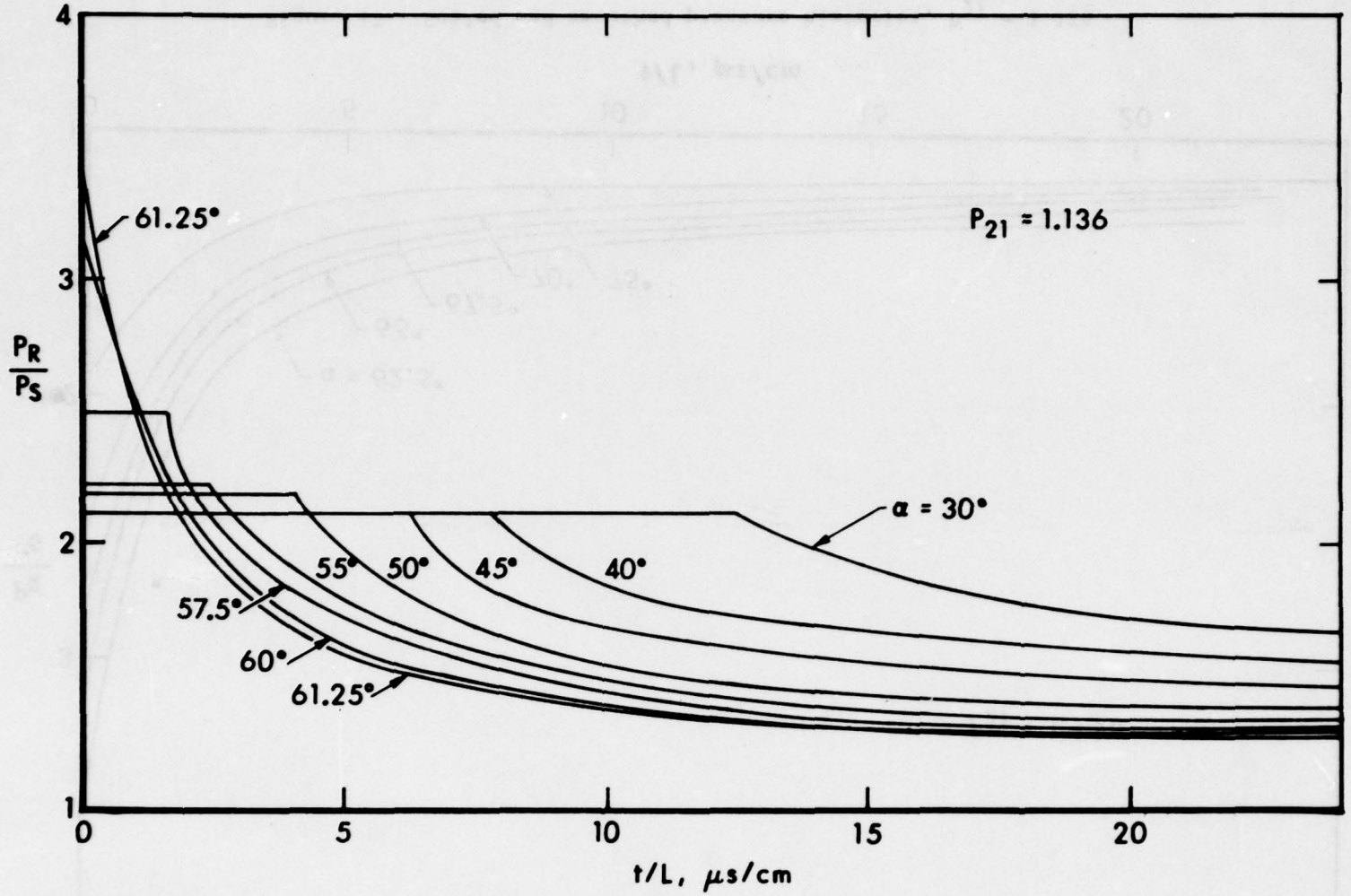

Figure 12. Scaled and smoothed pressure histories, P_{21} = 1.136.

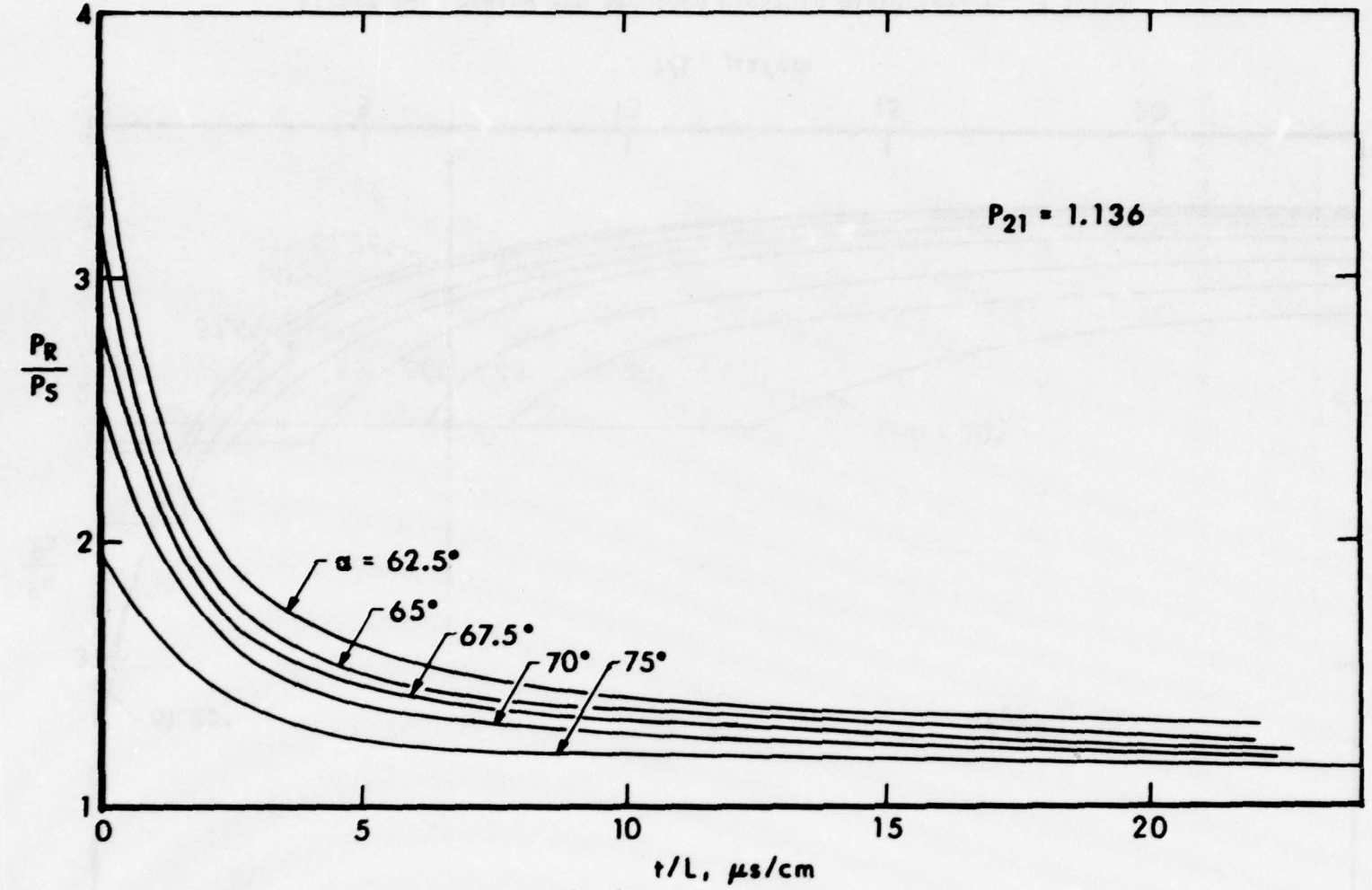

Figure 13. Scaled and smoothed pressure histories, P_{21} = 1.136.

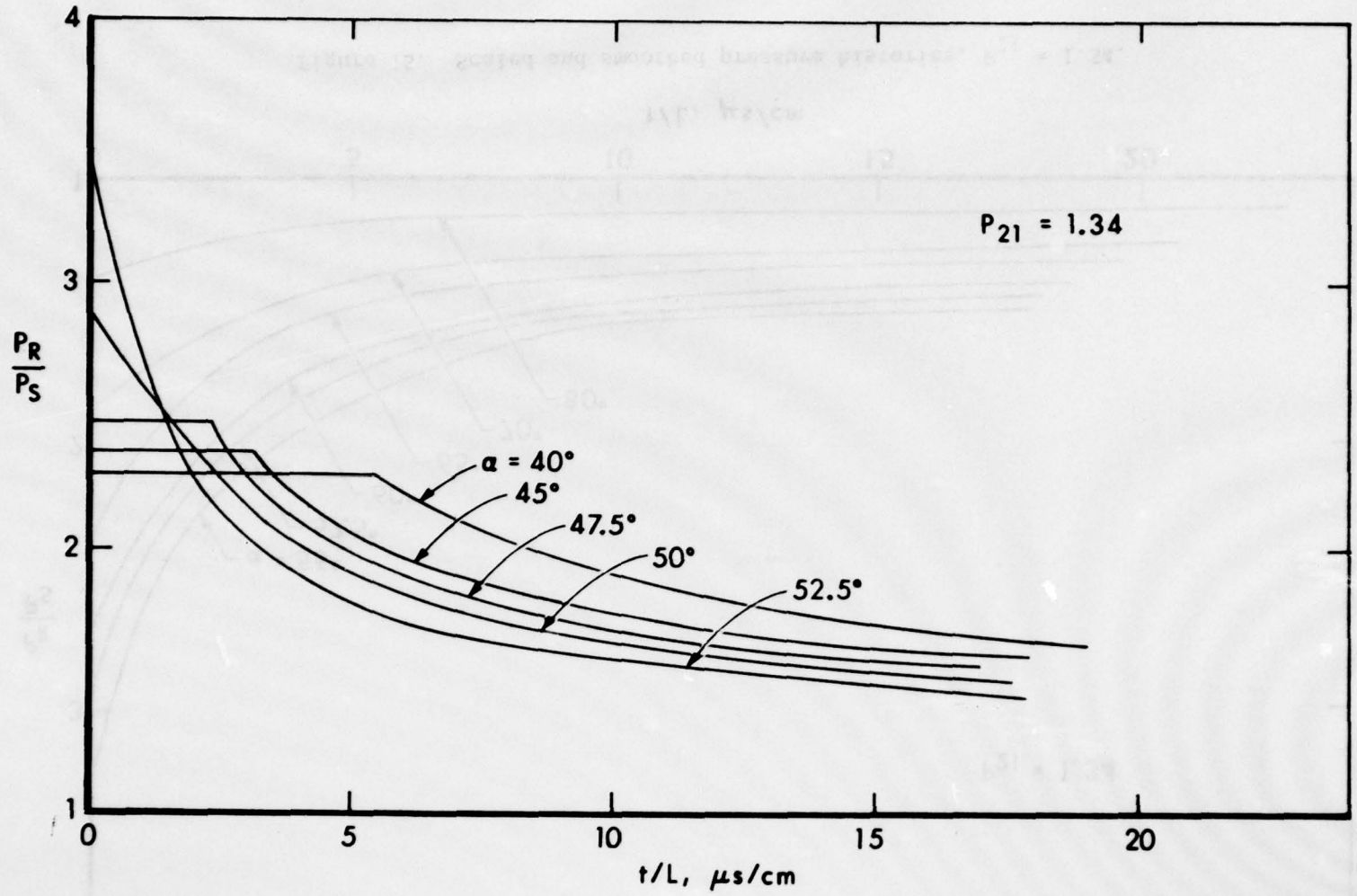

Figure 14. Scaled and smoothed pressure histories, P_{21} = 1.34.

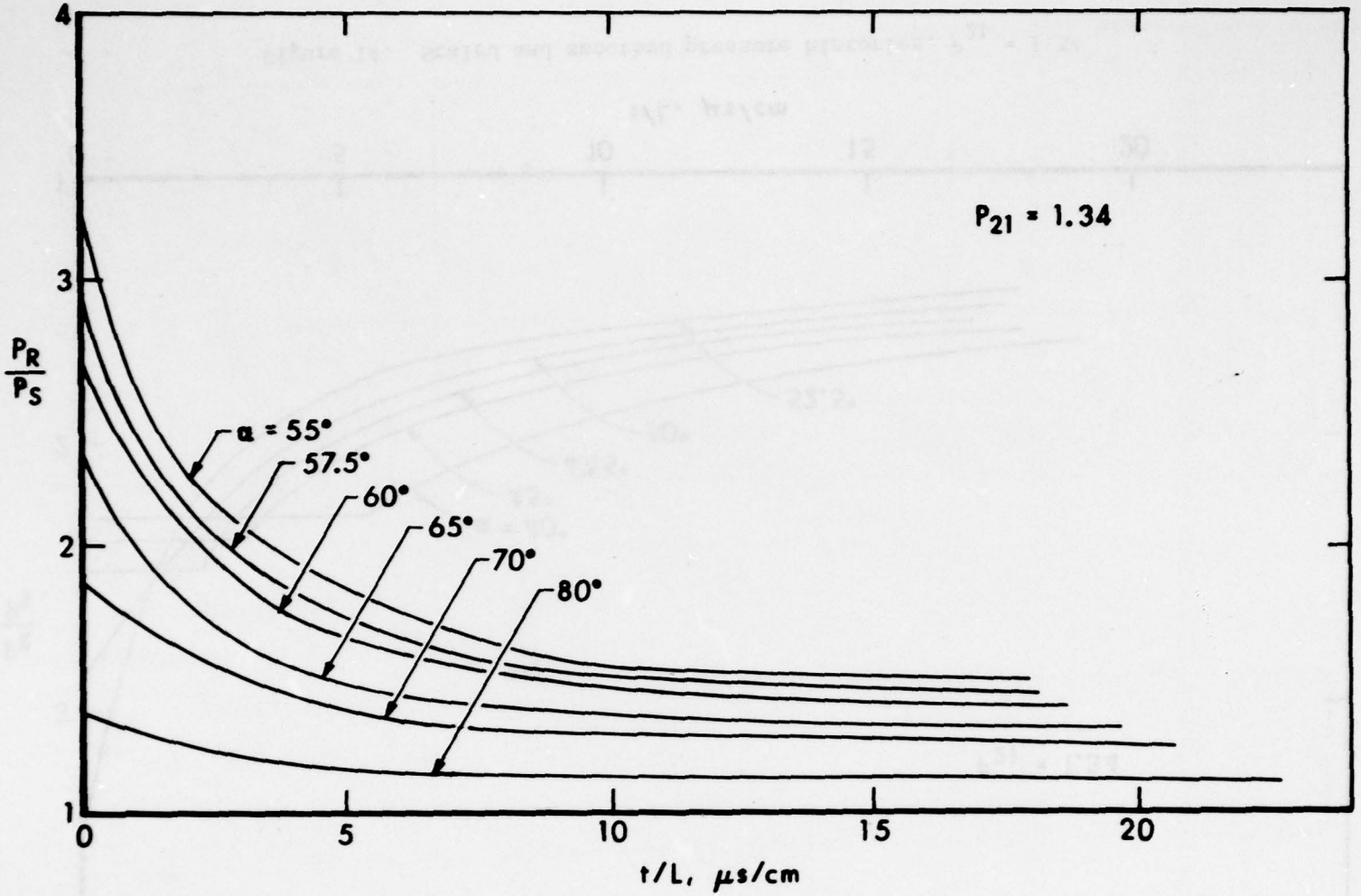

Figure 15. Scaled and smoothed pressure histories, P_{21} = 1.34.

from the proposed curves of Figures 8 and 9. The pressure histories have been smoothed to eliminate the irregularities caused by transducer acceleration sensitivity.

Figures 12 through 15 can be used to develop instantaneous pressure distributions for these two shock strengths on a section of a flat wedge surface when one may be interested in determining the response of that section to blast. Since the data are scaled by distance from the leading edge of the wedge, the arrival of shocks or rarefaction waves from other edges or surfaces would terminate the period for which the data can be used. The data are further limited by the maximum t/L of about 25 used during these tests. There were only two shots run at 62 ½° for 13.8 kPa overpressure at slow recording sweep rates that gave P_R/P_S of 1.26 and 1.18 at t/L of 68 and 130, respectively. Since the primary interest was in obtaining good resolution of the pressure close to the shock front, fast sweep rates were used for the remainder of the tests, limiting t/L to about 25.

The following discussion shows how the present data can be used to determine the pressure distribution on a section of a flat wedge surface:

A. For a panel between 60 and 120 cm from the leading edge, assume these input values:

$$P_S = 13.8 \text{ kPa}$$
$$P_1 = 101.3 \text{ kPa}$$
$$T_1 = 294^\circ \text{ K}$$
$$a_1 = 34442 \text{ cm/s}$$
$$\alpha = 62.5^\circ$$
$$P_{21} = 1.136 .$$

B. Calculate the speed of the reflection along the wedge. At this shock strength, 62½° is the boundary between transition and Mach reflection so the speed can be calculated assuming either case. Assume for example transition reflection with

$$W_{11} = \sqrt{\frac{6P_{21} + 1}{7}} = 1.057,$$

$$W_1 = W_{11}\, a_1,$$

and the speed of the reflection point along the wedge is

$$W_T = W_1/\sin \alpha = 41031 \text{ cm/s}.$$

One could also assume Mach reflection in this case, and find from Figure 7 that $P_R/P_S = 3.6$.

Then

$$P_R = \left(\frac{P_R}{P_S}\right) P_S = 49.7 \text{ kPa}$$

and from the shock speed equation

$$W_{T1} = \sqrt{\frac{6(P_R + 1)+1}{7}} = 1.192$$

so $W_T = W_{T1} a_1 = 41050$ cm/s, about the same as the regular reflection value.

C. Calculate the time of arrival (T.O.A.) of the shock at equally spaced points of interest on the wedge. A spacing of 5 cm is used in this example.

D. For each point used in C, determine the time Δt between shock arrival at that point and shock arrival at the furthermost point of interest, 120 cm in the present case.

E. Calculate $\Delta t/L$ for each point and determine P_R/P_S using Figures 12 through 15 for that $\Delta t/L$.

Table V lists the values calculated for this example. Figure 16 depicts the pressure distribution on the panel between 60 and 120 cm from the leading edge at t = 2923 μs, just as the shock arrives at 120 cm.

V. SUMMARY AND CONCLUSIONS

Reflected shock pressure histories for several positions on a wedge have been obtained for angles of incidence from 0 to 90 degrees for shock strengths of 1.136 and 1.34. Pressure histories have been shown to scale with distance from the leading edge of the wedge. Enhanced pressures of angles of incidence above 40 degrees in the regular, transition, and Mach reflection regions have been documented. Values of peak pressures in the transition and Mach reflection regions have been estimated. The application of the data to predictions of instantaneous blast loads has been demonstrated.

The measured pressure data in the regular reflection region support the two shock theory. Although the transducers, because of their finite size, cannot quite resolve the maximum pressure near α_s, there is no reason to expect that the predicted values are incorrect up to α_c. Furthermore, the measured increase in the pressure with distance from the leading edge at $\alpha > \alpha_M$ lends support to acceptance of the values calculated using Mach stem speed in that region. Since the rarefaction originating at the leading edge reaches point T at α_c, which

Table V. Example Tabulation for Instantaneous Blast Loads

L, cm	TOA, μs	Δt, μs	Δt/L	P_R/P_S	P_S, kPa
120	2923	0	0	3.6	49.7
115	2802	121	1.05	2.55	35.2
110	2680	243	2.21	1.98	27.3
105	2558	365	3.48	1.75	24.2
100	2436	487	4.87	1.62	22.4
95	2314	609	6.41	1.52	21.0
90	2191	731	8.12	1.45	20.0
85	2071	852	10.0	1.40	19.3
80	1949	974	12.2	1.37	18.9
75	1827	1096	14.6	1.35	18.6
70	1705	1218	17.4	1.33	18.4
65	1583	1340	20.6	1.31	18.1
60	1462	1462	24.4	1.30	17.9

INPUT CONDITIONS

$P_{21} = 1.136$

$\alpha = 62\frac{1}{2}°$

$P_1 = 101.3$ kPa

$T_1 = 294°$ K

$a_1 = 34442$ cm/s

$W_T = 41050$ cm/s

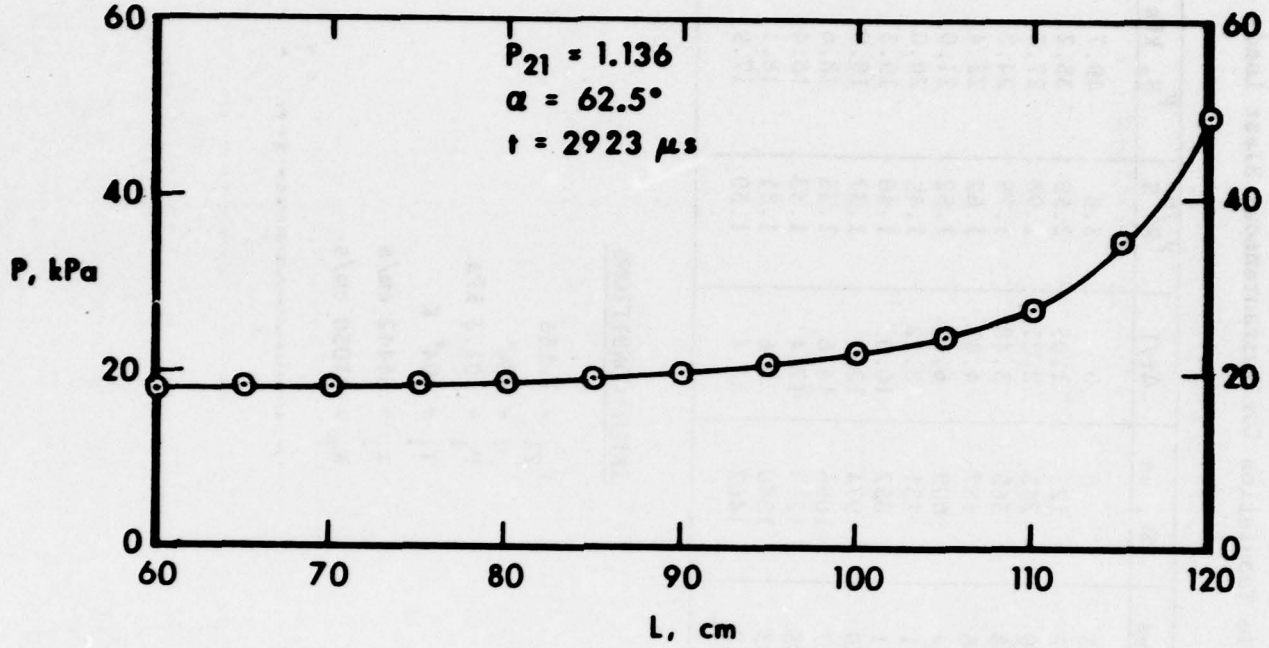

Figure 16. Example of instantaneous pressure loads on a flat surface.

is less than α_E by a fraction of one degree, it appears that the pressure predicted with the two shock theory for α_E is not quite reached. The measurements obtained in these tests in the transition region clearly show that the pressure at angles above α_c rises above the pressure predicted by the two shock theory for α_c and reaches a maximum at α_M. It appears that the actual peak overpressures in the transition region begin with the regular reflection-predicted value at α_c, terminate with the velocity-determined value at α_M and increase smoothly in the interval.

ACKNOWLEDGEMENTS

I thank Mr. George Coulter for his assistance in preparation of the experiments, and Mr. Rodney Abrahams for his assistance with instrumentation set-up and data reduction.

APPENDIX A

Typical Pressure History Records $P_{21} = 1.136$

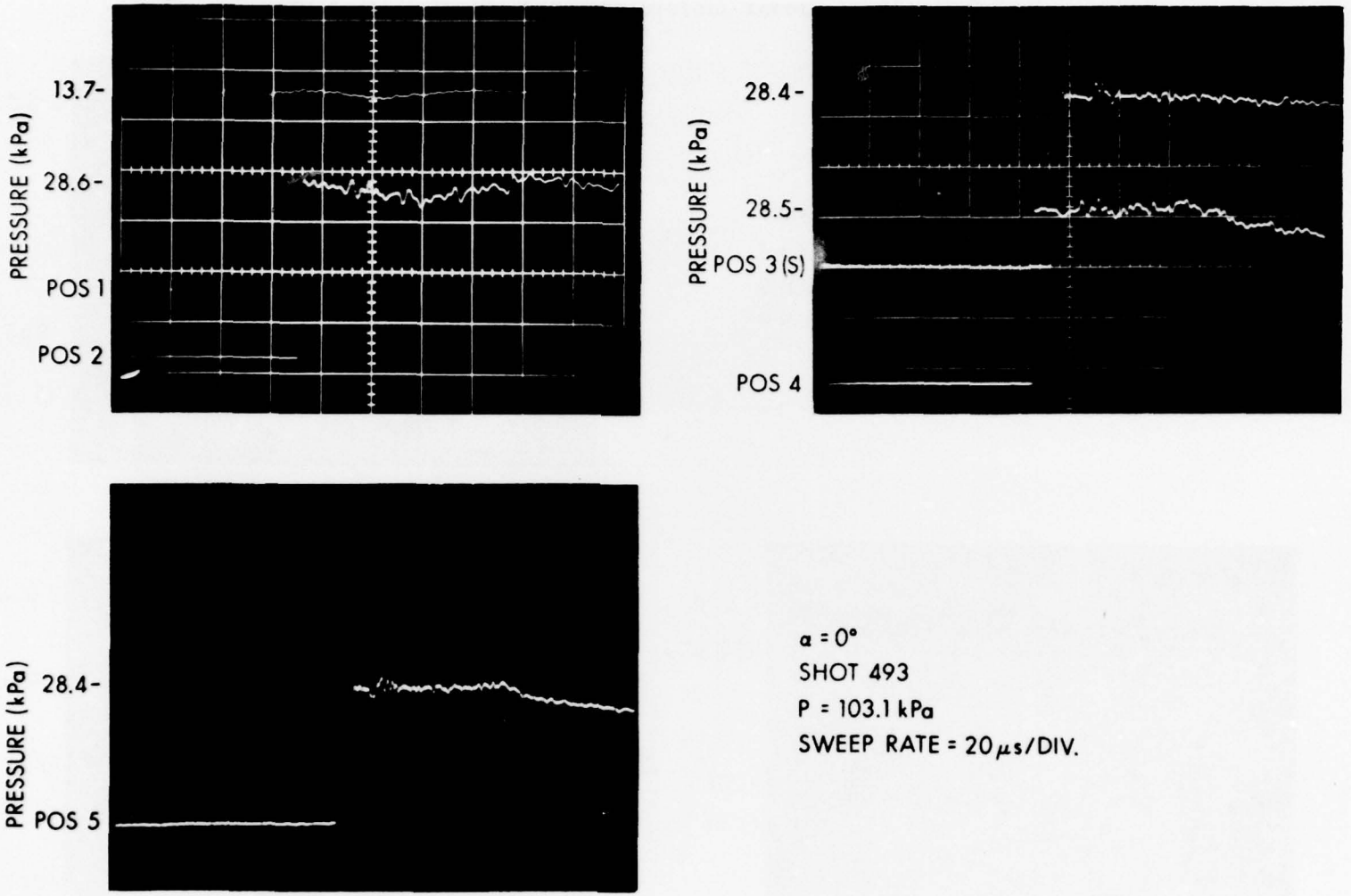

Figure A1. Typical pressure history records, P_{21} = 1.136.

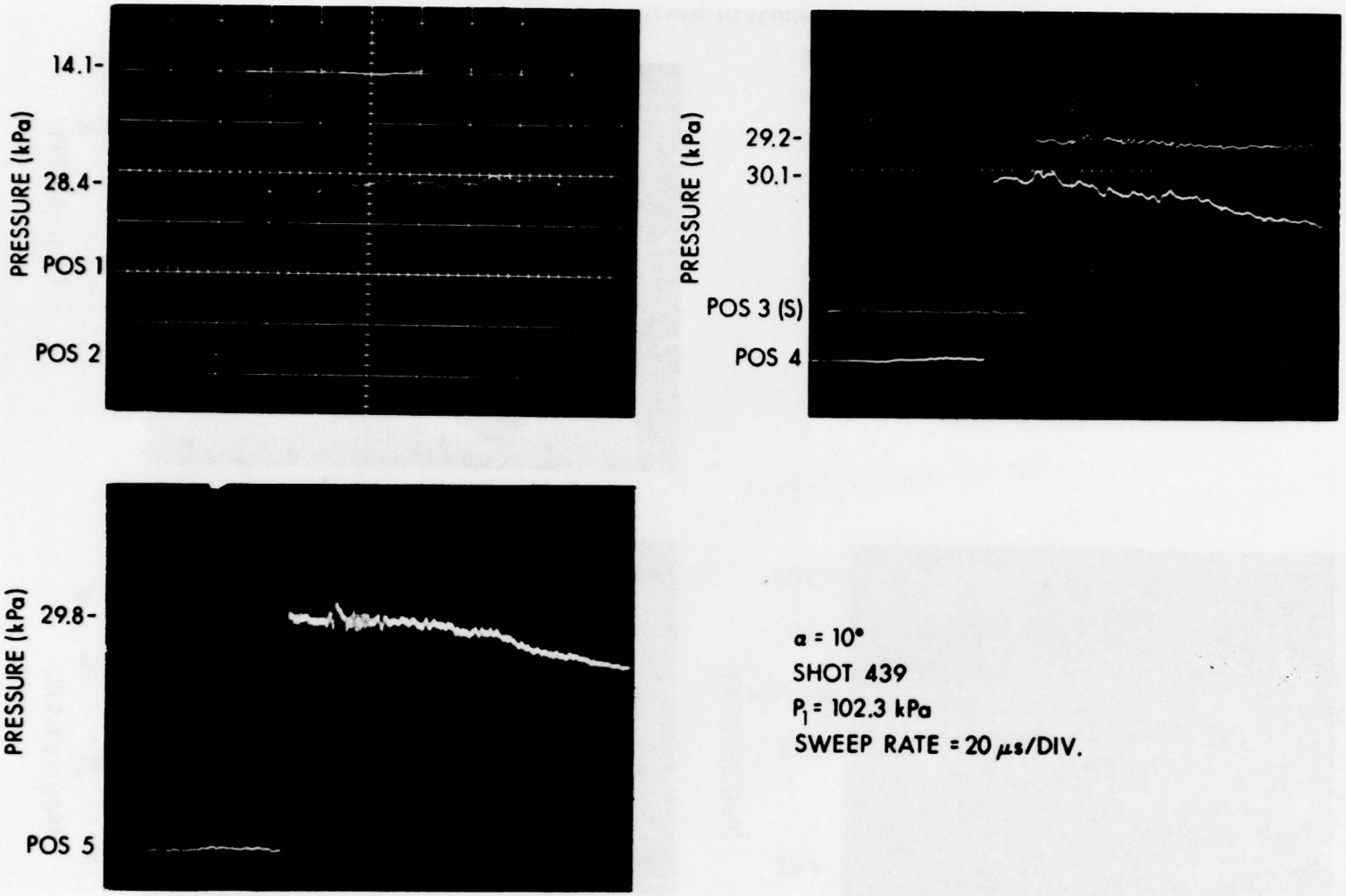

Figure A2. Typical pressure history records, P_{21} = 1.136.

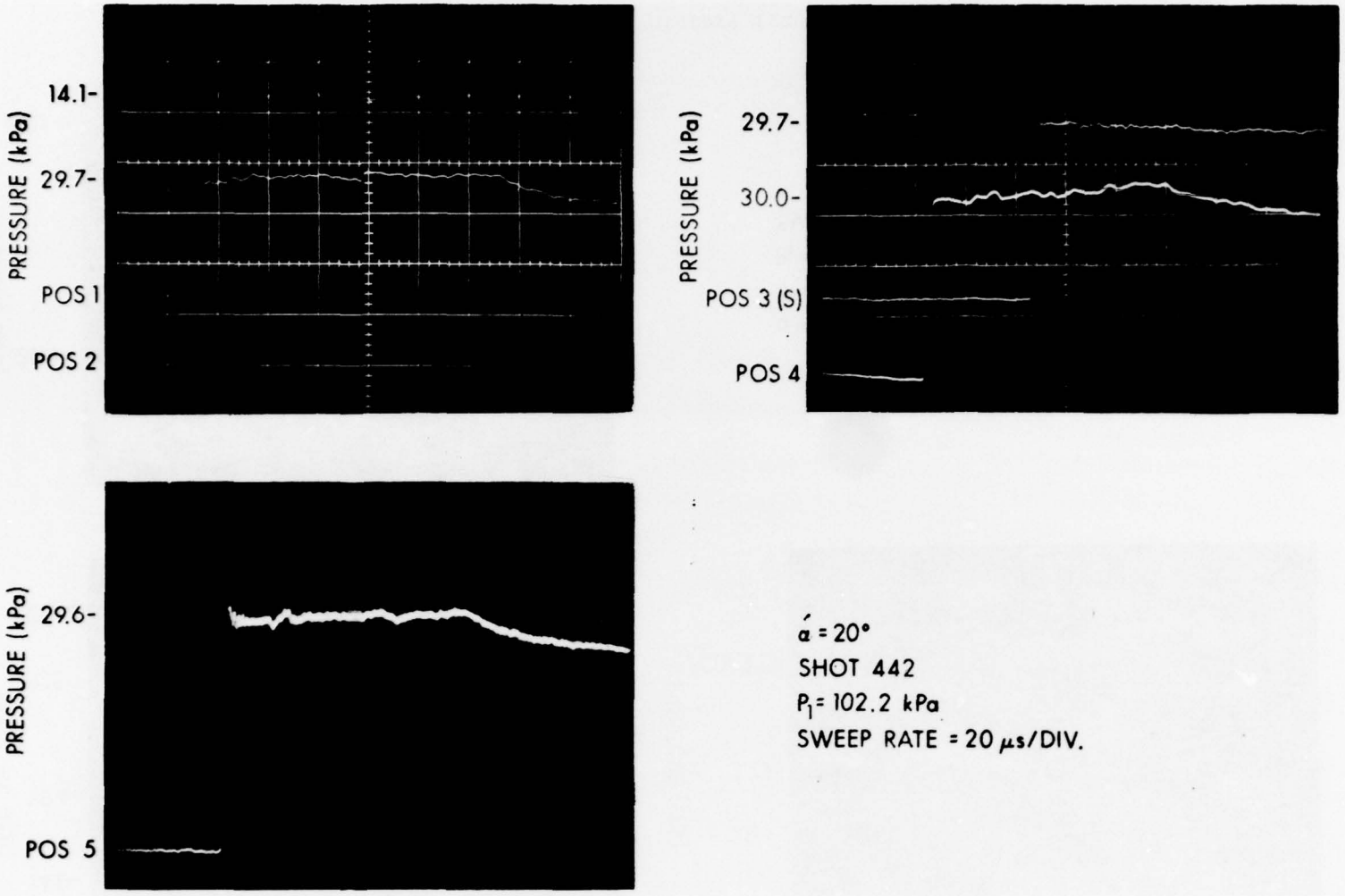

Figure A3. Typical pressure history records, P_{21} = 1.136.

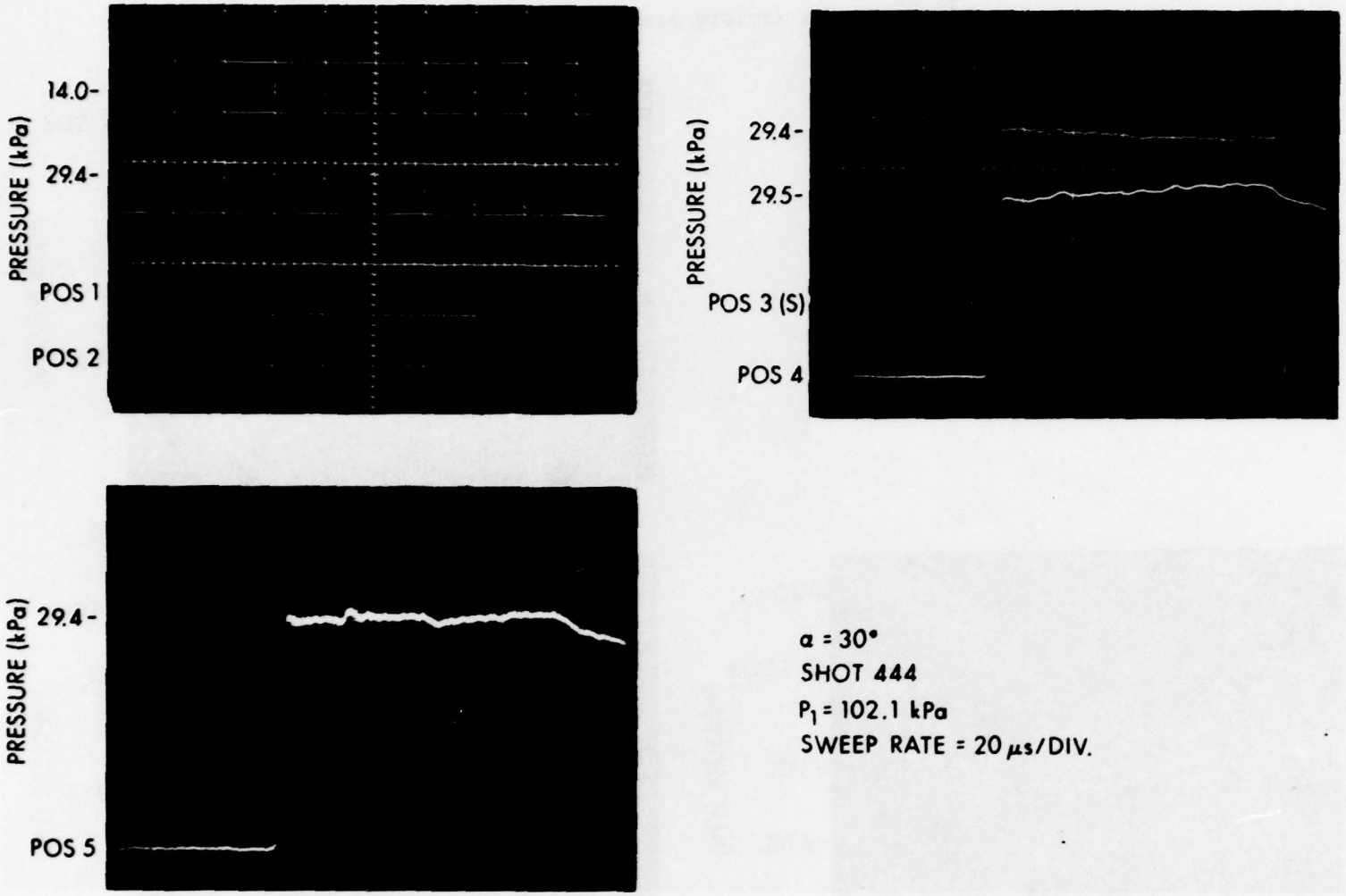

Figure A4. Typical pressure history records, P_{21} = 1.136.

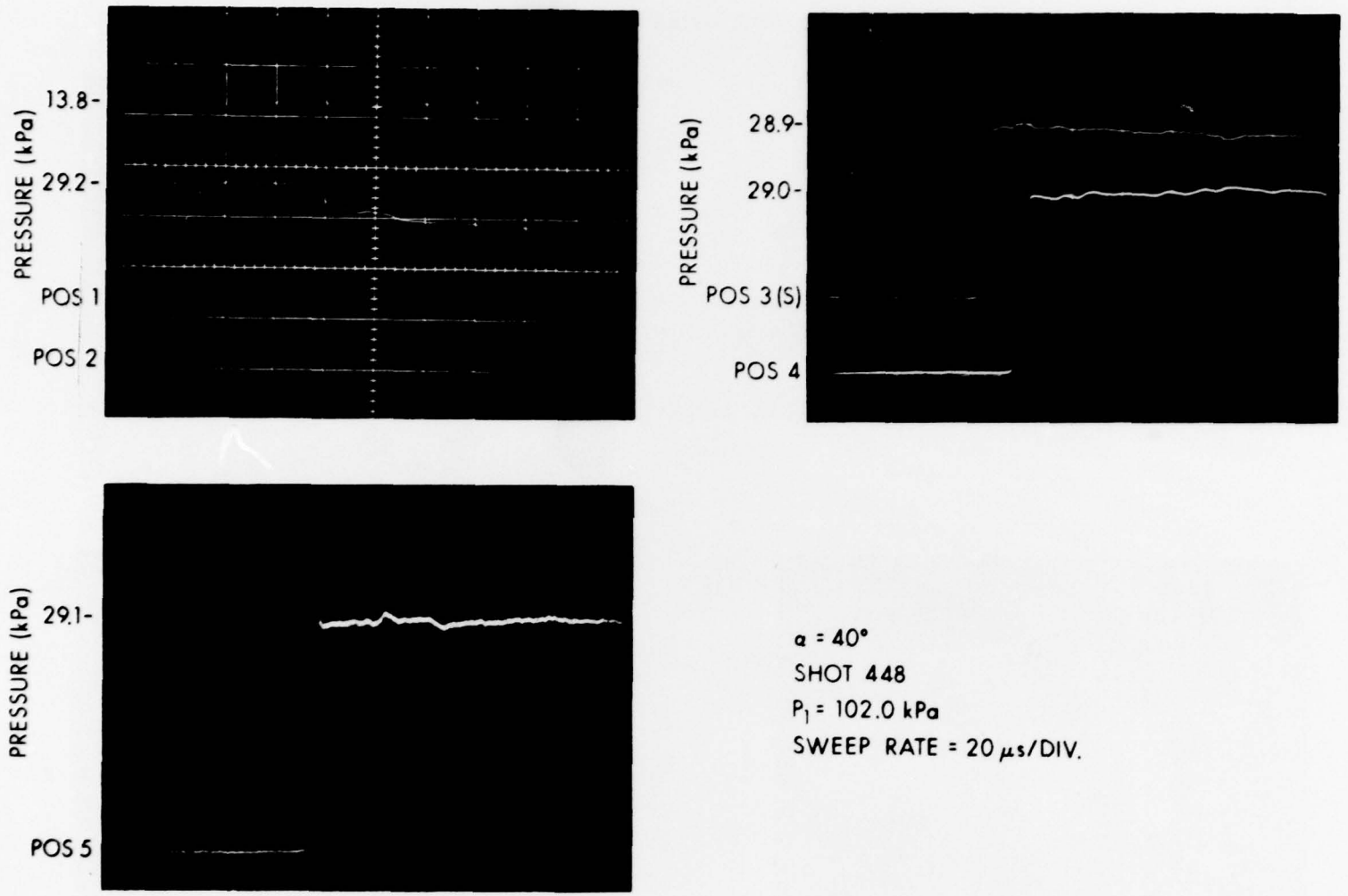

Figure A5. Typical pressure history records, P_{21} = 1.136.

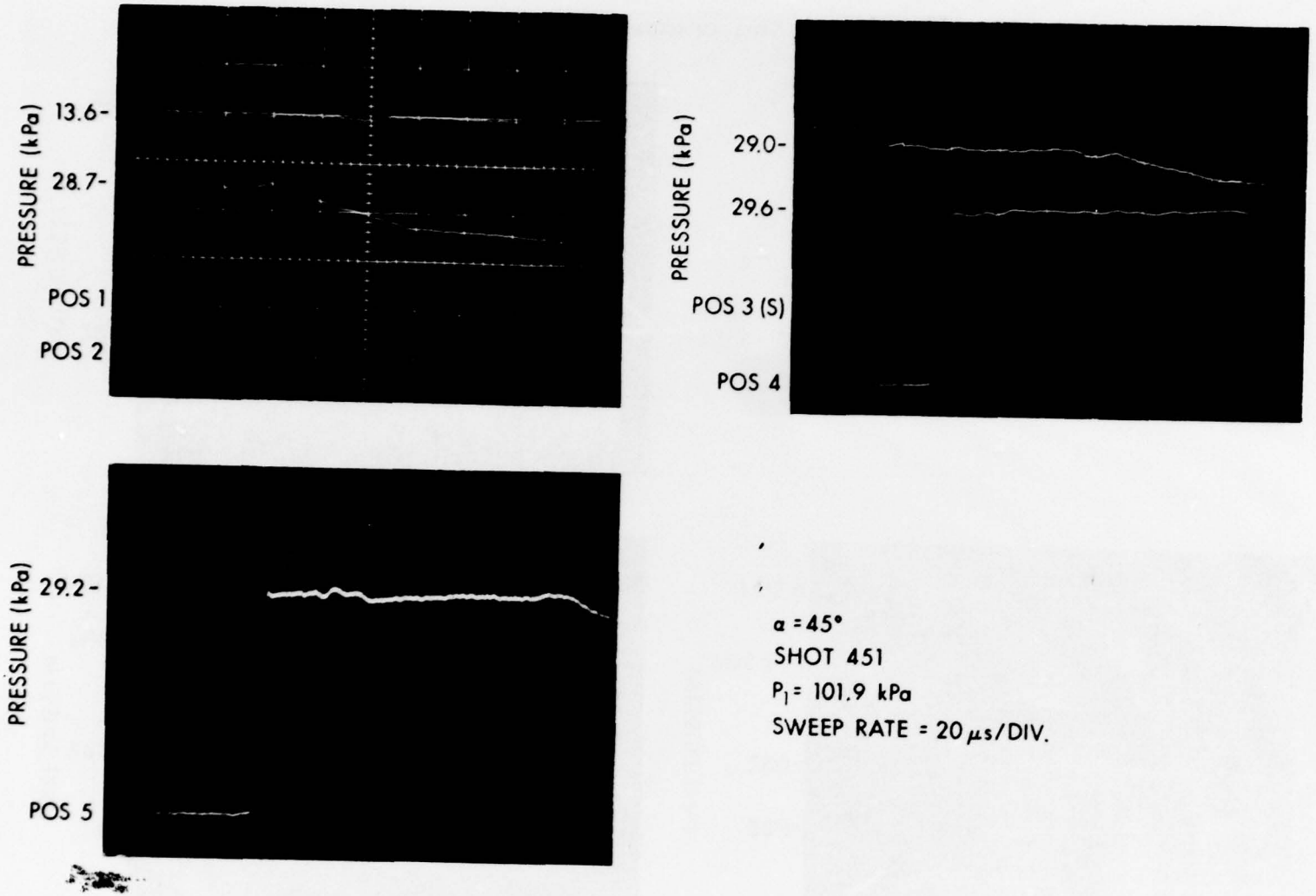

Figure A6. Typical pressure history records, P_{2i} = 1.136.

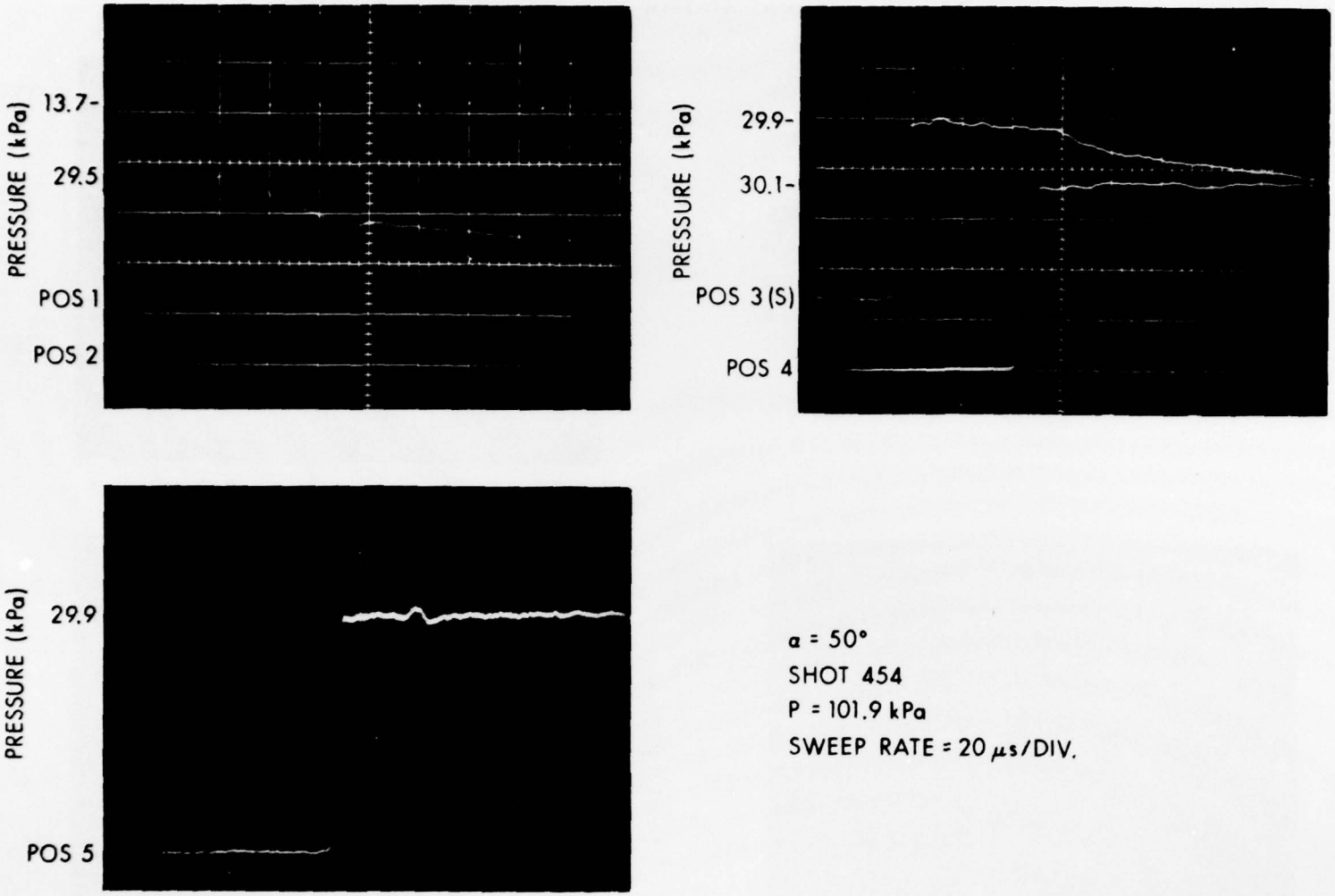

Figure A7. Typical pressure history records, P_{21} = 1.136.

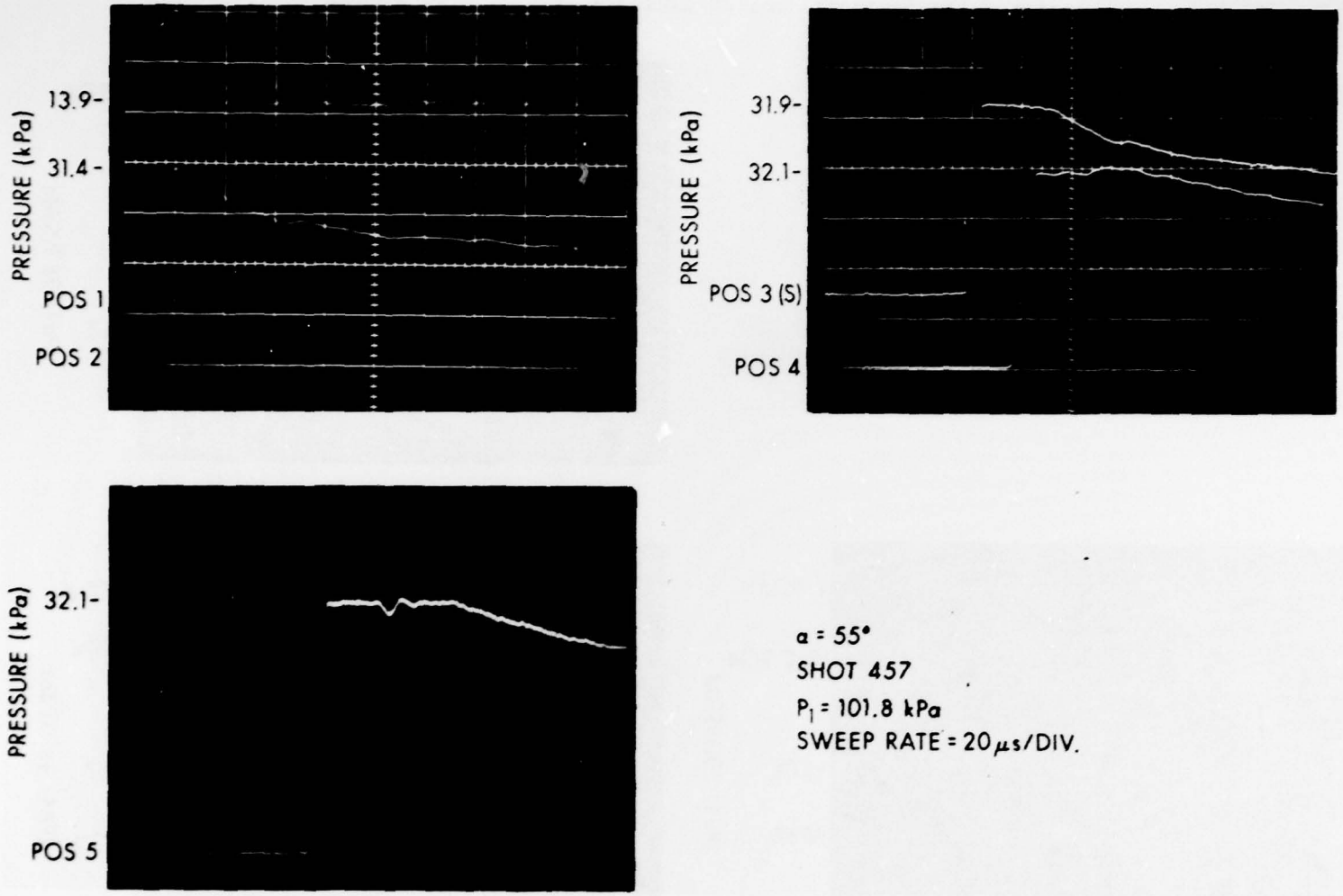

Figure A8. Typical pressure history records, P_{21} = 1.136.

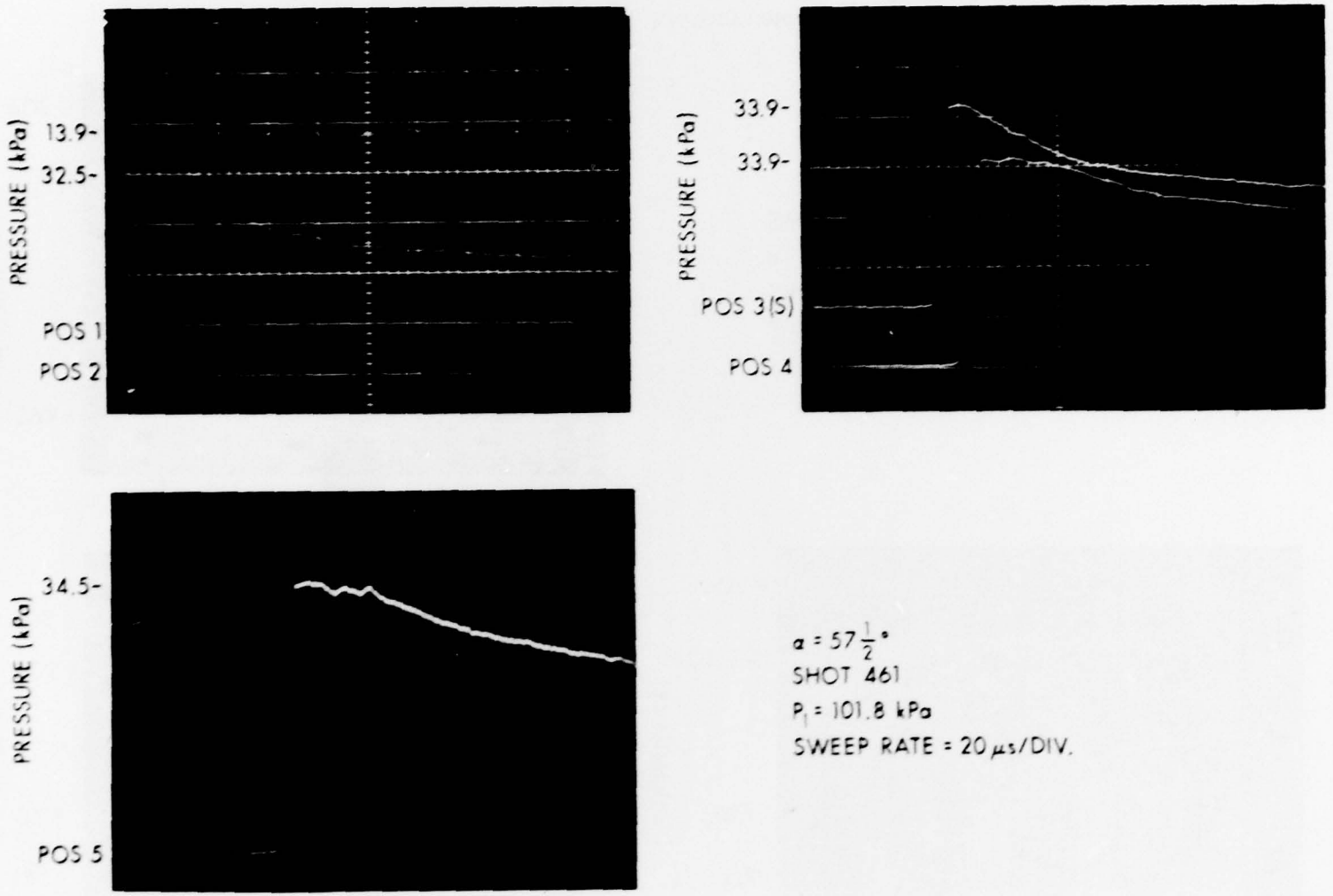

Figure A9. Typical pressure history records, P_{21} = 1.136.

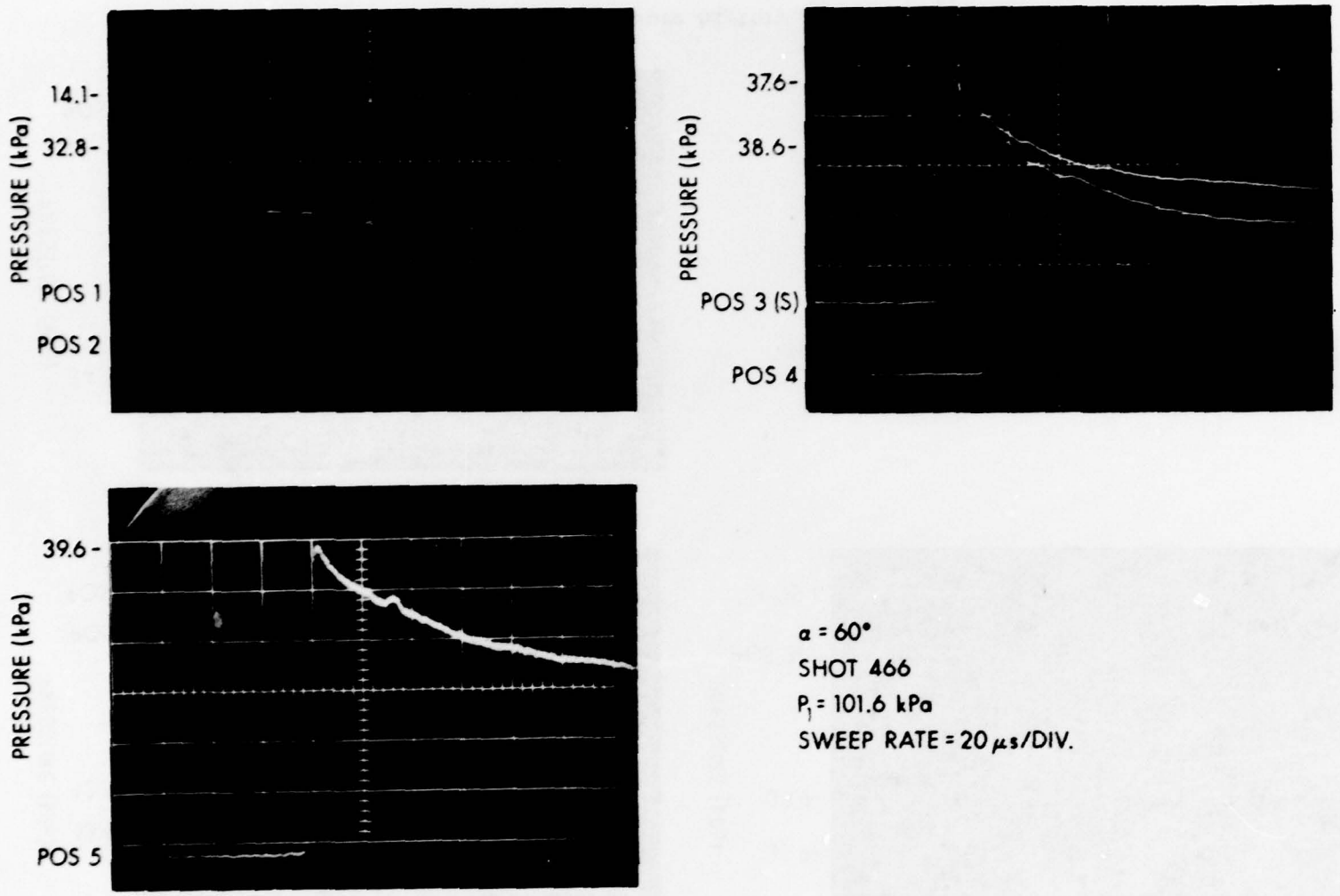

Figure A10. Typical pressure history records, P_{21} = 1.136.

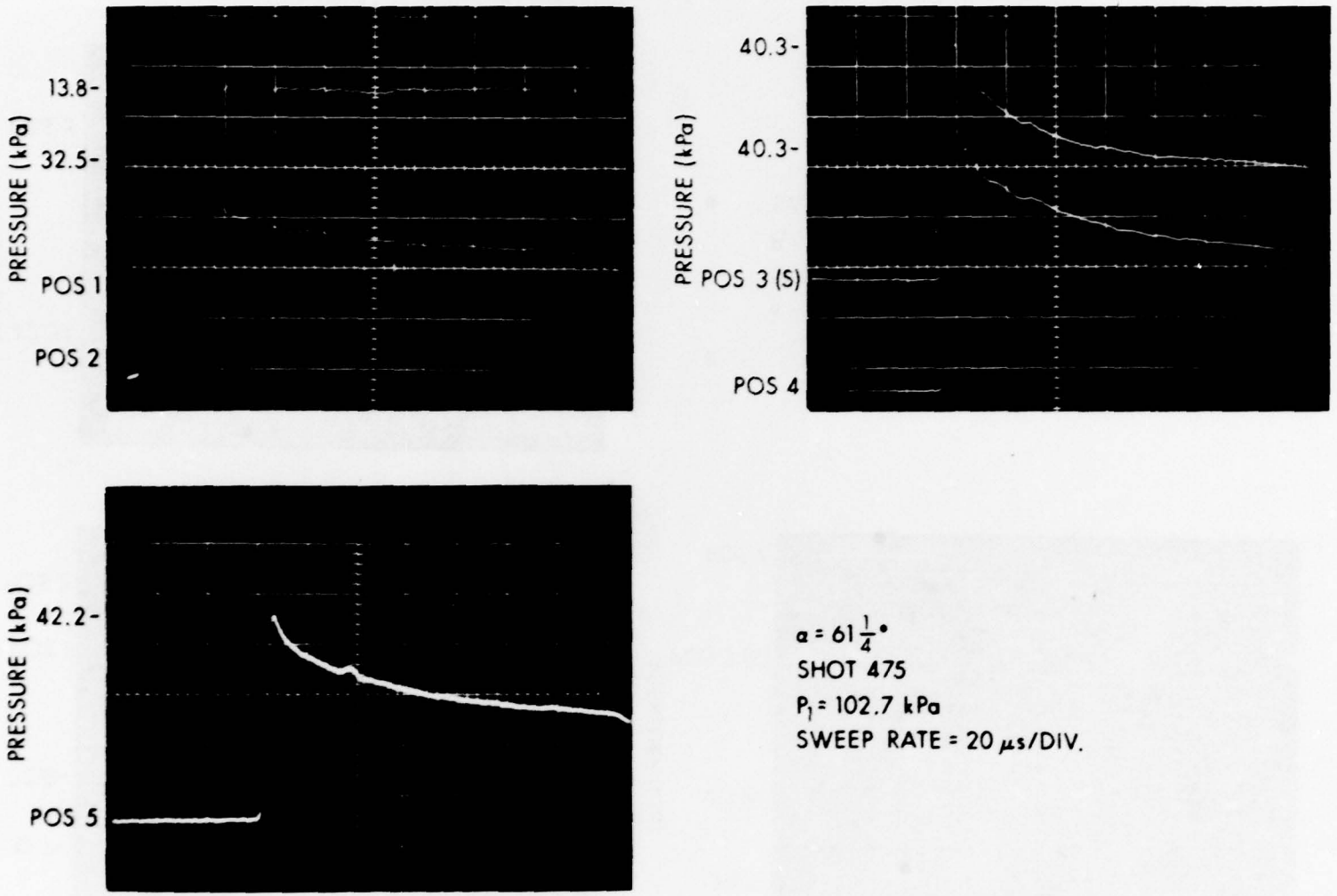

Figure A11. Typical pressure history records, P_{21} = 1.136.

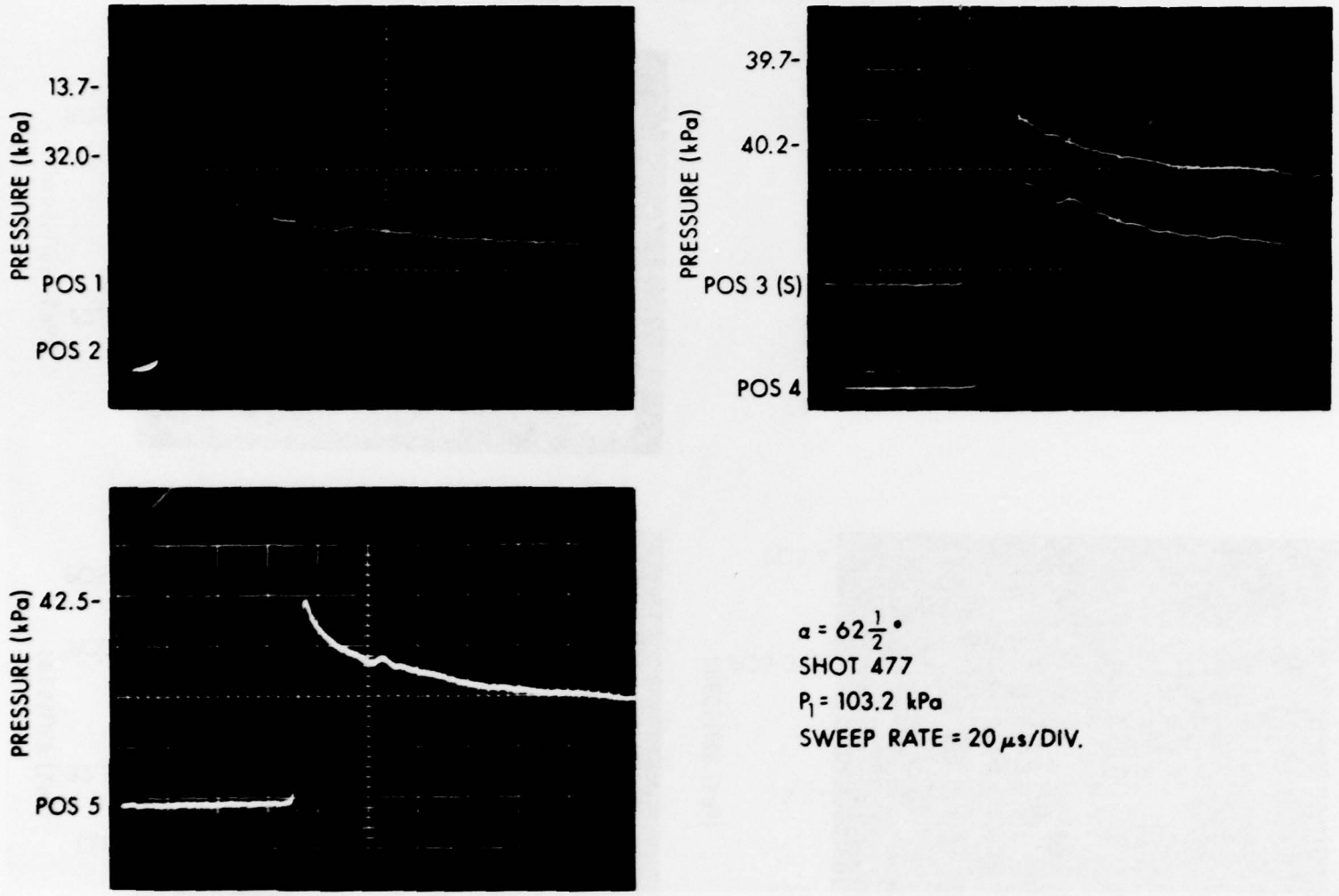

Figure A12. Typical pressure history records, P_{21} = 1.136.

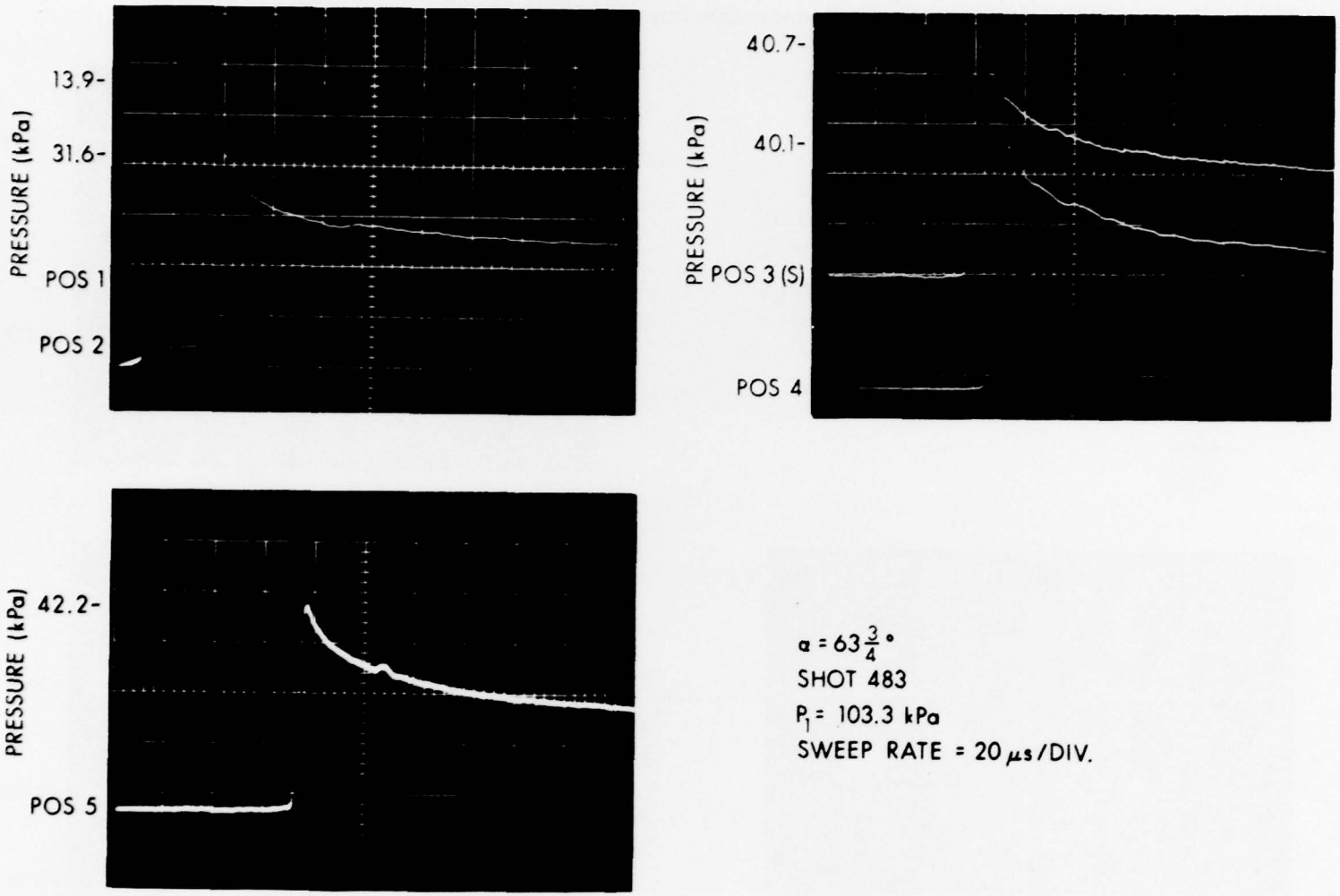

Figure A13. Typical pressure history records, P_{21} = 1.136.

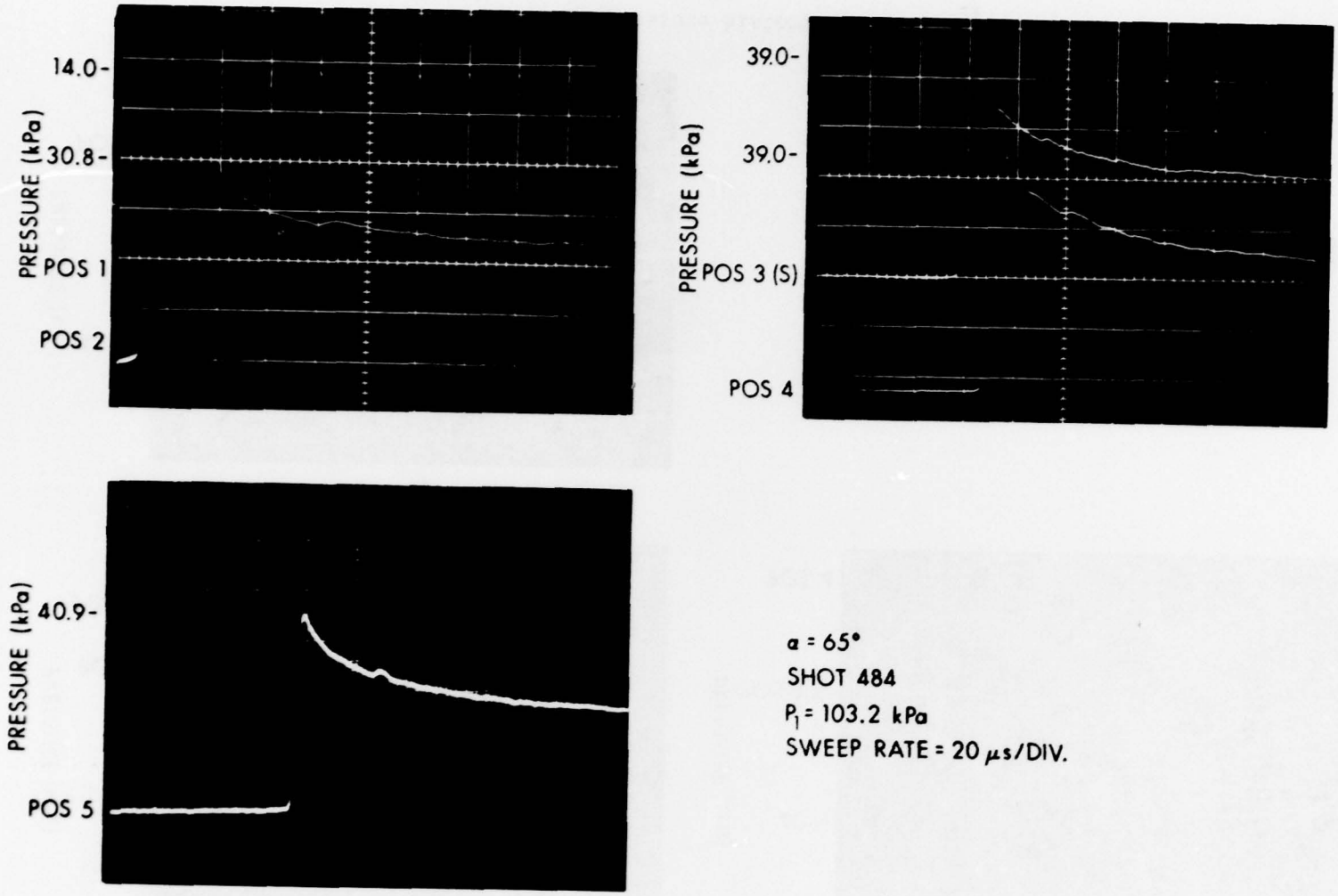

Figure A14. Typical pressure history records, P_{21} = 1.136.

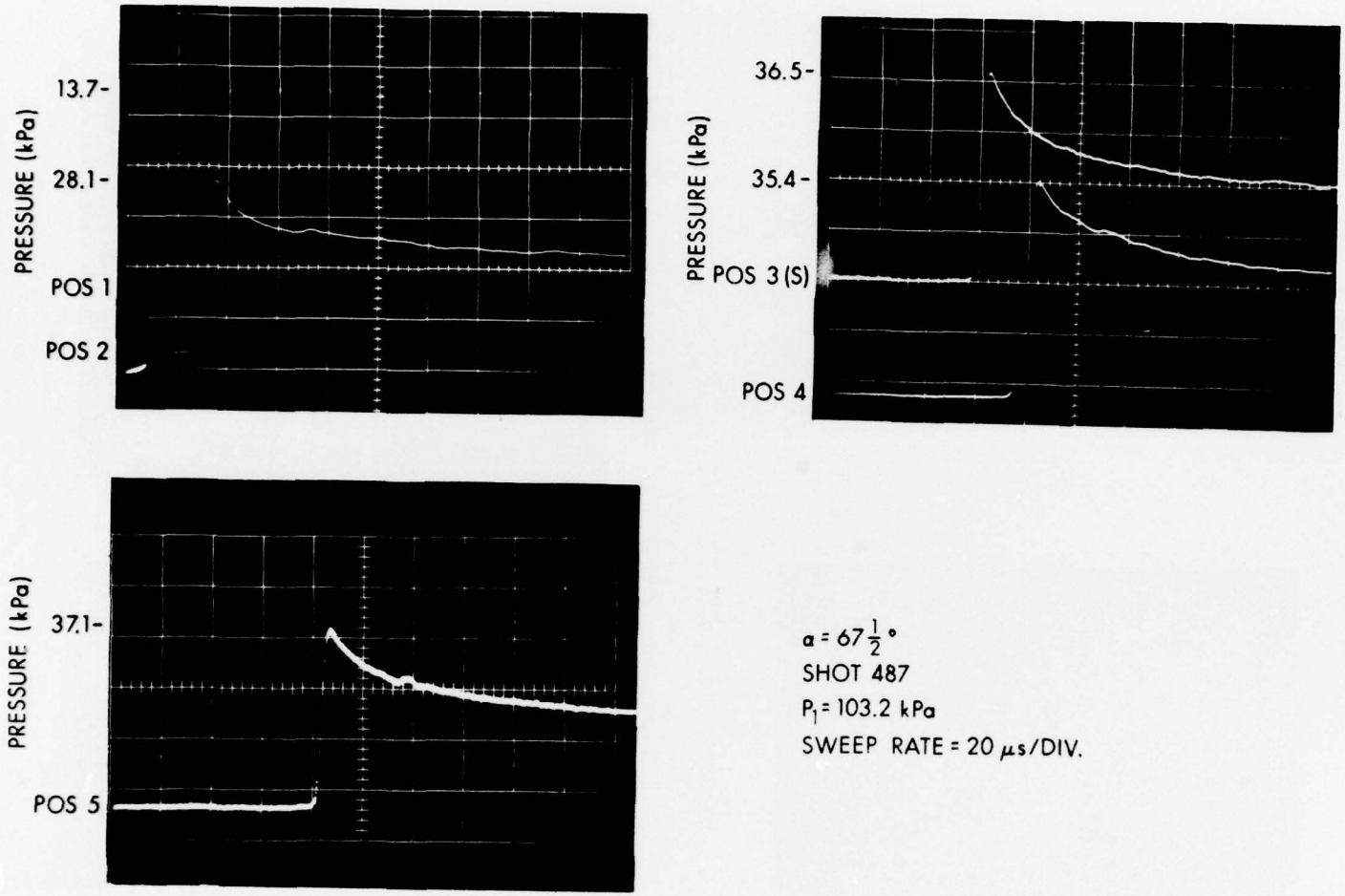

Figure A15. Typical pressure history records, P_{21} = 1.136.

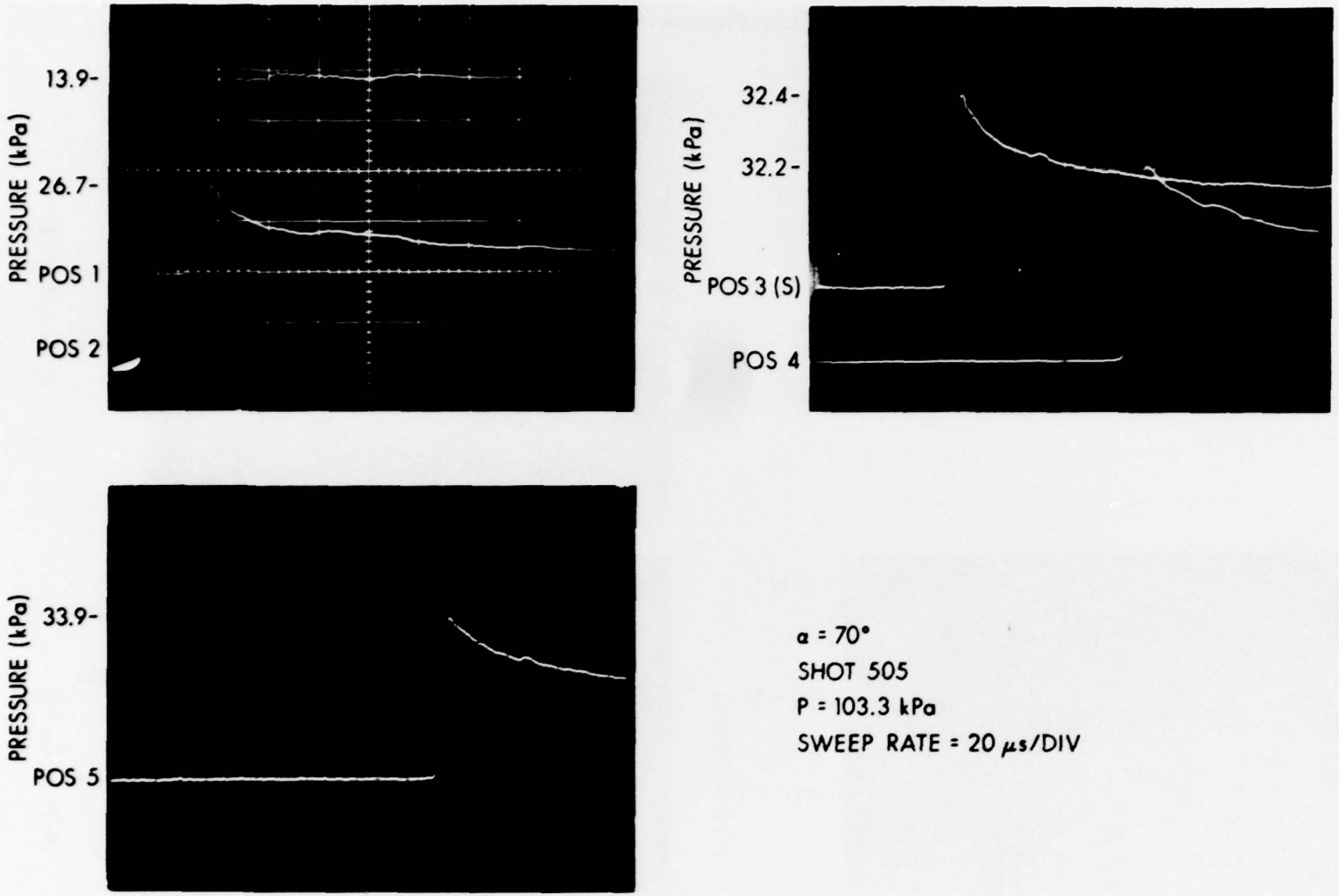

Figure A16. Typical pressure history records, P_{21} = 1.136.

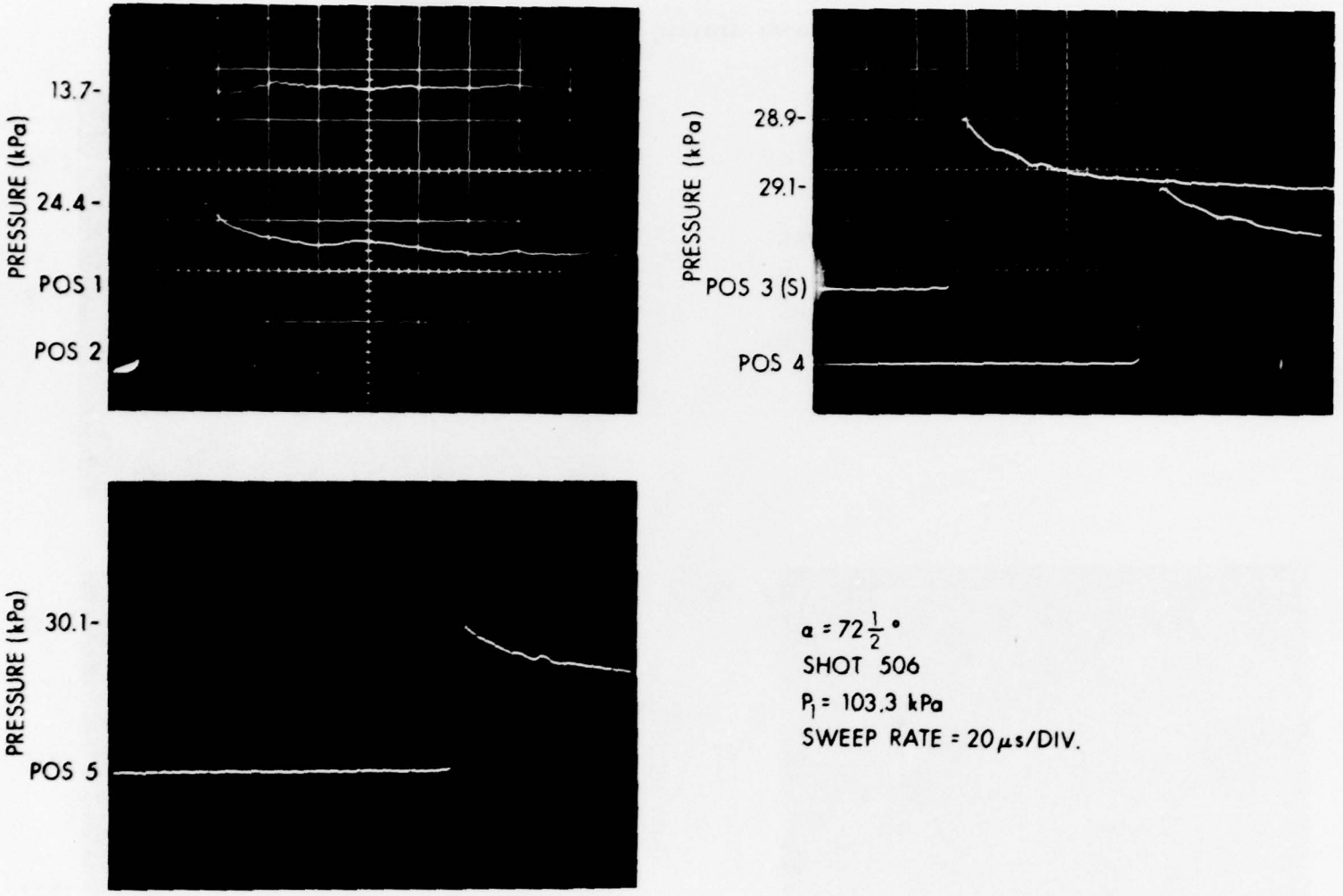

Figure A17. Typical pressure history records, P_{21} = 1.136.

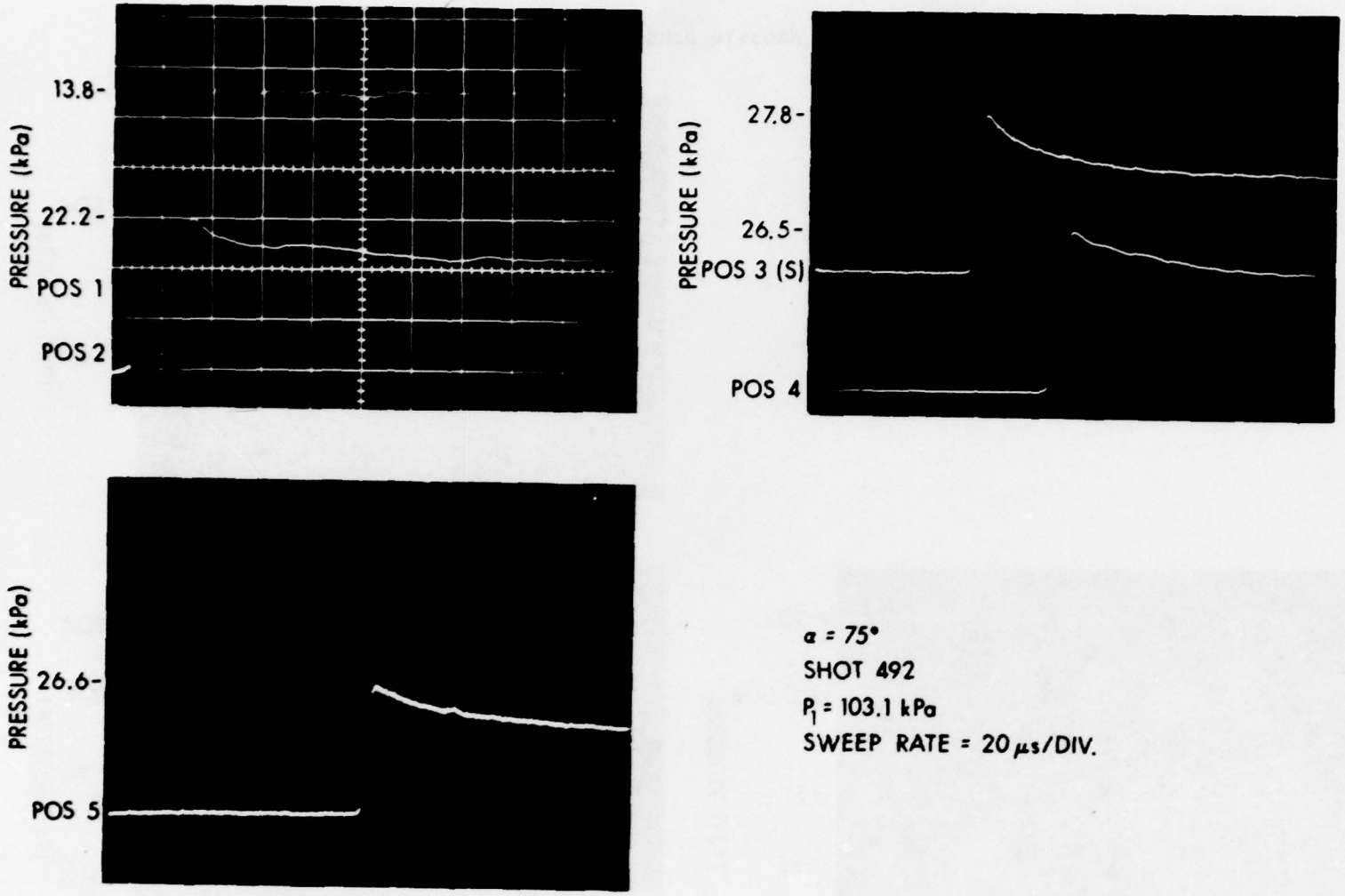

Figure A18. Typical pressure history records, P_{21} = 1.136.

APPENDIX B

Typical Pressure History Records, $P_{21} = 1.34$

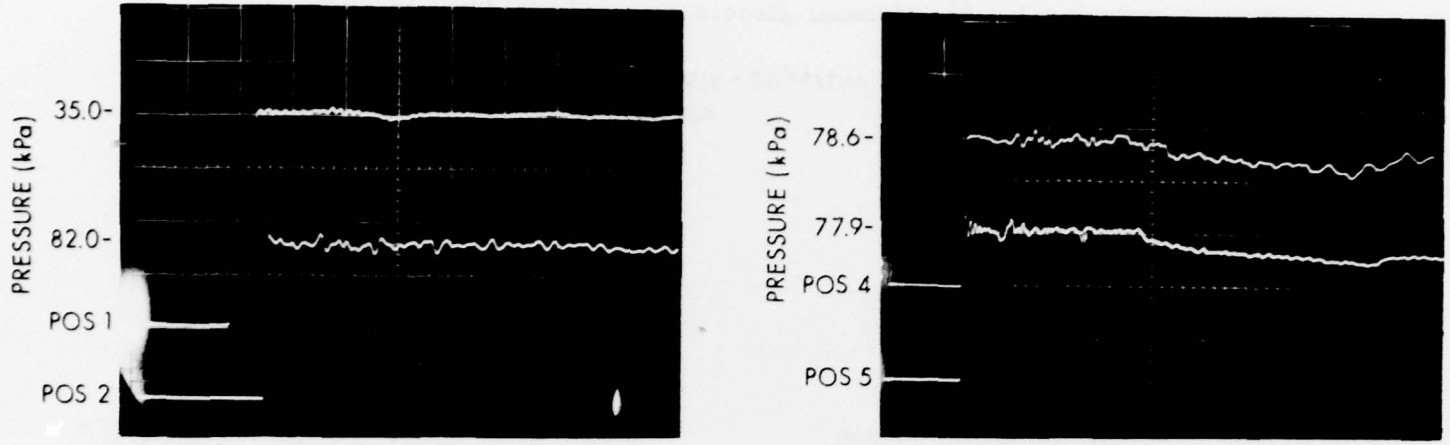

α = 0°
SHOT 372
P = 102.0 kPa
SWEEP RATE = 20 μs/DIV.

Figure B1. Typical pressure history records, P_{21} = 1.34.

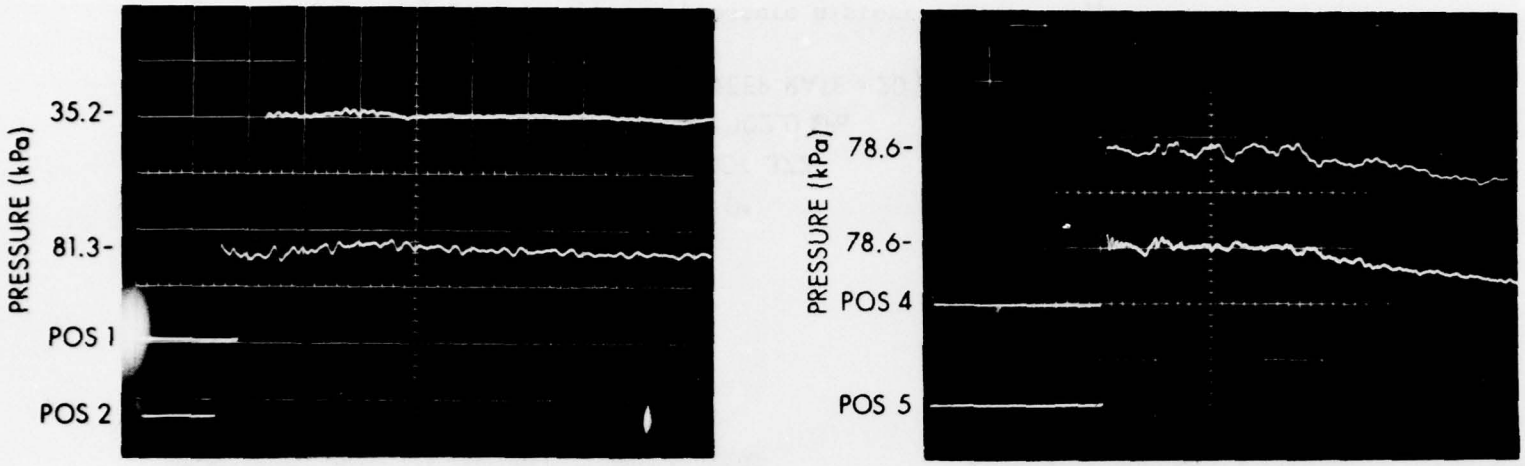

$\alpha = 5°$
SHOT 373
$P_1 = 102.0$ kPa
SWEEP RATE = 20 μs/DIV.

Figure B2. Typical pressure history records, $P_{21} = 1.34$.

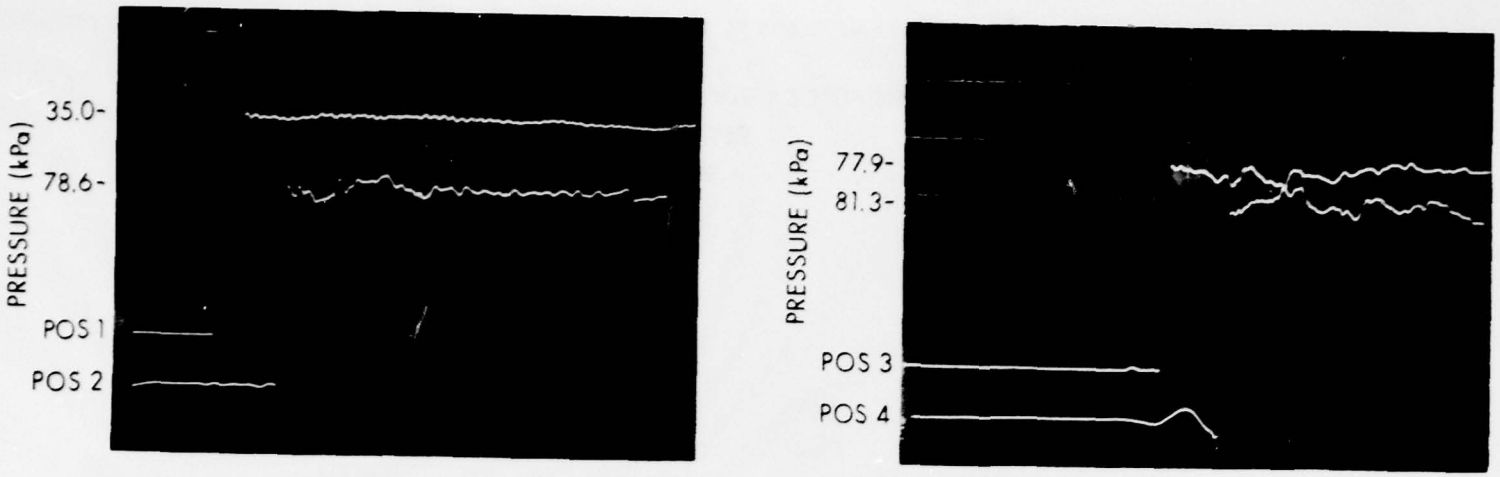

$\alpha = 10°$
SHOTS 306
$P_1 = 102.6$
SWEEP RATE = 20 μs/DIV.

Figure B3. Typical pressure history records, $P_{21} = 1.34$.

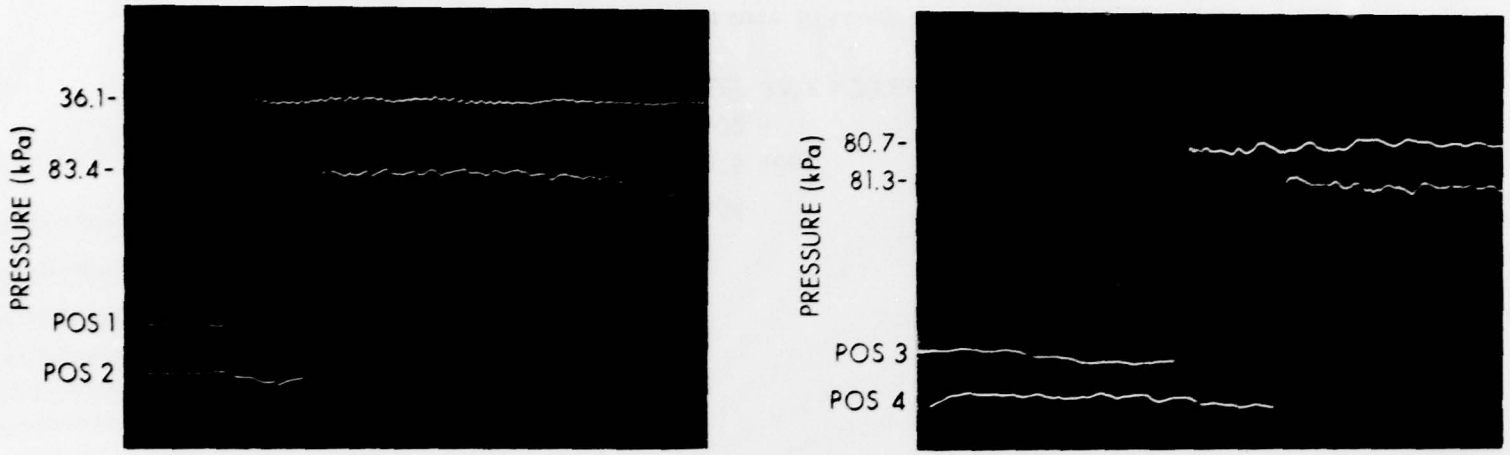

$\alpha = 20°$
SHOT 308
$P_1 = 102.6$ kPa
SWEEP RATE = 20 μs/DIV.

Figure B4. Typical pressure history records, $P_{21} = 1.34$.

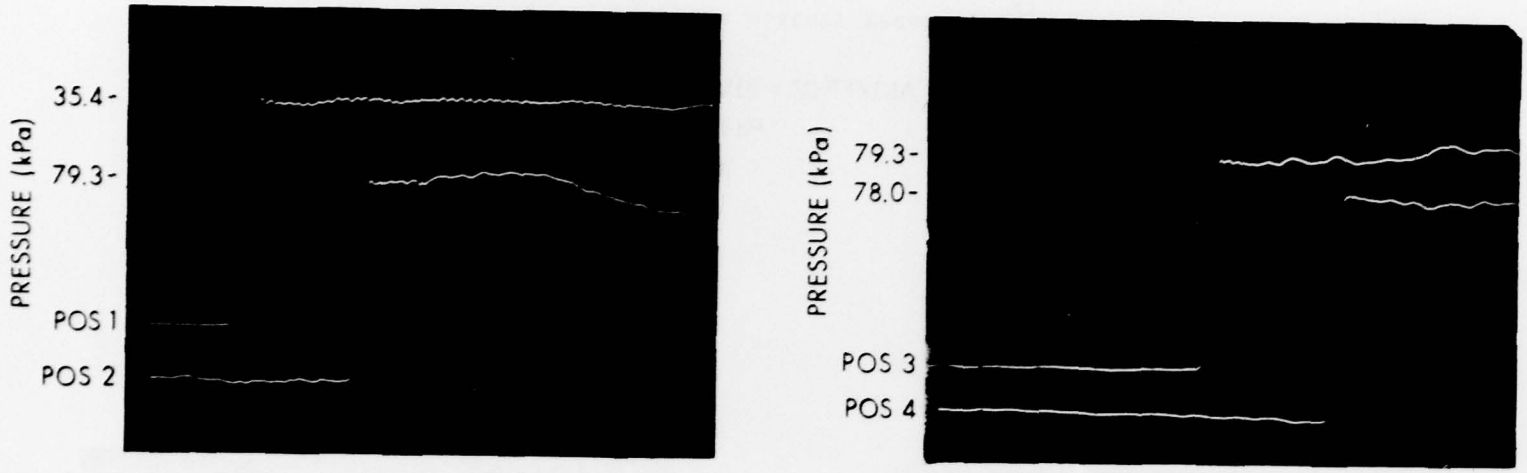

$\alpha = 30°$
SHOT 311
$P_1 = 102.6$ kPa
SWEEP RATE = 20 μs/DIV.

Figure B5. Typical pressure history records, $P_{21} = 1.34$.

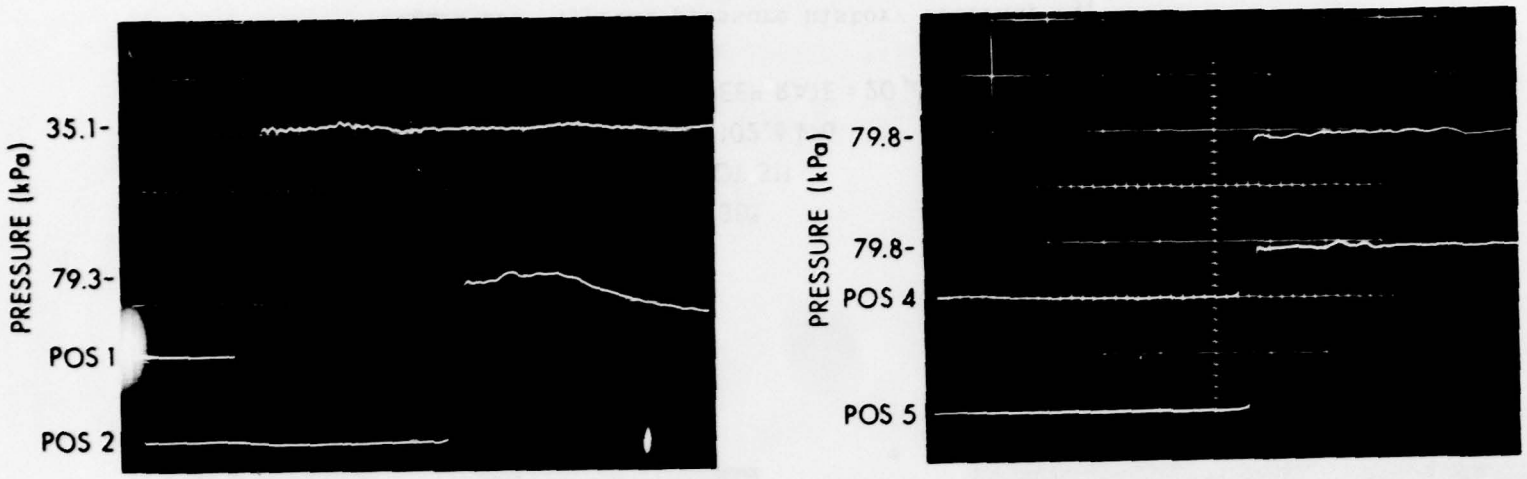

$\alpha = 39\frac{1}{4}°$
SHOT 393
P_1 = 102.6 kPa
SWEEP RATE = 20 μs/DIV.

Figure B6. Typical pressure history records, P_{21} = 1.34.

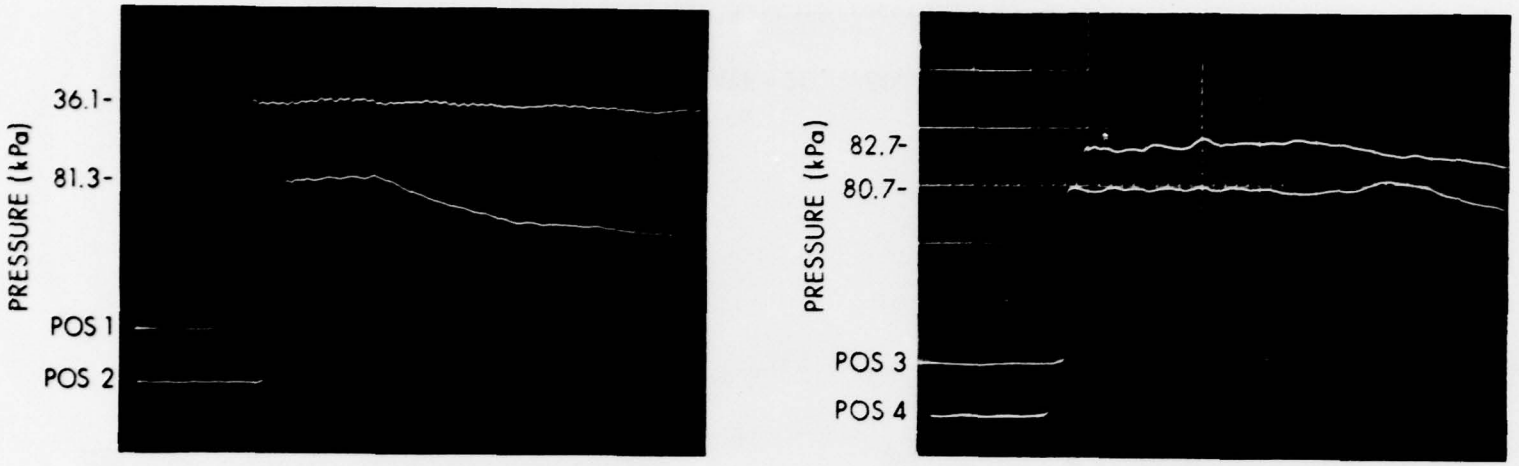

$\alpha = 40°$
SHOT 315
$P_1 = 102.3$ kPa
SWEEP RATE = 20 μs/DIV.

Figure B7. Typical pressure history records, $P_{21} = 1.34$.

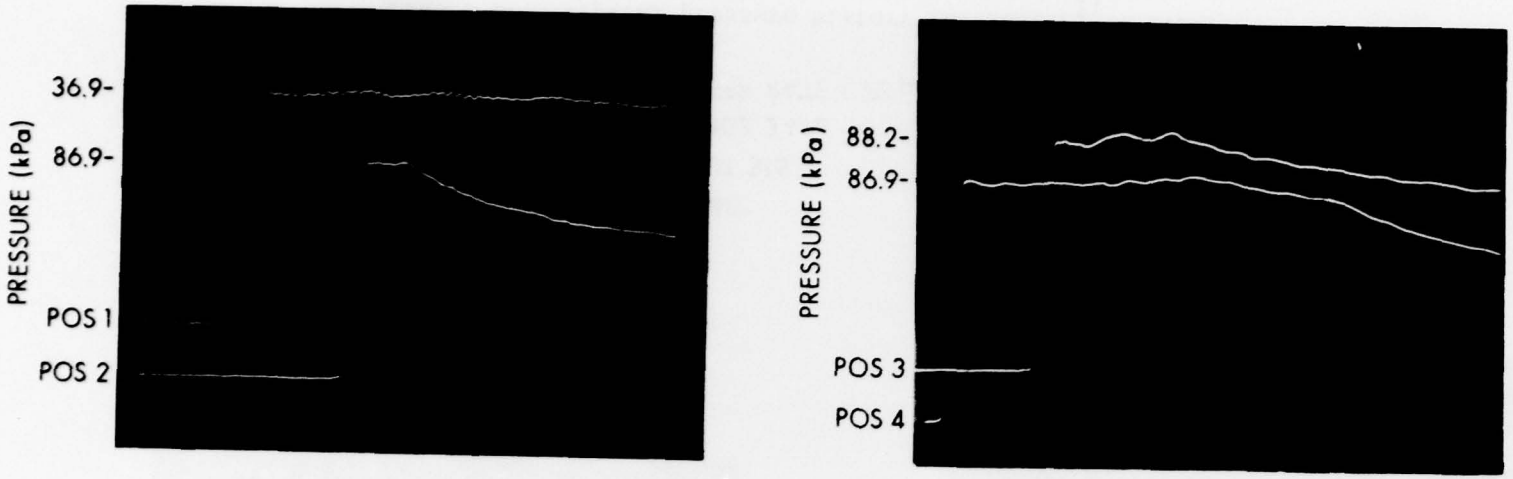

α = 45°
SHOT 316
P_1 = 102.2 kPa
SWEEP RATE = 20 μs/DIV.

Figure B8. Typical pressure history records, P_{21} = 1.34.

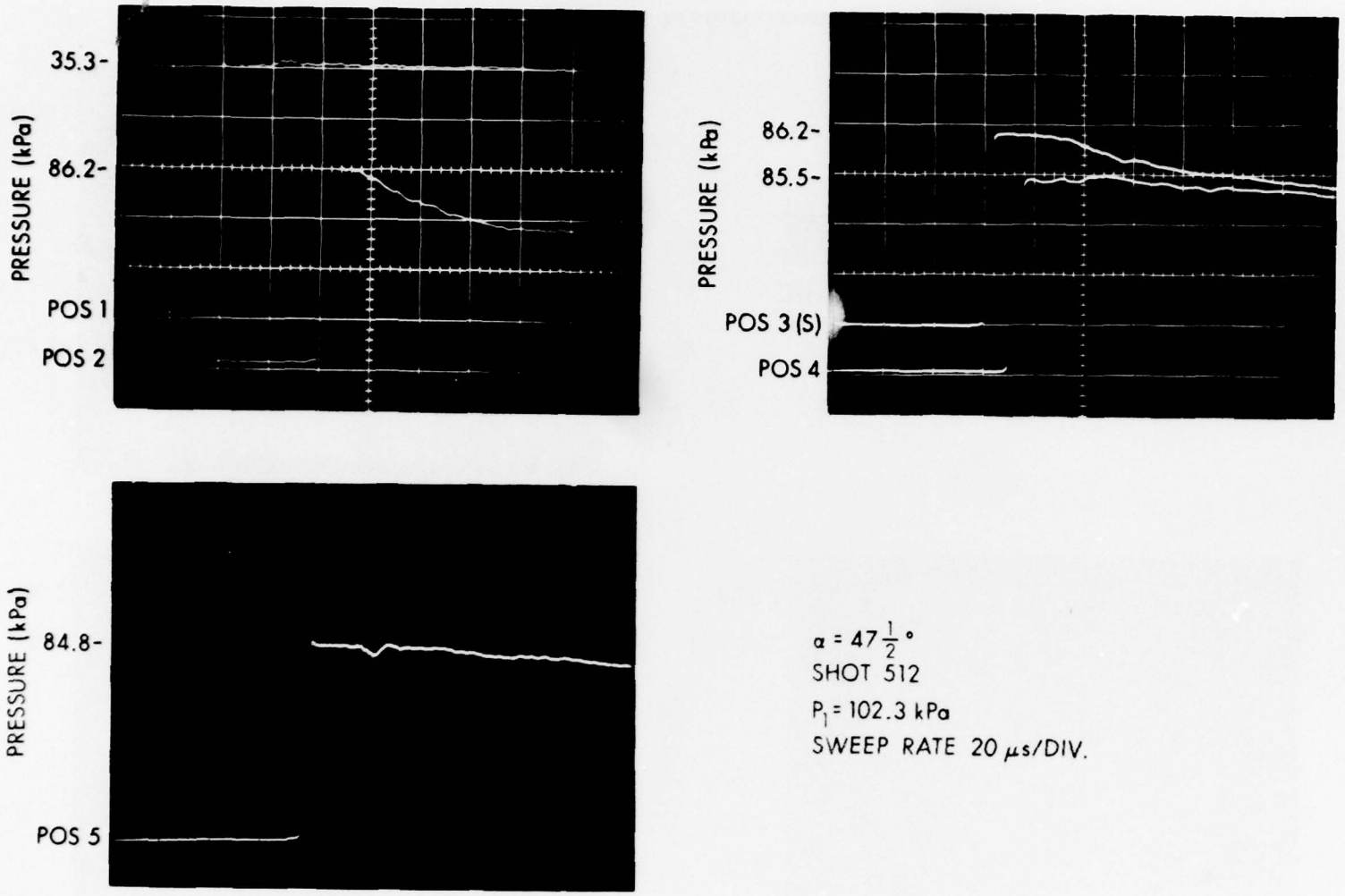

Figure B9. Typical pressure history records, P_{21} = 1.34.

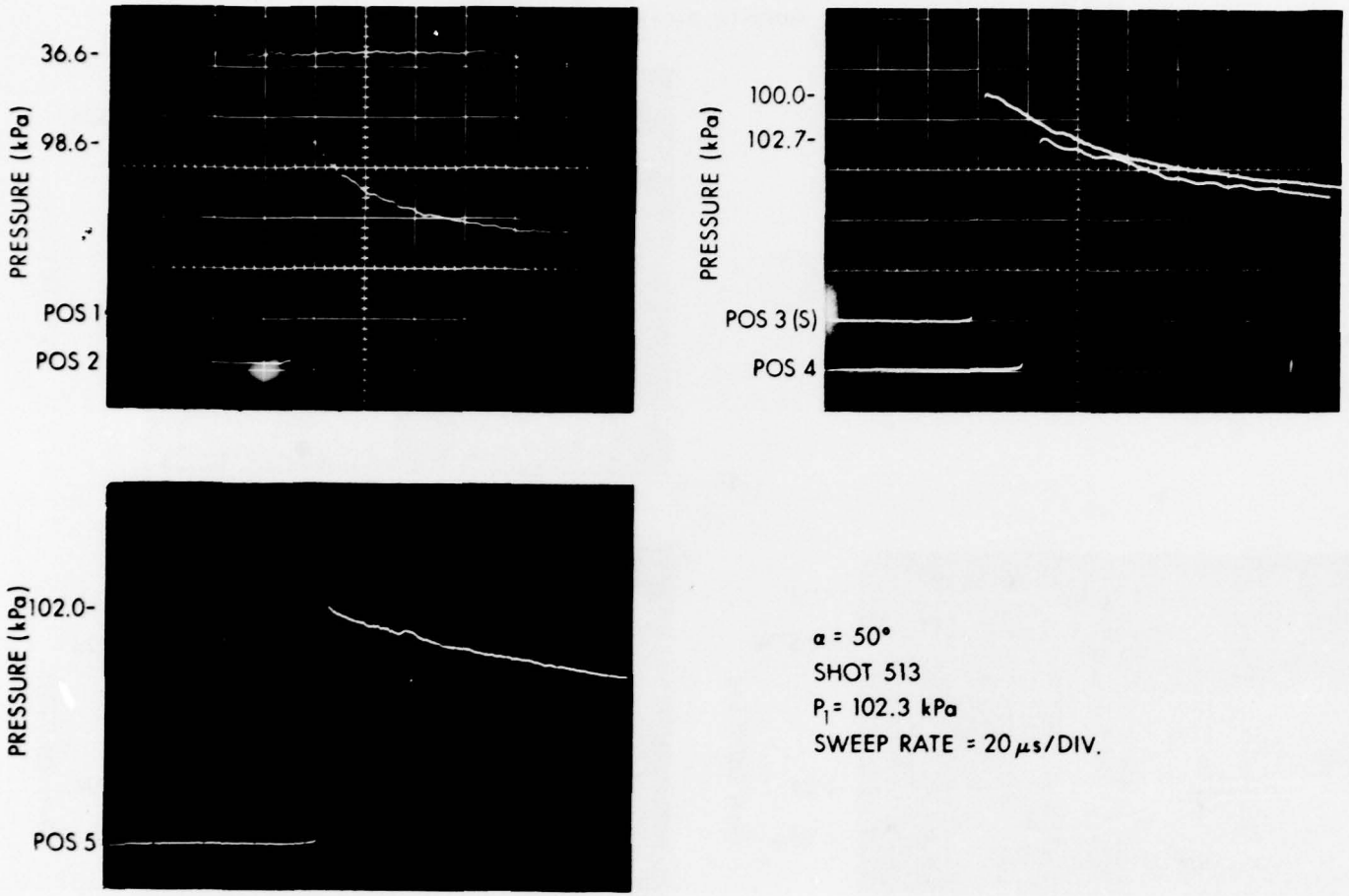

Figure B10. Typical pressure history records, P_{21} = 1.34.

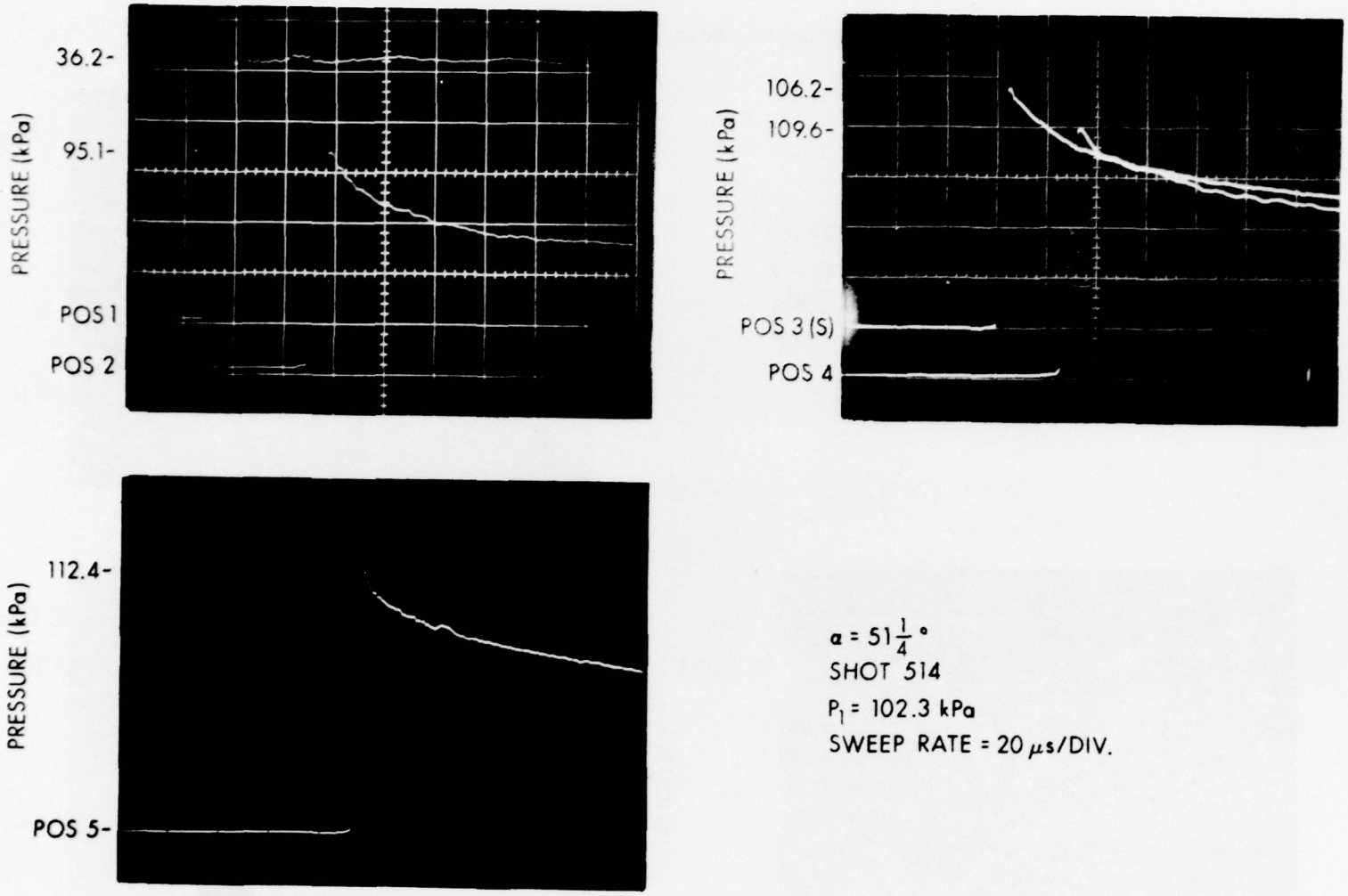

Figure B11. Typical pressure history records, P_{21} = 1.34.

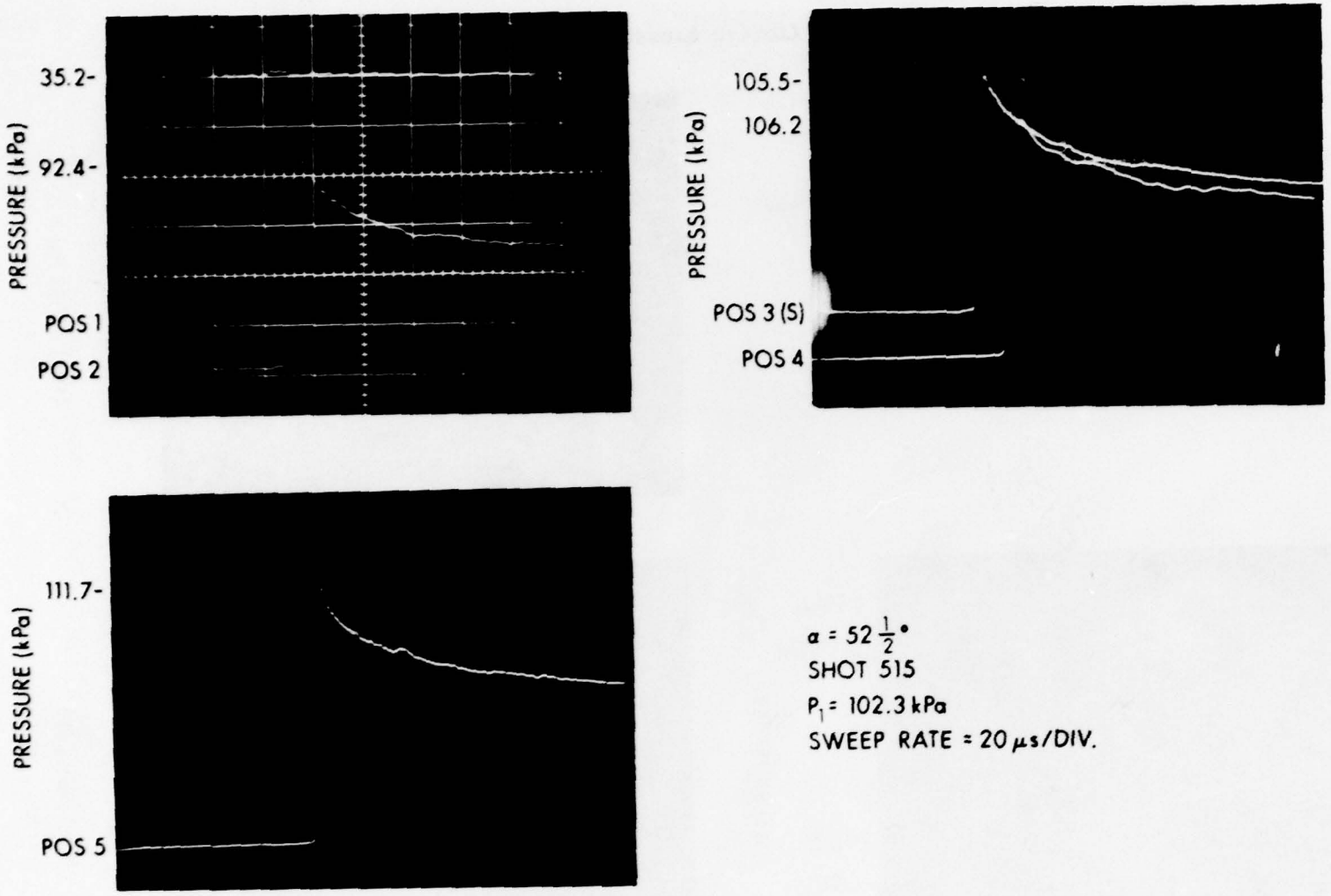

Figure B12. Typical pressure history records, P_{21} = 1.34.

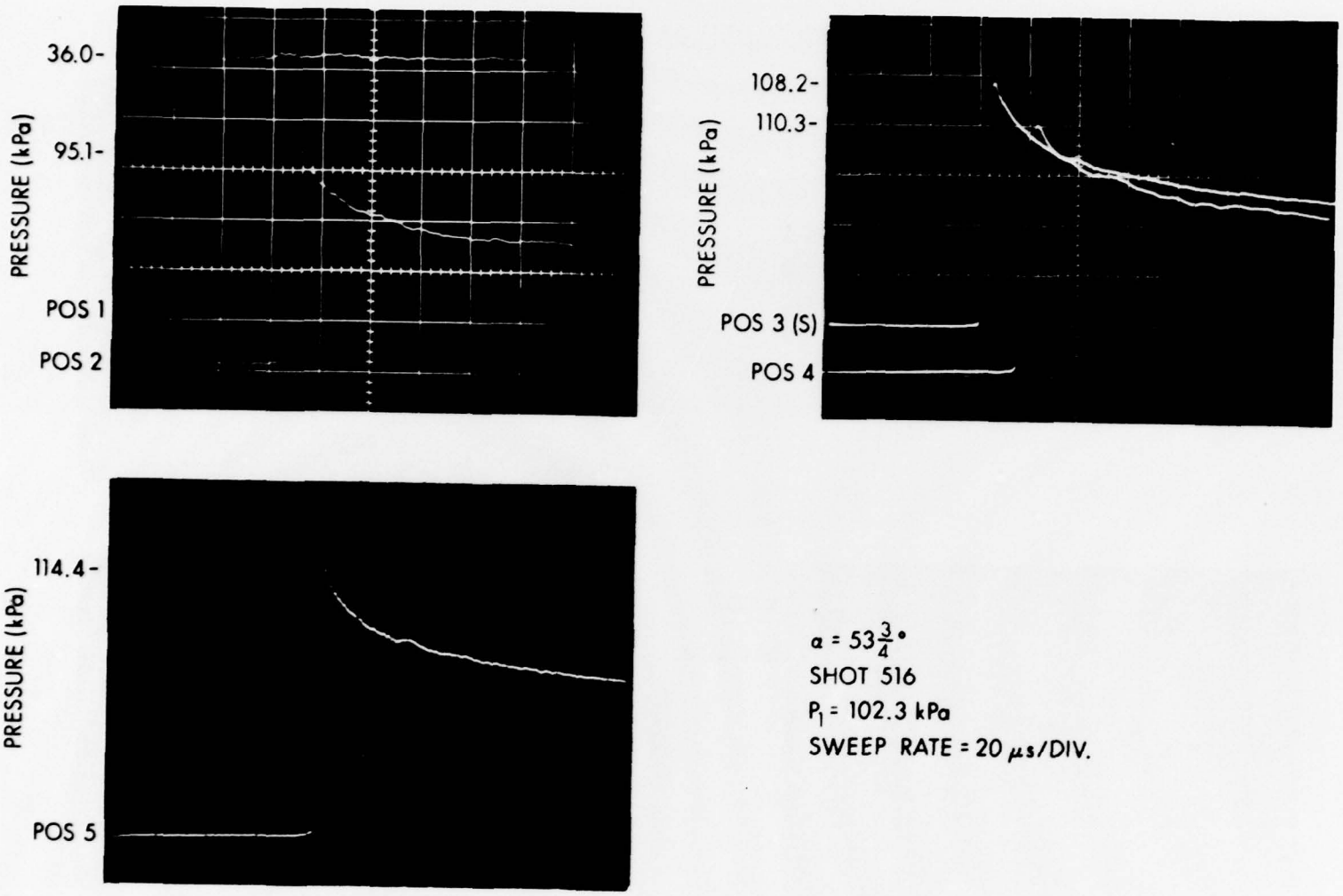

Figure B13. Typical pressure history records, P_{21} = 1.34.

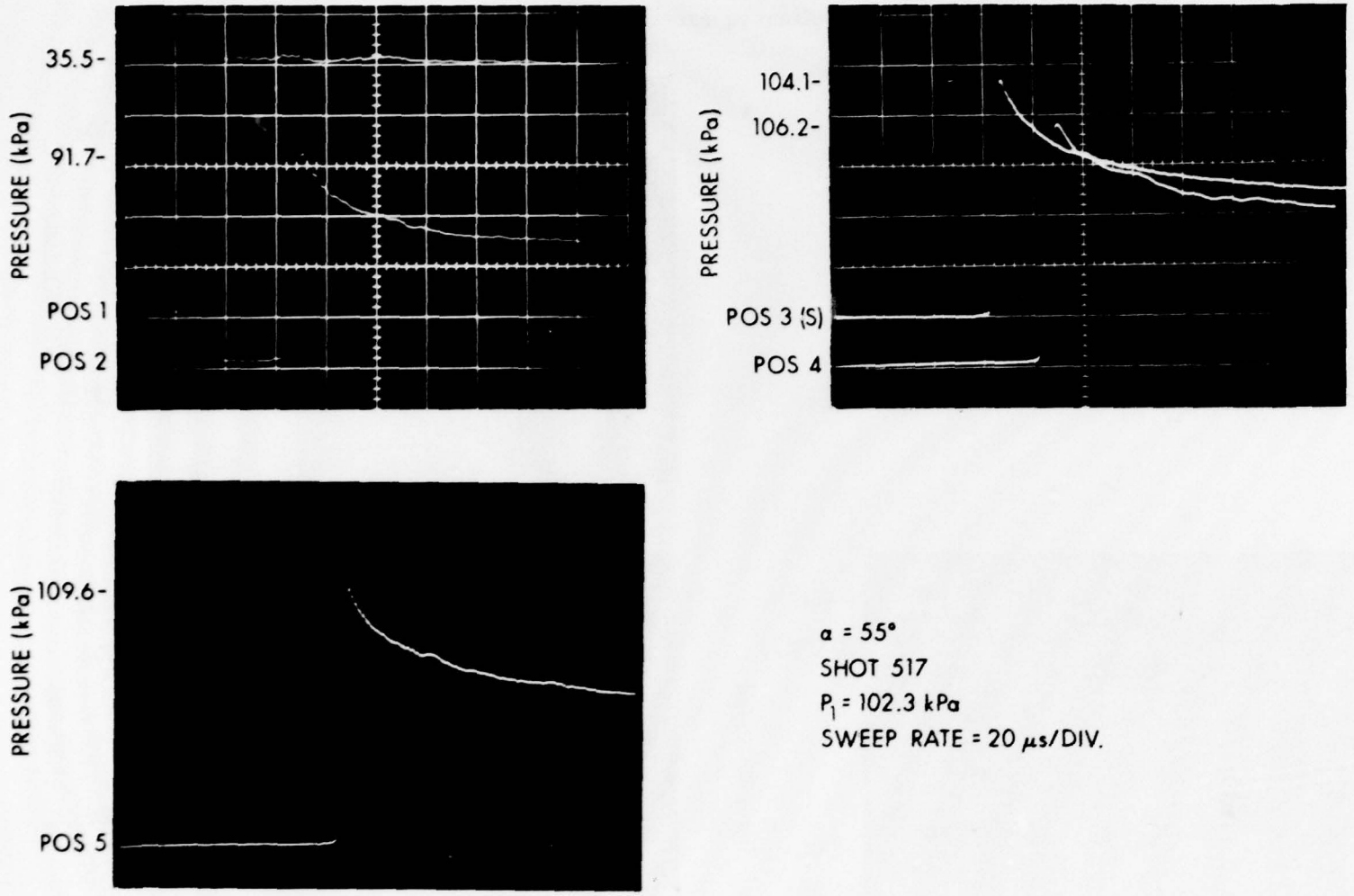

Figure B14. Typical pressure history records, P_{21} = 1.34.

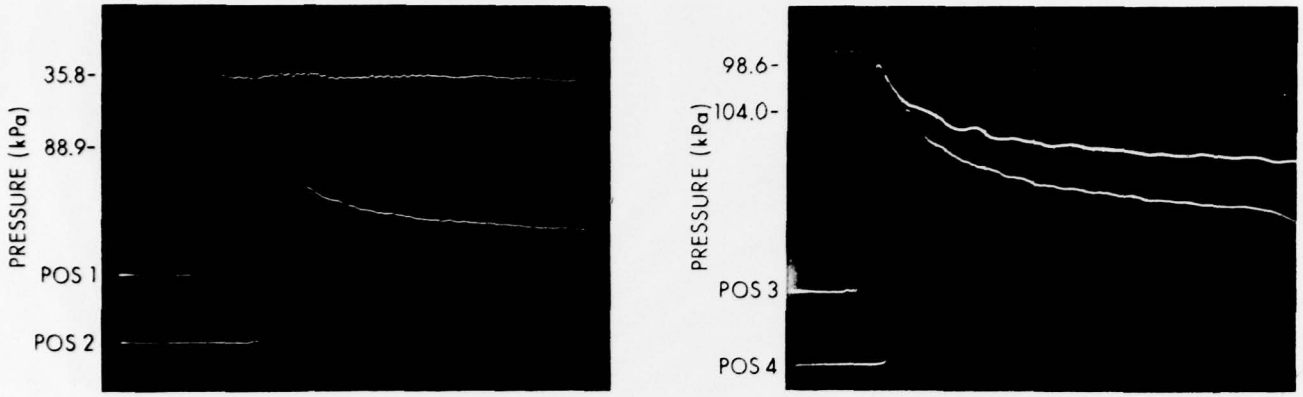

$\alpha = 56\frac{1}{4}°$
SHOT 344
P_1 = 103.5 kPa
SWEEP RATE = 20 μs/DIV.

Figure B15. Typical pressure history records, P_{21} = 1.34.

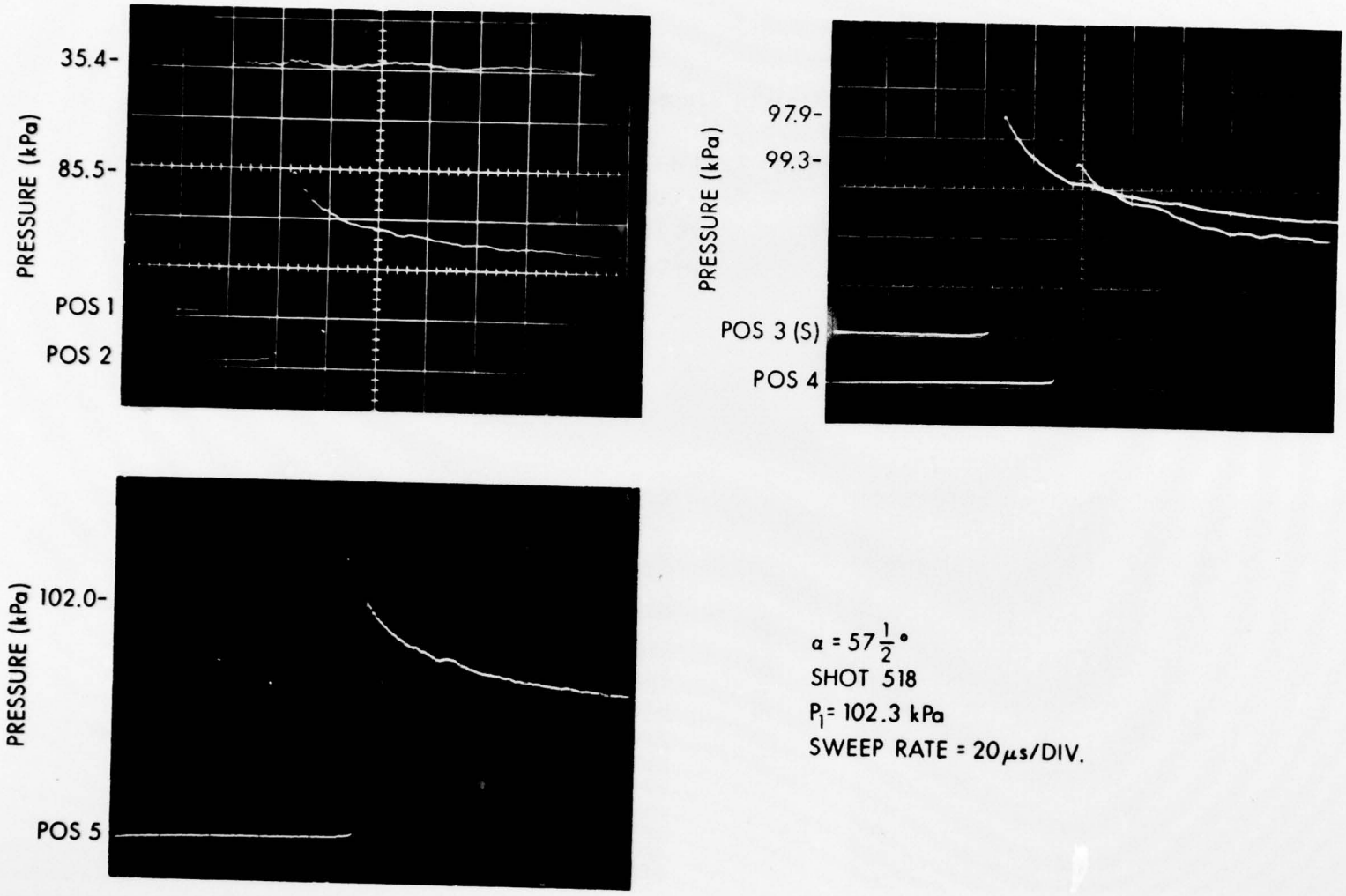

Figure B16. Typical pressure history records, P_{21} = 1.34.

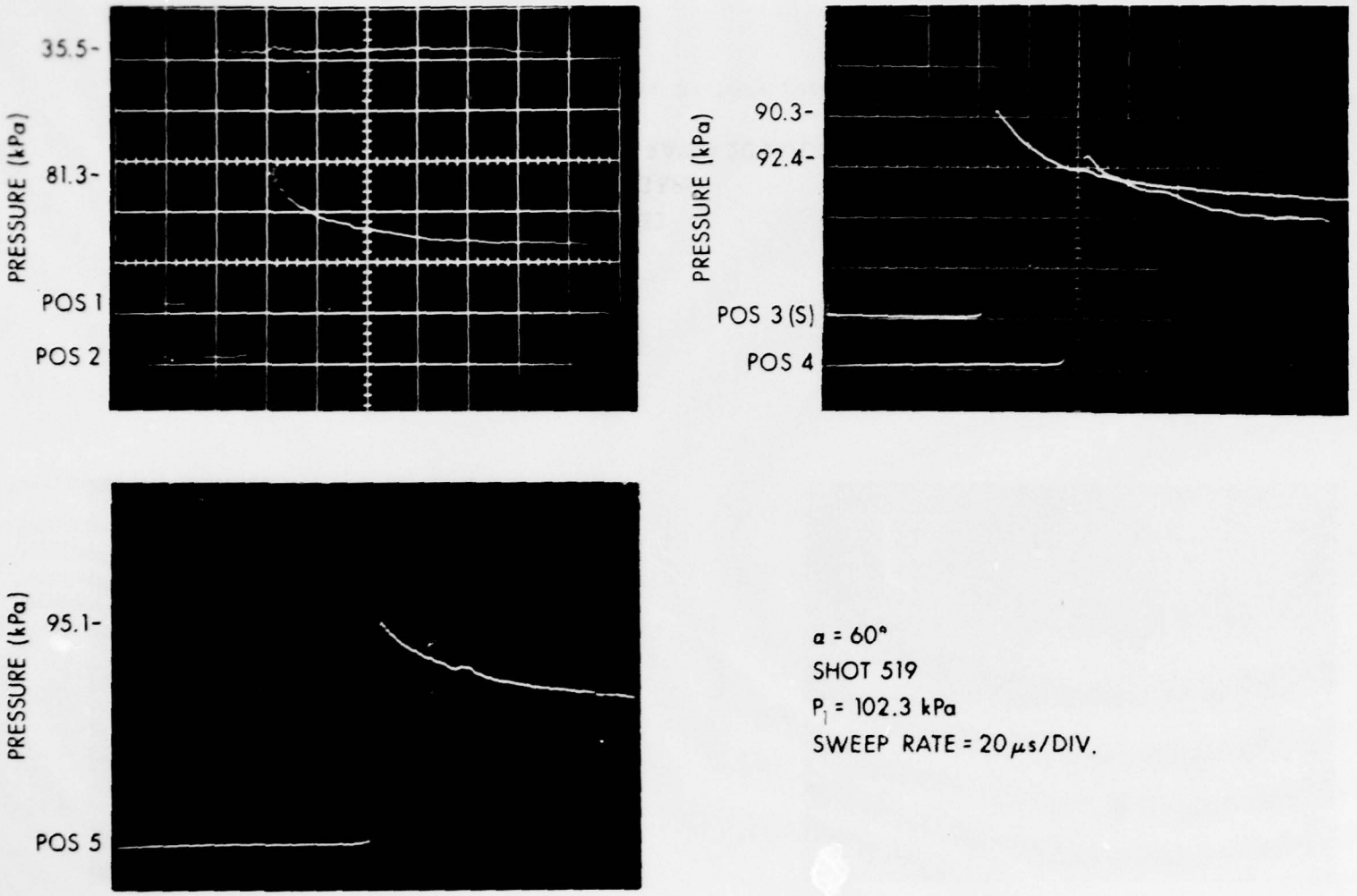

Figure B17. Typical pressure history records, P_{21} = 1.34.

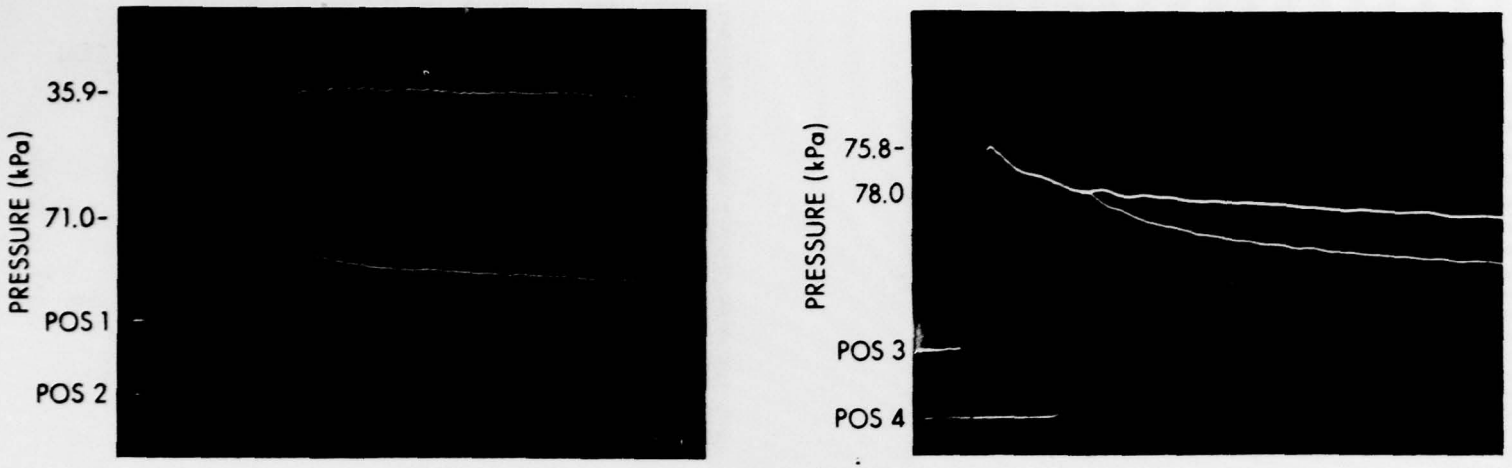

α = 65°
SHOT 353
P_1 = 103.3 kPa
SWEEP RATE = 20 μs/DIV

Figure B18. Typical pressure history records, P_{21} = 1.34.

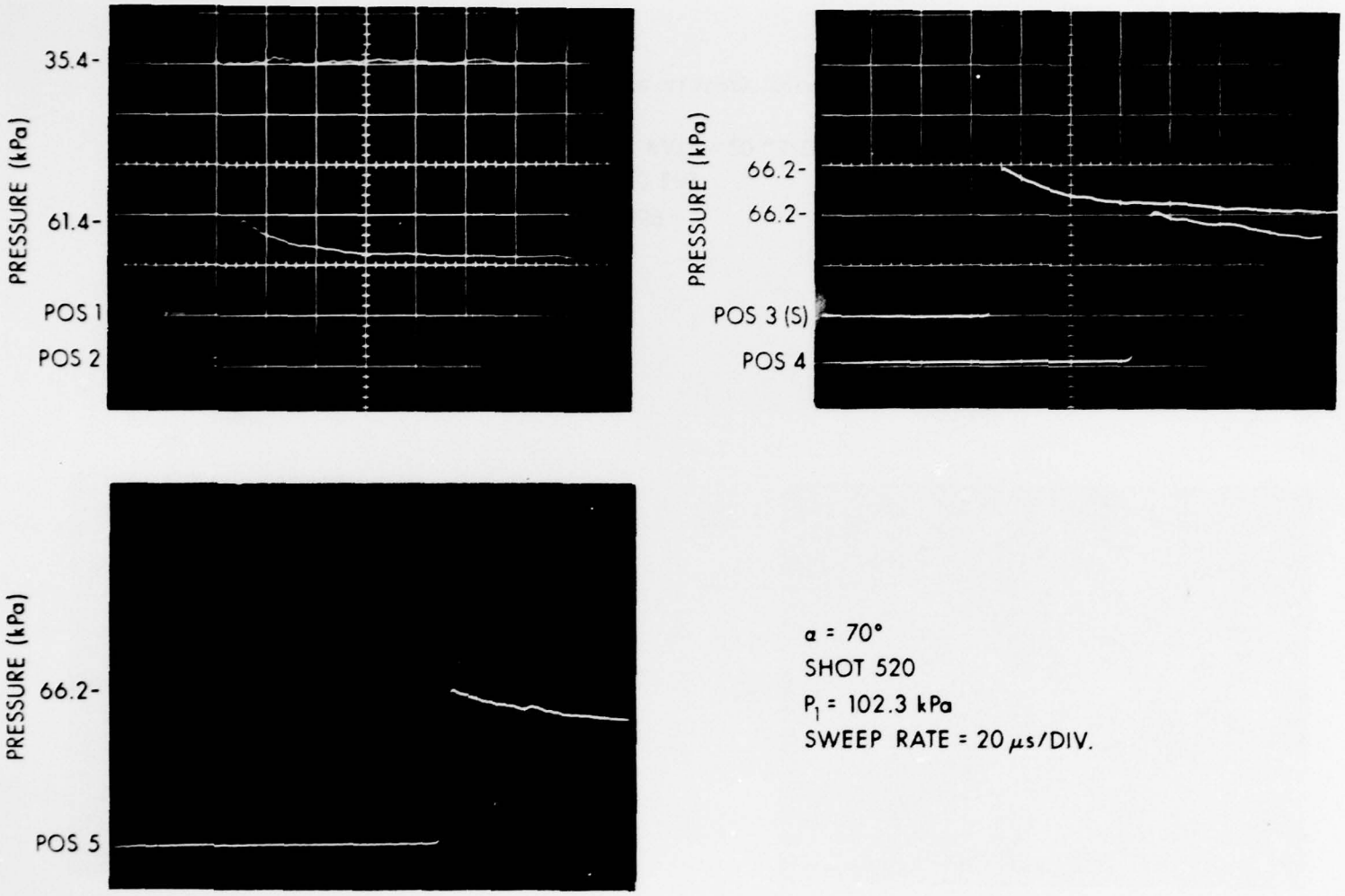

Figure B19. Typical pressure history records, P_{21} = 1.34.

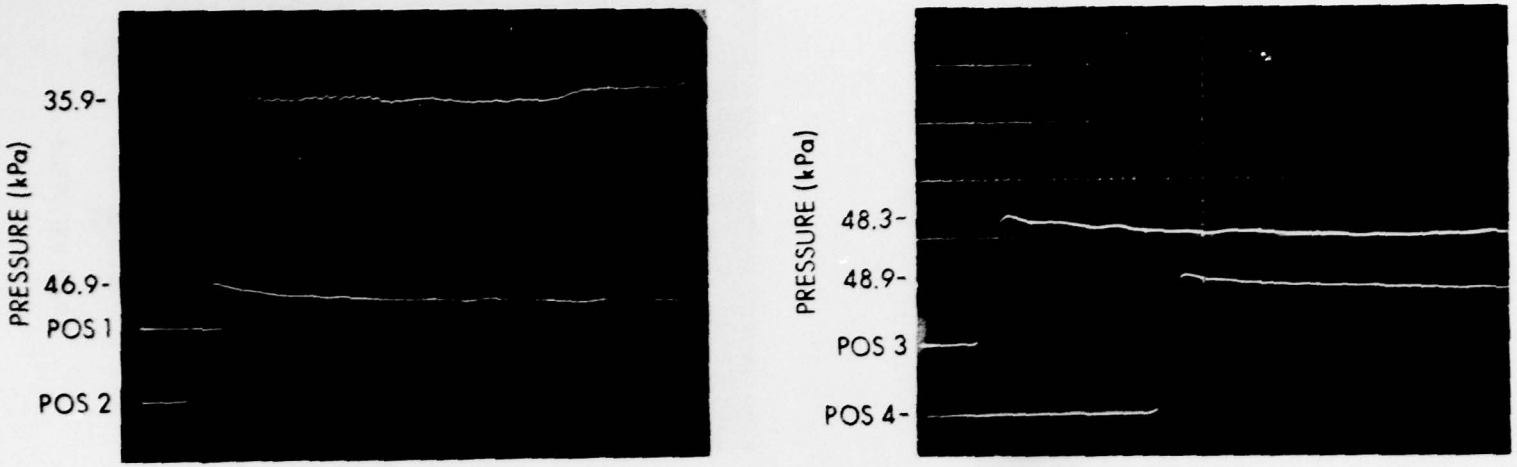

α = 80°
SHOT 359
P_1 = 103.3 kPa
SWEEP RATE = 20 μs/DIV.

Figure B20. Typical pressure history records, P_{21} = 1.34.

APPENDIX C

Scaled Measured Pressure Histories, $P_{21} = 1.136$

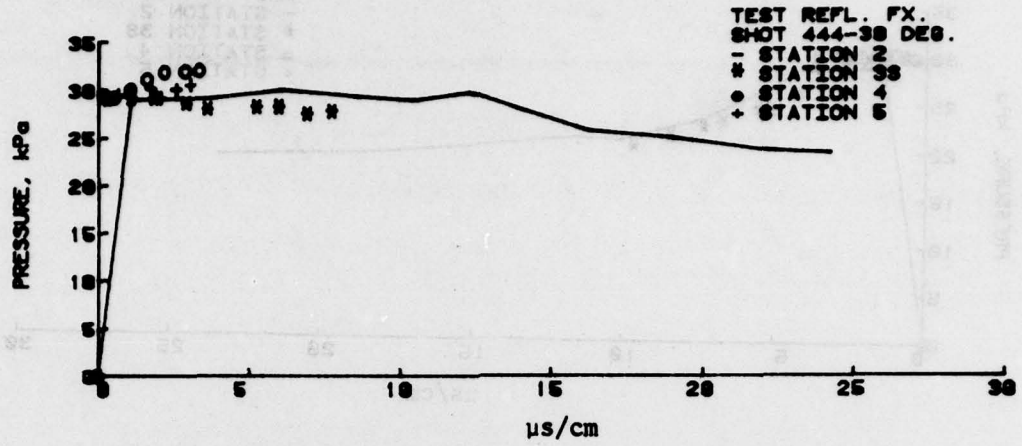

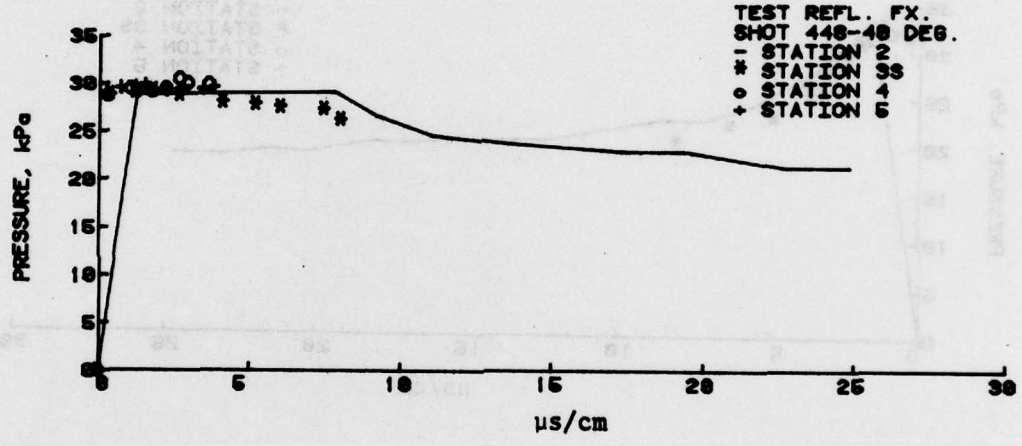

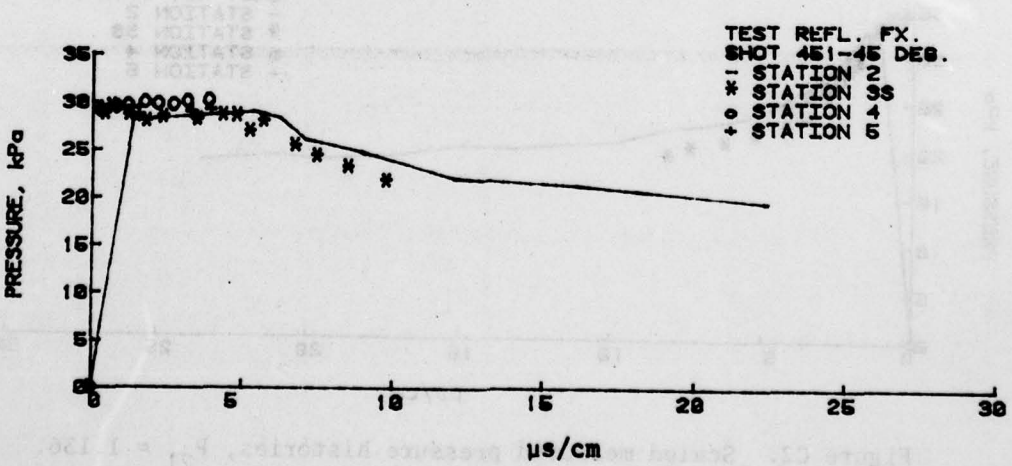

Figure C1. Scaled measured pressure histories, P_{21} = 1.136.

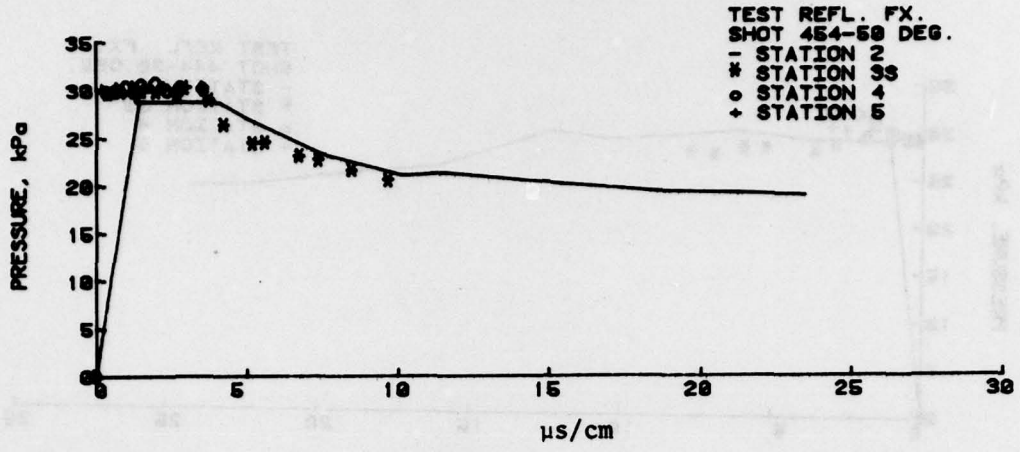

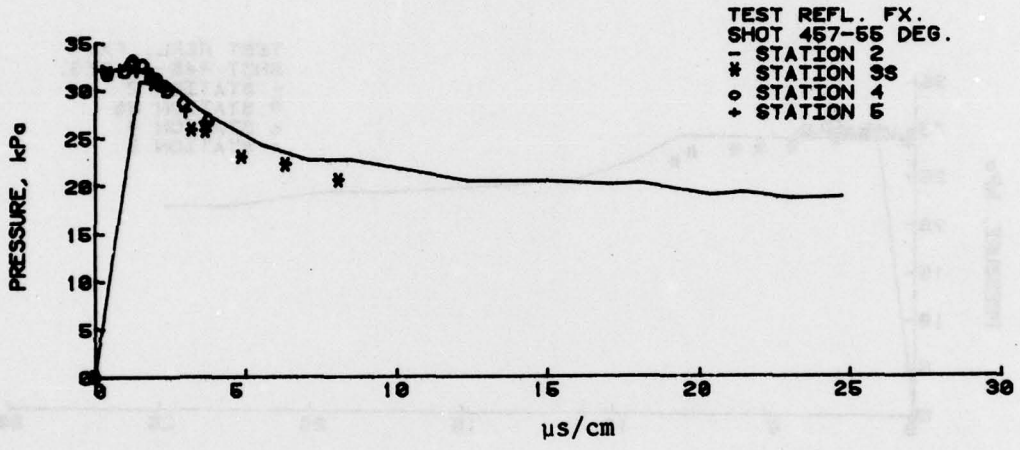

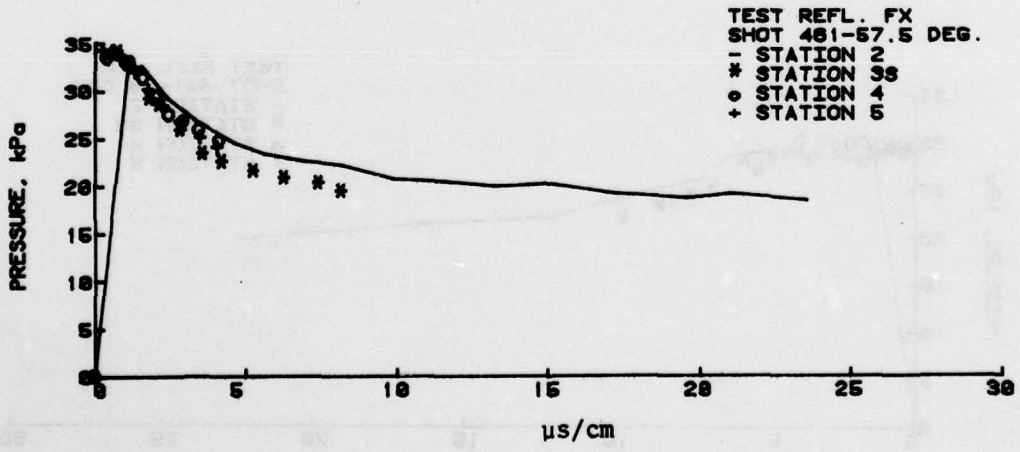

Figure C2. Scaled measured pressure histories, P_{21} = 1.136.

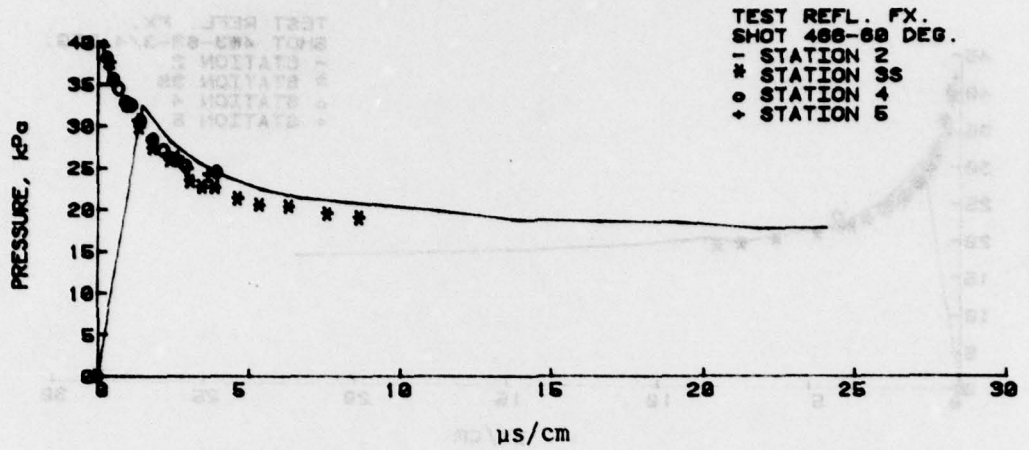

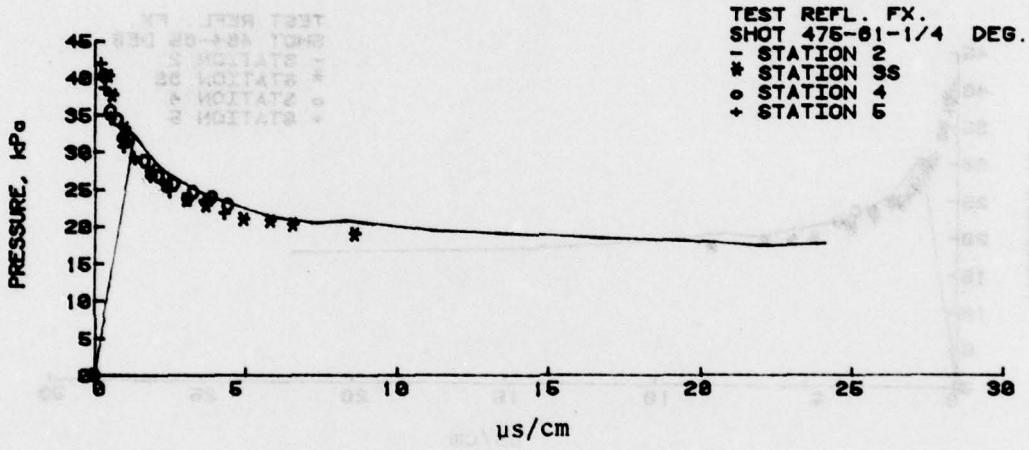

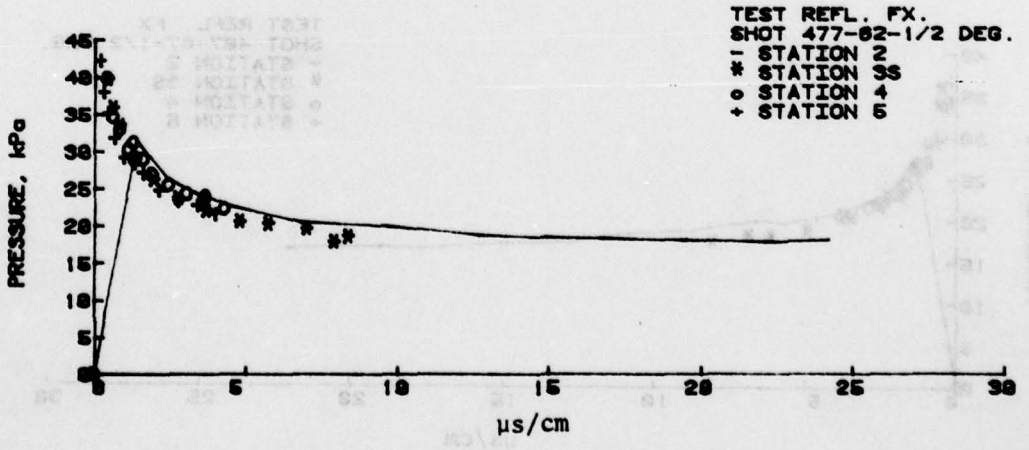

Figure C3. Scaled measured pressure histories, P_{21} = 1.136.

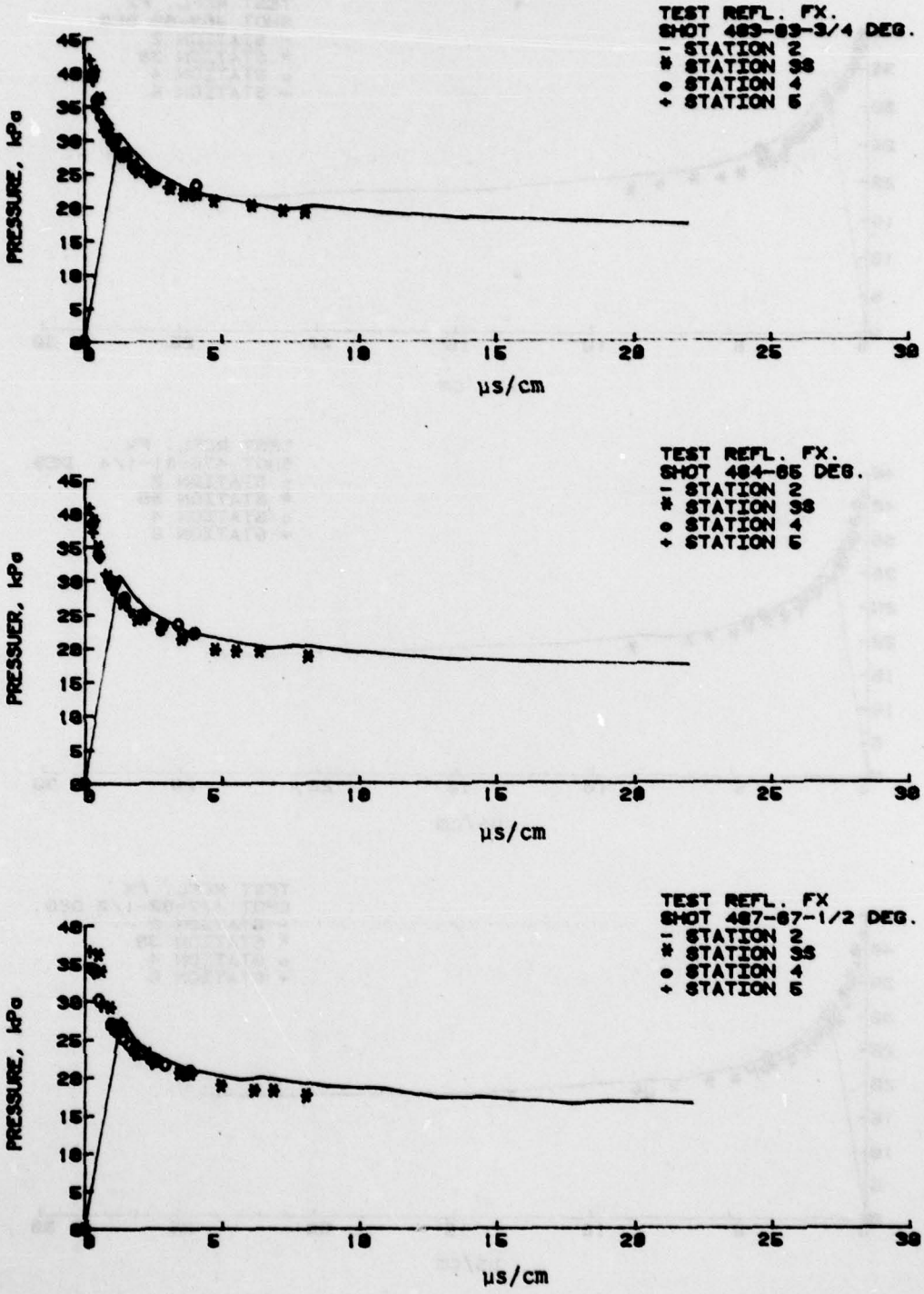

Figure C4. Scaled measured pressure histories, P_{21} = 1.136.

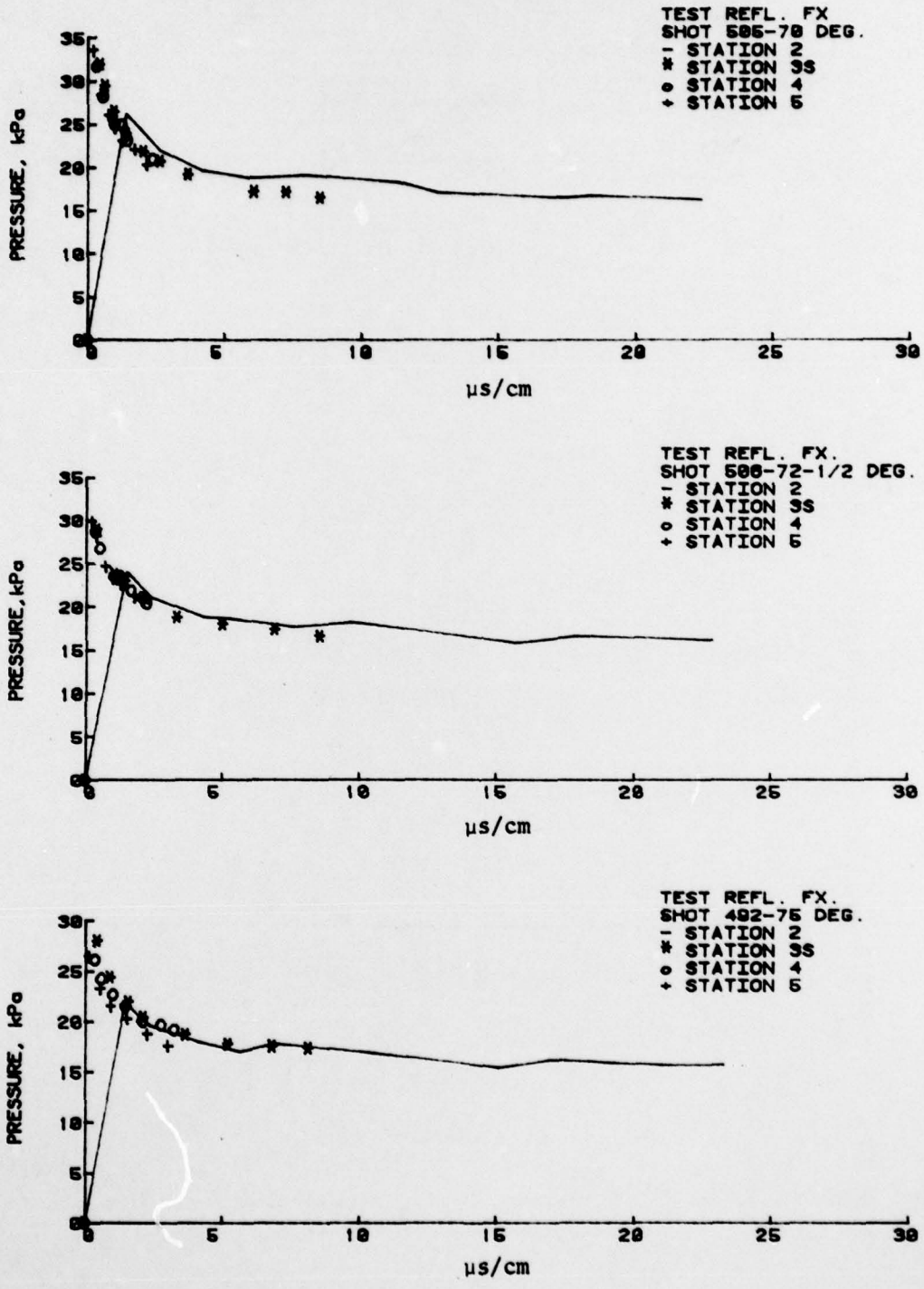

Figure C5. Scaled measured pressure histories, P_{21} = 1.136.

APPENDIX D

Scaled Measured Pressure Histories, $P_{21} = 1.34$

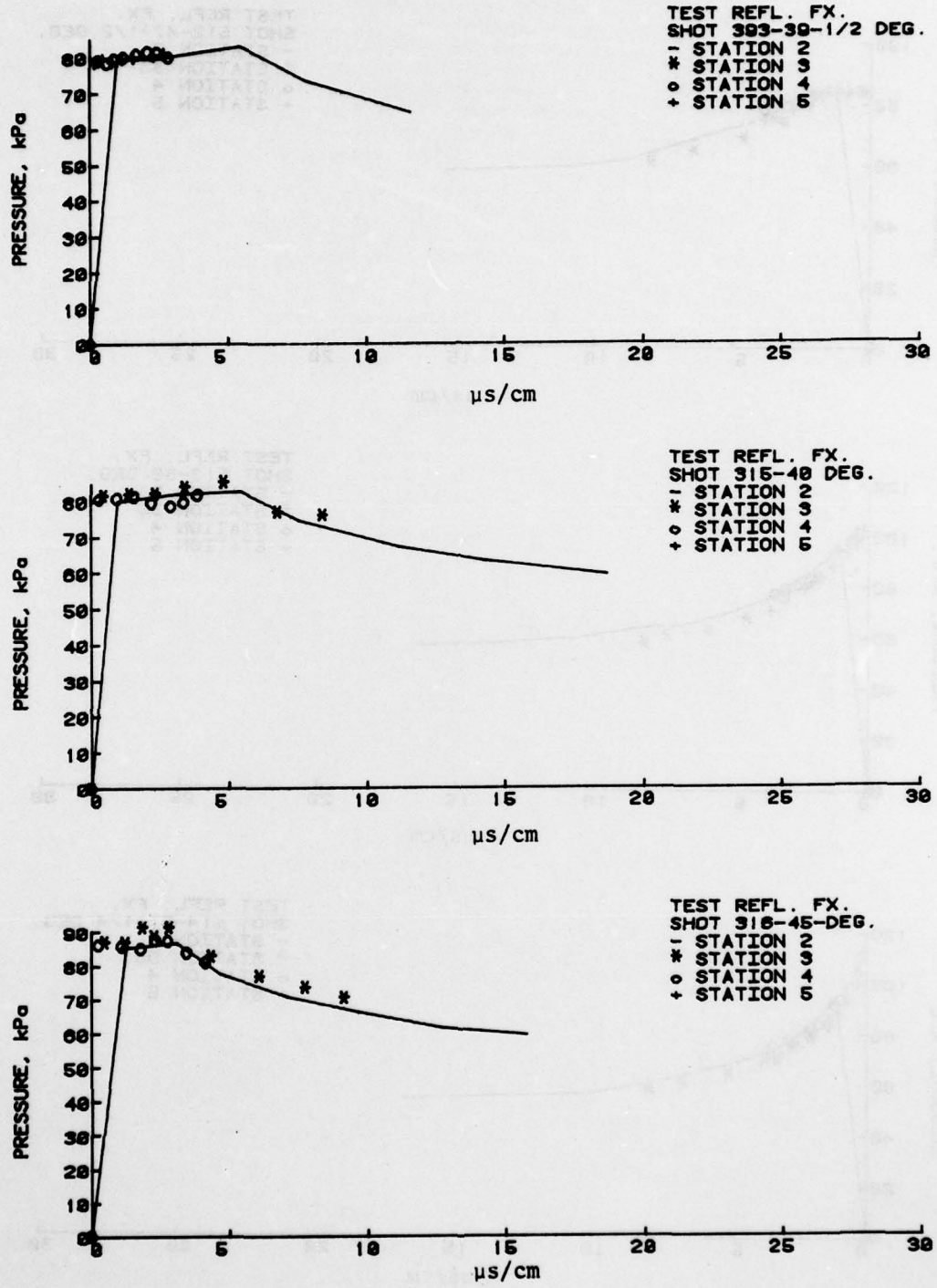

Figure D1. Scaled measured pressure histories, P_{21} = 1.34.

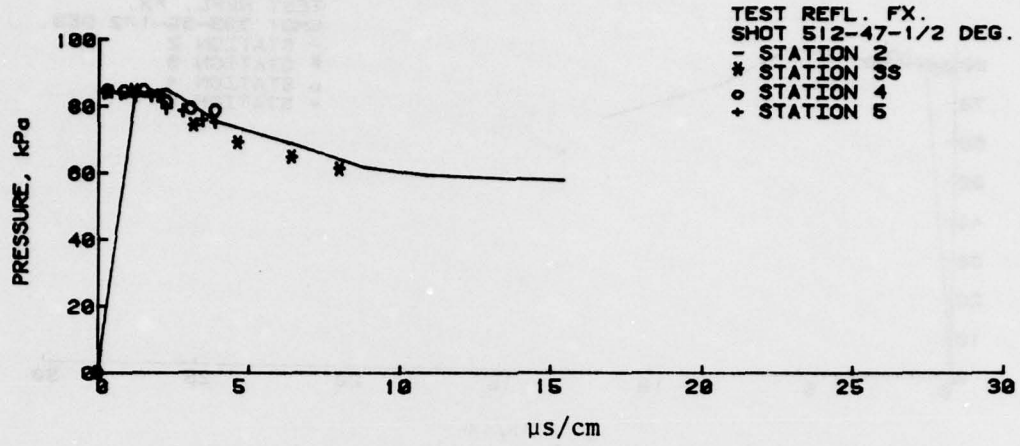

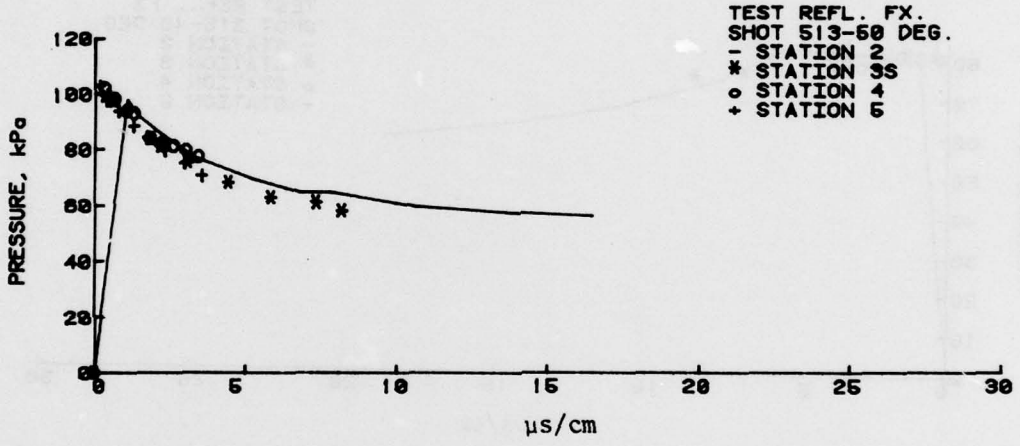

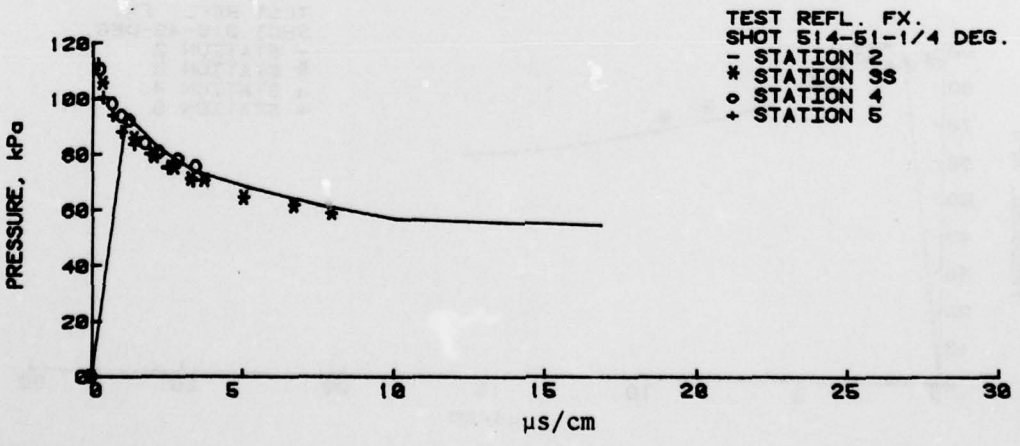

Figure D2. Scaled measured pressure histories, P_{21} = 1.34.

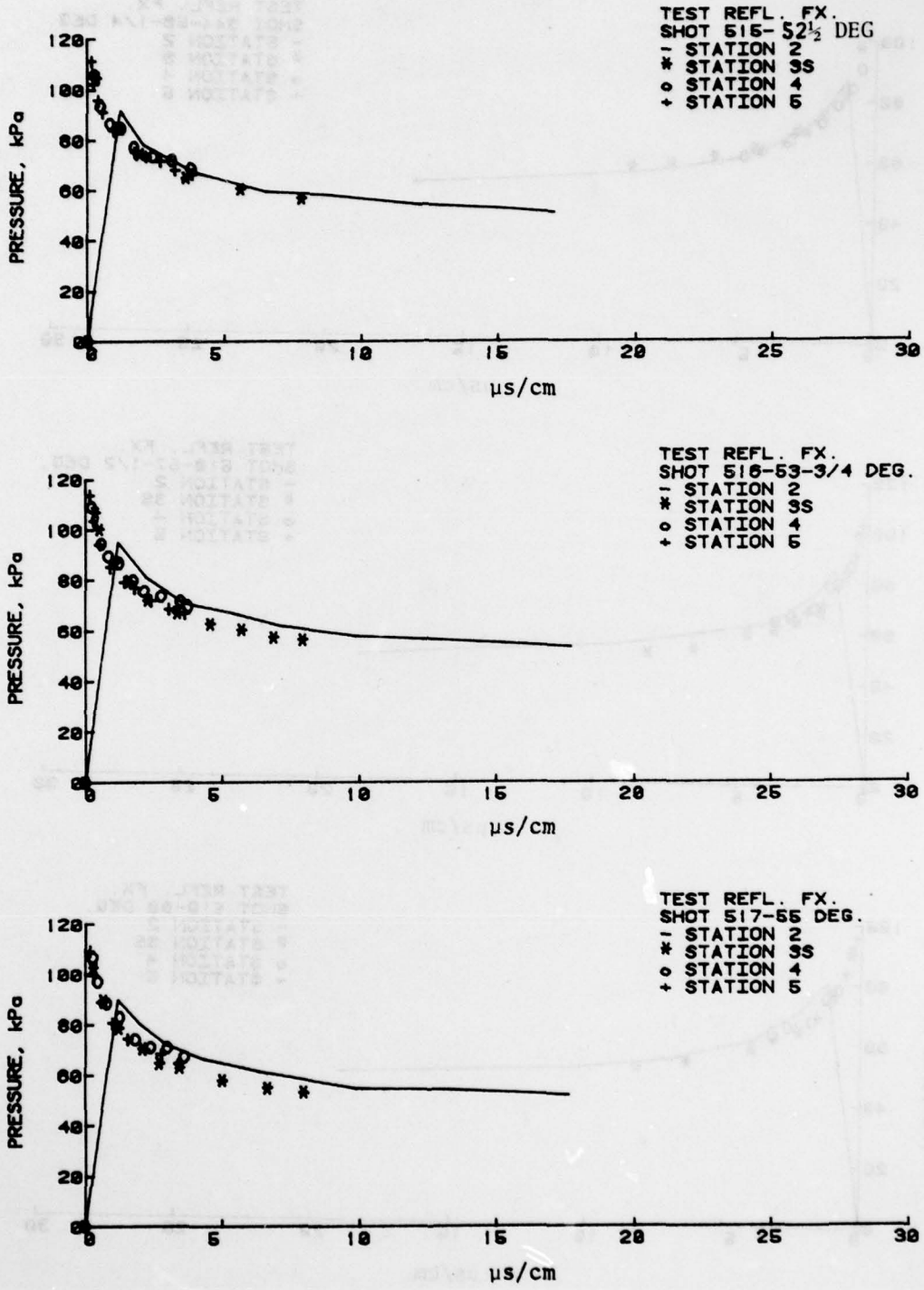

Figure D3. Scaled measured pressure histories, P_{21} = 1.34.

AD-A080 539 ARMY ARMAMENT RESEARCH AND DEVELOPMENT COMMAND ABERD--ETC F/G 20/4
MEASUREMENTS OF WEAK SHOCK WAVE REFLECTED PRESSURE HISTORIES ON--ETC(U)
OCT 79 B P BERTRAND

UNCLASSIFIED ARBRL-MR-02966 SBIE -AD-E430 357 NL

2 OF 2
AD
A080539

END
DATE
FILMED
3-80
DDC

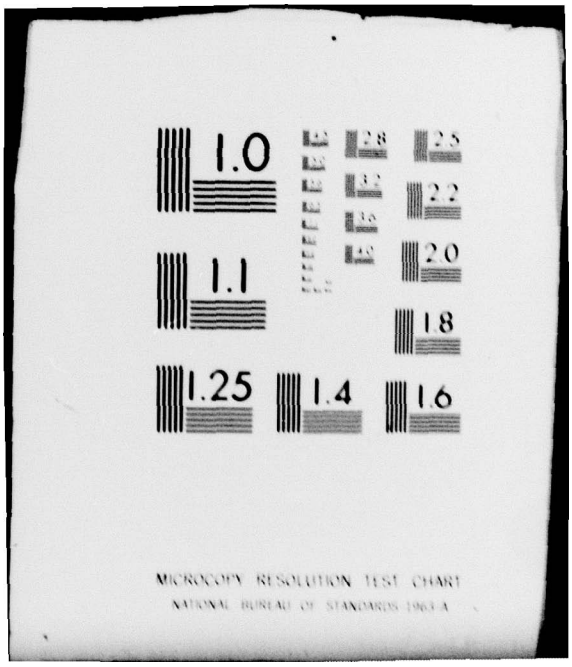
1.0
1.1
1.25
1.4
1.6
2.8
3.2
3.6
4.0
2.5
2.2
2.0
1.8
MICROCOPY RESOLUTION TEST CHART
NATIONAL BUREAU OF STANDARDS 1963-A

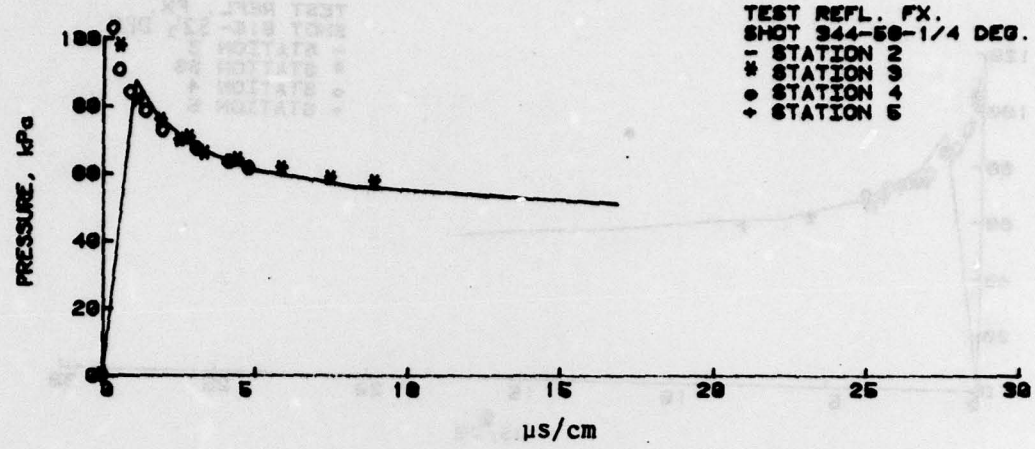

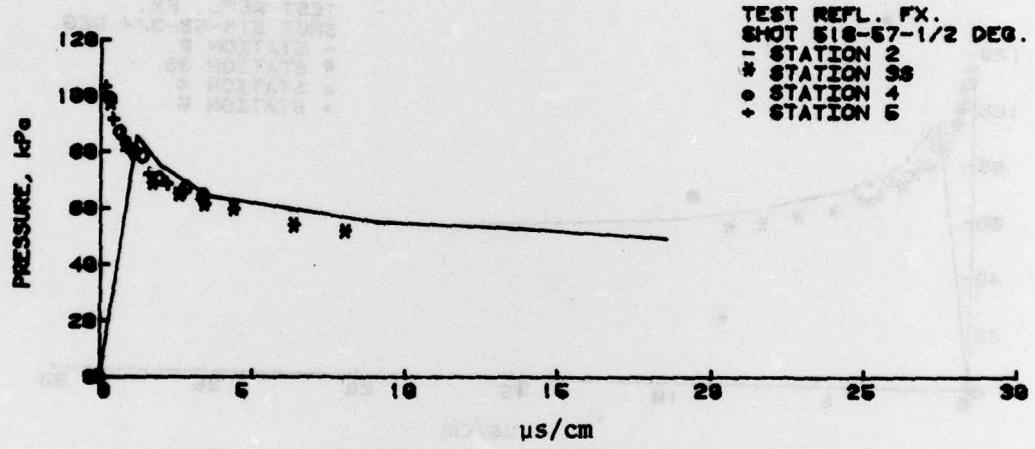

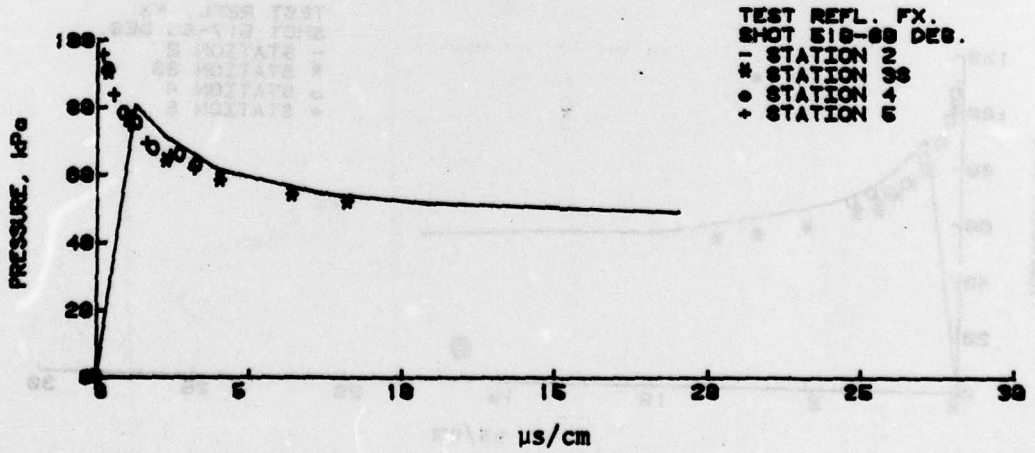

Figure D4. Scaled measured pressure histories, P_{21} = 1.34.

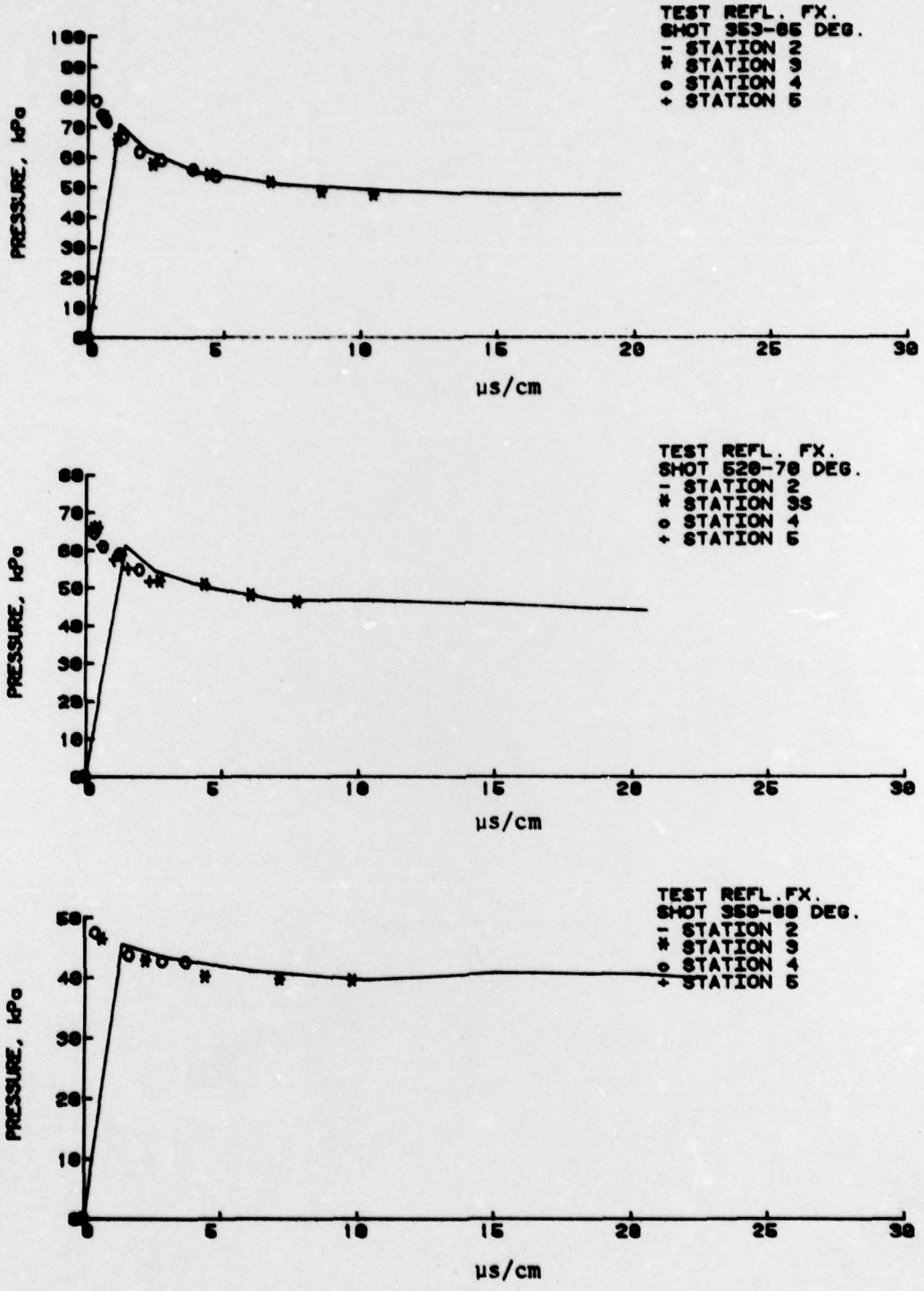

Figure D5. Scaled measured pressure histories, P_{21} = 1.34.

LIST OF SYMBOLS

a_1	ambient sound speed
d	diameter of transducer sensitive element
L	distance from leading edge of wedge to transducer position
P_1	ambient pressure
P_2	shock pressure
P_{21}	P_2/P_1
P_{12}	P_1/P_2
P_5	reflected shock pressure
P_{51}	P_5/P_1
P_{52}	P_5/P_2
P_S	$P_2 - P_1$
P_R	$P_5 - P_1$
T_1	ambient temperature
t	time
V	calibration voltage
W_1	shock velocity
W_{11}	W_1/a_1
W_T	speed of shock along the surface of wedge
W_{T1}	W_T/a_1
α	angle between shock front and reflecting surface
α_c	catch up angle
α_E	largest angle for which two shock theory has solutions
α_M	smallest angle at which Mach reflection occurs
γ	ratio of specific heats
Δt	time increment following shock arrival at a point

DISTRIBUTION LIST

No. of Copies	Organization
12	Commander Defense Documentation Center ATTN: DDC-DDA Cameron Station Alexandria, VA 22314
4	Director of Defense Research & Engineering ATTN: DD/TWP DD/S&SS DD/I&SS AD/SW Washington, DC 20301
3	Director Defense Advanced Research Projects Agency ATTN: Technical Library NMRO PMO 1400 Wilson Boulevard Arlington, VA 22209
6	Director Defense Nuclear Agency ATTN: STTL (Tech Lib, 2 cys) SPAS, Mr. J. Moulton DDST, Mr. P. H. Haas SPSS, Dr. George Ullrich SPAS, Mr. D. Kohler Washington, DC 20305
2	Commander Field Command, DNA ATTN: FCTMOF Kirtland AFB, NM 87115
2	Department of Defense Explosives Safety Board ATTN: R. Perkins Dr. Tom Zaker Room GS-270, Forrestal Bldg Washington, DC 20314
1	Commander US Army Materiel Development and Readiness Command ATTN: DRCDMD-ST 5001 Eisenhower Avenue Alexandria, VA 22333
4	Commander US Army Armament Research & Development Command ATTN: DRDAR-TSS (2 cys) P. Angelotti Mr. Demitrack Dover, NJ 07801
2	Commander US Army Armament Materiel Readiness Command ATTN: SARRI-LR, B. Morris DRSAR-LEP-L, Tech Lib Rock Island, IL 61229
1	Commander US Army Aviation Research and Development Command ATTN: DRSAV-E 12th and Spruce Streets St. Louis, MO 63166
1	Director US Army Air Mobility Research & Development Laboratory Ames Research Center Moffett Field, CA 94035
1	Commander US Army Electronics Research & Development Command Tech Spt Activity ATTN: DELSD-L Fort Monmouth, NJ 07703

DISTRIBUTION LIST

No. of Copies	Organization
3	Commander US Army Missile R&D Command ATTN: DRDMI-R DRDMI-YDL DRDMI-S, Chief Scientist Redstone Arsenal, AL 35809
2	Commander US Army Tank Automotive Research & Development Command ATTN: DRDTA-UL DRDTA-RHT, LT P. Hasek Warren, MI 48090
4	Commander US Army Harry Diamond Laboratories ATTN: DRXDO-TI/012 DRXDO-NP, F. Wimenitz DRXDO-NP, J. Gaul DRXDO-NP, J. Gwaltney 28 Powder Mill Road Adelphi, MD 20783
1	Director US Army Materials and Mechanics Research Center ATTN: Technical Library Watertown, MA 02172
1	Commander US Army Foreign Science and Technology Center ATTN: Research & Data Branch 220 7th Street, NE Charlottesville, VA 22901
3	Commander US Army Nuclear Agency ATTN: ATCN-W, CAPT M. Bowling CDINS-E Technical Library 7500 Backlick Road, Bldg 2073 Springfield, VA 22150
1	Director US Army TRADOC Systems Analysis Activity ATTN: ATAA-SL, Tech Library White Sands Missile Range New Mexico 88002
1	HGDA (DAMA-AR, NCB Division) Washington, DC 20310
3	Director US Army Advanced BMD Technology Center ATTN: Mr. B. E. Kelley Mr. M. Capps Mr. Marcus Whitfield P. O. Box 1500 Huntsville, AL 35807
1	Commander US Army Ballistic Missile Defense Systems Command ATTN: SSC-DH, H. Solomonson P. O. Box 1500 Huntsville, AL 35807
1	Commander US Army Ballistic Missile Defense Program Office ATTN: DACS-SAE-S, J. Shea 5001 Eisenhower Avenue Alexandria, VA 22333
2	Commander US Army Engineer Waterways Experiment Station ATTN: Library W. Flateau P. O. Box 631 Vicksburg, MS 39180

DISTRIBUTION LIST

No. of Copies	Organization
3	Commander David Taylor NSRDC ATTN: Code 1740.4, S.L. WANG C. NG Lib Div., Code 522 Bethesda, MD 20084
2	Chief of Naval Research Department of the Navy ATTN: T. Quinn, Code 461 J. L. Warner, Code 461 Washington, DC 20360
2	Commander Naval Ship Eng'g Center ATTN: J. R. Sullivan NSEC 6105-G Technical Library Hyattsville, MD 20782
4	Commander Naval Surface Weapons Center ATTN: Code 1224, Navy Nuclear Programs Office Code 241, J. Petes Code 730, Tech Library J. Pittman Silver Spring, MD 20910
1	Commander Naval Weapons Evaluation Fac ATTN: Document Control Kirtland AFB, NM 87117
1	Commander Naval Civil Engineering Lab ATTN: Dr. W. A. Shaw, Code L31 Port Hueneme, CA 93041
3	Director Naval Research Laboratory ATTN: M. Persechino G. Cooperstein Tech Lib, Code 2027 Washington, DC 20375
1	HQ USAFSC (DLCAW, Tech Library) Andrews AFB Washington, DC 20331
1	AFOSR (OAR) Bolling AFB, DC 20332
1	RADC (Document Lib, FMTLD) Griffis AFB, NY 13440
4	AFWL (CA, Dr. A. Guenther DYT, Charles Needham DYT, MAJ G. Gonong; S. Melzer) Kirtland AFB, NM 87117
1	AFCRL L. G. Hanscom Field Bedford, MA 01730
1	SAMSO (Library) P. O. Box 92960 Los Angeles, CA 90009
3	AFTC (K. Rosenlof R. McBride G. Leises) Patrick AFB, FL 32925
2	AFML (G. Schmitt, MAS; D. Schmidt) Wright-Patterson AFB, OH 45433
2	Energy Research & Development Administration Department of Military Application ATTN: R&D Branch Library Branch, G-043 Washington, DC 20545
2	Director Los Alamos Scientific Laboratory ATTN: Dr. J. Taylor Technical Library P. O. Box 1663 Los Alamos, NM 87554

DISTRIBUTION LIST

No. of Copies	Organization
1	Director, NASA ATTN: Code 04.000 Langley Research Center Langley Station Hampson, VA 23365
1	Director NASA Scientific & Technical Information Facility ATTN: SAK/DL P. O. Box 8757 Baltimore/Washington International Airport, MD 21240
1	National Academy of Sciences ATTN: Dr. Donald Groves 2101 Constitution Avenue, NW Washington, DC 20418
1	Aerospace Corporation ATTN: Tech Information Svcs, Bldg 105, Rm 2220 P. O. Box 92957 Los Angeles, CA 90009
1	Agbabian Associates ATTN: Dr. J. Malthan 250 N. Nash Street El Segundo, CA 90245
1	AVCO Government Products Group ATTN: Dr. W. Bade 201 Lowell Street Wilmington, MA 01887
1	AVCO-Everett Research Laboratory ATTN: Technical Library 2385 Revere Beach Parkway Everett, MA 02149
1	John A. Blume & Associates ATTN: Dr. John A. Blume Sheraton-Palace Hotel 100 Jessie Street San Francisco, CA 94105
1	CALSPAN Corporation ATTN: Library P. O. Box 235 Buffalo, NY 14221
1	Effects Technology, Inc. ATTN: E. Anderson 5383 Holister Avenue Santa Barbara, CA 93105
1	General Electric Co. - TEMPO ATTN: DASIAC 816 State Street, Drawer QQ Santa Barbara, CA 93102
1	General Electric Co. - TEMPO ATTN: Dr. Lynn Kennedy 7800 Marble Avenue, NE, Suite 5 Albuquerque, NM 87110
1	H-Tech Laboratories, Inc. ATTN: B. Hartenbaum P. O. Box 1686 Santa Monica, CA 90406
1	Hughes Aircraft Company Systems Development Laboratory ATTN: Dr. A. Puckett Centinela and Teale Streets Culver City, CA 92032
1	Ion Physics Corporation ATTN: Technical Library South Bedford Street Burlington, MA 01803

DISTRIBUTION LIST

No. of Copies	Organization
1	Kaman Sciences Corporation ATTN: Dr. D. Sachs 1500 Garden of the Gods Road Colorado Springs, CO 80907
1	Kaman Avidyne, Division of Kaman Sciences ATTN: Dr. J. Ray Ruetenik 83 2nd Ave, NW Industrial Park Burlington, MA 01803
1	KTECH Corporation ATTN: Dr. Donald V. Keller 911 Pennsylvania NE Albuquerque, NM 87110
1	Lockheed Missiles & Space Co, Division of Lockheed Aircraft Corp ATTN: J. Nickell P. O. Box 504 Sunnyvale, CA 94088
1	Management Science Associates ATTN: Kenneth Kaplan P. O. Box 239 Los Altos, CA 94022
1	Martin Marietta Aerospace Orlando Division ATTN: A. Ossin P. O. Box 5837 Orlando, FL 32805
1	Maxwell Laboratories, Inc. ATTN: A. Kolb 9244 Balboa Avenue San Diego, CA 92123
1	McDonnell Douglas Astronautics Corporation 5301 Bolsa Avenue Huntington Beach, CA 92647
1	Philco Ford Corporation Aeronutronic Division ATTN: L. K. Goodwin Newport Beach, CA 92663
2	Physics International Company ATTN: Document Control Fred Sauer 2700 Merced Street San Leandro, CA 94577
3	R&D Associates ATTN: Technical Library Jerry Carpenter Allen Kuhl P. O. Box 9695 Marina del Rey, CA 90291
1	Sandia Laboratories ATTN: Dr. J. Kennedy P. O. Box 5800 Albuquerque, NM 87115
2	Science Applications, Inc ATTN: Mr. J. W. Miller Dr. John Cockayne 8400 West Park Drive McLean, VA 22101
1	Shock Hydrodynamics, Inc. ATTN: L. Zernow 4710-16 Vineland Avenue N. Hollywood, CA 91602
1	Systems, Science & Software ATTN: Technical Library P. O. Box 1620 La Jolla, CA 92036

DISTRIBUTION LIST

No. of Copies	Organization
1	Teledyne-Brown Engineering ATTN: Dr. M. Batel Research Park Huntsville, AL 35807
1	Union Carbide Corporation Oak Ridge National Laboratory ATTN: Technical Library P. O. Box X Oak Ridge, TN 37830
1	URS Research Company ATTN: Technical Library 155 Bovet Road San Mateo, CA 94002
1	Battelle Memorial Institute ATTN: Technical Library 505 King Avenue Columbus, Ohio 43201
2	Denver Research Institute University of Denver ATTN: Mr. John Wisotski P. O. Box 10127 Denver, CO 90210
1	Director Applied Physics Laboratory The Johns Hopkins University Johns Hopkins Road Laurel, MD 20810
1	Lovelace Rsch Institute ATTN: Dr. D. Richmond P. O. Box 5890 Albuquerque, NM 87108
1	Massachusetts Institute of Technology Aerophysics Laboratory Cambridge, MA 02139
1	New Mexico Institute of Mining and Technology ATTN: Mr. P. McClain Socorro, NM 87801
1	Northwestern Michigan College ATTN: Prof. D. C. Kennard, Jr. Traverse City, MI 49584
1	Southwest Research Institute ATTN: Dr. W. Baker 8500 Culebra Road San Antonio, TX 78206
1	Stevens Institute of Technology Dept of Electrical Engineering ATTN: Prof. R. Geldmacher Castle Point Station Hoboken, NJ 07039
1	Research Institute of Temple University ATTN: Technical Library Philadelphia, PA 19144
1	Texas Tech University Dept of Civil Engineering ATTN: Mr. Joseph E. Minor Lubbock, TX 79409
1	Univeristy of Arkansas Department of Physics ATTN: Prof. O. Zinke Fayetteville, AR 72701
1	University of California Lawrence Livermore Laboratory Technical Information Division ATTN: Technical Library Dr. Donald N. Montan P. O. Box 808 Livermore, CA 94550

DISTRIBUTION LIST

No. of Copies	Organization
1	University of Illinois Consulting Engineering Services ATTN: Nathan M. Newmark 1211 Civil Engineering Building Urbana, IL 61801
1	University of Maryland Department of Physics ATTN: Dr. E. Oktay College Park, MD 20742
1	The University of Michigan Gas Dynamics Laboratory ATTN: Z. Gabrijel Aerospace Engineering Building Ann Arbor, MI 48109
1	The University of New Mexico Eric H. Wang Civ Eng'g Res Fac ATTN: Technical Library University Station, Box 188 Albuquerque, NM 87131
1	University of Oklahoma Department of Physics ATTN: Prof. R. Fowler Norman, OK 73069

Aberdeen Proving Ground

Director, USAMSAA
ATTN: Dr. J. Sperrazza
Mr. R. Norman, GWD
DRXSY-MP, H. Cohen
Cdr, USATECOM
ATTN: DRSTE-TO-F
Dir, Wpns, Sys Concepts Team
Bldg E3516, EA
ATTN: DRDAR-ACW

USER EVALUATION OF REPORT

Please take a few minutes to answer the questions below; tear out this sheet and return it to Director, US Army Ballistic Research Laboratory, ARRADCOM, ATTN: DRDAR-TSB, Aberdeen Proving Ground, Maryland 21005. Your comments will provide us with information for improving future reports.

1. BRL Report Number _____

2. Does this report satisfy a need? (Comment on purpose, related project, or other area of interest for which report will be used.)

_____

_____

_____

3. How, specifically, is the report being used? (Information source, design data or procedure, management procedure, source of ideas, etc.) _____

_____

_____

4. Has the information in this report led to any quantitative savings as far as man-hours/contract dollars saved, operating costs avoided, efficiencies achieved, etc.? If so, please elaborate.

_____

_____

5. General Comments (Indicate what you think should be changed to make this report and future reports of this type more responsive to your needs, more usable, improve readability, etc.) _____

_____

_____

_____

6. If you would like to be contacted by the personnel who prepared this report to raise specific questions or discuss the topic, please fill in the following information.

Name: _____

Telephone Number: _____

Organization Address: _____

_____

_____